2009

Tensile strength and failure criterion of analog lithophysal rock

James A. Nott
University of Nevada Las Vegas

TENSILE STRENGTH AND FAILURE CRITERION

OF ANALOG LITHOPHYSAL ROCK

by

James A. Nott

Bachelor of Science
University of Maryland
College Park, Maryland
1956

Master of Science in Engineering
George Washington University
Washington, D.C.
1962

A dissertation submitted in partial fulfillment
of the requirements for the

Doctor of Philosophy Degree in Engineering
Department of Civil and Environmental Engineering
Howard R. Hughes College of Engineering

Graduate College
University of Nevada, Las Vegas
December 2009

UNLV
UNIVERSITY OF NEVADA LAS VEGAS

THE GRADUATE COLLEGE

We recommend that the dissertation prepared under our supervision by

James Allen Nott

entitled

Tensile Strength and Failure Criterion of Analog Lithophysal Rock

be accepted in partial fulfillment of the requirements for the degree of

Doctor of Philosophy in Engineering
Civil and Environmental Engineering

Moses Karakouzian, Committee Chair

Nadar Ghafoori, Committee Member

Douglas Rigby, Committee Member

Samaan Ladkany, Committee Member

Samir Moujaes, Graduate Faculty Representative

Ronald Smith, Ph. D., Vice President for Research and Graduate Studies
and Dean of the Graduate College

December 2009

ABSTRACT

Tensile Strength and Failure Criterion of Analog Lithophysal Rock

by

James A. Nott

Dr. Moses Karakouzian, Examination Committee Chair
Professor of Civil and Environmental Engineering
University of Nevada, Las Vegas

This project determines the tensile strength of lithophysal analog rock and presents failure criteria that can be used by geotechnical engineers to evaluate underground structures in rock. The physical and mechanical properties that are related to the failure criterion, such as porosity, compressive strength and modulus of elasticity, are also discussed.

Experimental tensile tests were made using direct uniaxial and indirect Brazilian tests. Three 4-inch specimens were fabricated and tested in direct uniaxial tensile tests using Hydro-Stone TB. The results showed that the elastic tensile modulus of elasticity was within two percent of existing data for the compressive modulus of elasticity. The direct tests were not successful in determining the ultimate tensile strength, as failure occurred at the connections.

Twenty 4-inch diameter by 2-inch long specimens were fabricated and tested using the indirect Brazilian tensile test method. Hydro-Stone TB was also used as the analog material in the Brazilian indirect tests. The Brazilian tests were successful in determining the splitting tensile strength and the effect of porosity on the ultimate tensile strength of the Hydro-Stone TB specimens. Results

showed that the tensile strength of the specimens was approximately 10 percent of the compressive strength. New test data were obtained for 0 (solid), 6.2, 12.5 and 18.7 percent porosities. Photographs, figures and graphs are shown for the test setups and results.

Computer simulations of both direct and indirect tensile testing were made using Itasca's UDEC 2D, 3.1 computer program. The computer results were then compared with the experimental data. The results showed that the UDEC computer models can successfully predict the cracking patterns of the experimental test specimens.

Results of the experimental tensile tests were combined with existing compressive test data and the Mohr-Coulomb, Mohr-Coulomb in s-t Space, Griffith and Power Failure Criteria were then formulated from these test data. Also, the four criteria were used to show the effect of porosity on the failure strength of the analog rock material for porosities between 0 and 18.7 percent.

ACKNOWLEDGMENTS

I am grateful and would like to thank the many people who made this project possible and supported me. Rock mechanics is a complex subject and involves large volumes of data and mathematical analyses. In particular, I would like to thank the following:

Dr. Moses Karakouzian, Professor of Civil Engineering, chief advisor and committee chairperson, for his guidance and helpful discussions throughout the project.

Dr. Nadar Ghafoori, Dr. Samaan Ladkany and Dr. Samir Moujaes, Professors of Engineering, for giving advice throughout the project and serving on my graduate committee.

Dr. Douglas Rigby, Senior Researcher, who assisted in the fabrication of Hydro-Stone TB specimens, gave instruction on the UDEC computer program for analyses in rock mechanics, provided data on the properties on Nevada tuff rock and Hydro-Stone TB, and served on my graduate committee.

Dr. Brendan O'Toole, Professor of Engineering, who made available the mechanical testing facilities in the UNLV Mechanical Engineering laboratory, and provided instruction on how to operate the test equipment.

Dr. Harriet Barlow, Associate Dean, Graduate College, who conducted the UNLV writing seminars, and provided instruction on the writing of this dissertation.

Dr. Richard Goodman, Dr. Francois Heuze and Dr. Herbert Einstein, Professors, who gave instruction at the American Rock Mechanics Association course in Rock Mechanics at Alexandria, VA.

Elyson Liao, Stacey Nelson and Jagadeep Thorta, Teaching Assistants, who assisted in the fabrication and tests of experimental Hydro-Stone TB specimens.

Allen Sampson and Jon Becker, shop supervisors, who assisted in the fabrication of test equipment and Hydro-Stone TB test specimens.

TABLE OF CONTENTS

LIST OF TABLES

LIST OF FIGURES

CHAPTER 1

INTRODUCTION

1.1 General

Lithophysal Topopah Tuff rock is a porous igneous rock that was formed in western Nevada 12.8 million years ago by volcanic action, when approximately 1,000 km^3 of pyroclastic flow material was deposited (Marshak, 2006). The pyroclastic debris is what formed the tuff rock, which is in the area of the DOE repository. Lithophysal rocks comprise about 85 percent of the volumetric space at the repository (Rigby, 2004). Figure 1 is a photograph of a sample of Topopah Tuff rock.

Data on tuff rock that are required for developing failure criteria are tensile strengths, compressive strengths and porosities. Also of interest is the modulus of elasticity, which is required when strain measurements are converted to stress.

Figure 1 Photograph of Topopah Rock

DOE has no tensile test results for either direct tensile testing or indirect Brazilian tensile testing on representative-sized lithophysal tuff. The tensile failure criteria assumed in DOE's use of the UDEC program has not been validated. Validation of the UDEC results for simulating lithophysal tuff with an analog material in compression was verified by recent tests (Rigby 2007).

This present research project is organized to show the comparison of the simulated UDEC behavior of lithophysal analog rock in tension with the experimental results. With both the compressive and tensile test results, a failure criterion can be developed for lithophysal analog rock. It should be noted that this research is to validate the UDEC simulations for analog lithophysal rock, and not the actual lithophysal tuff.

1.2 Objectives

The objectives of this project are to:

1. Determine experimentally the tensile strengths of porous tuff rock with various porosities by using the analog material of Hydro-Stone TB,
2. Combine the new tensile test data with existing compressive test data,
3. Analyze the data using Itaca's UDEC computer program of block analyses and Microsoft's computer program EXCEL, and
4. Develop failure criteria for analog lithophysal rock that can be used for analyses of actual tuff rock.

1.3 Organization

This report is organized as follows:

Chapter 2 is a literature review of:

1. Tuff rock,
2. Tensile and compressive strengths of rock,
3. Tests on analog materials,
4. Numerical computer modeling, and
5. Rock failure criteria.

Chapter 3 is a description and discussion of experimental tensile tests.

Chapter 4 is a UDEC 2D computer analysis of tensile test models.

Chapter 5 is a discussion of failure criteria.

Chapter 6 is a summary of discussions, conclusions and recommendations.

The Appendixes show test results and data that are utilized in the text.

CHAPTER 2

LITERATURE REVIEW

2.1 Tuff Rock

Tuff rock is described as a pyroclastic volcanic deposit (Marshak 2006). The pyroclastic volcanic sediments are classified as:

1. Volcanic ash that has a grain size from 0.002 to 0.075 mm, and
2. Lapilli, which are fine rock fragments and crystals that have grain sizes from 2 mm to 64 mm (Goodman, 1993).

Tuff rocks have lithophysal cavities that vary in shape. Cavity shapes can be gash-like, ellipsoids or spheres. Most cavities have their long dimension in a near horizontal position. Some large cavities have irregular boundaries and are formed from a number of smaller cavities. Different minerals coat the interior surfaces of the cavities, as shown by the different shades of darkness on the cavity walls on Figure 1. Cubic specimens that were made from core samples had sizes of lithophysae on the surface that ranged from 0.1 to 5.0 cm. Porosity can range up to 30 percent by volume (Hudyma, Avar and Karakouzian, 2004).

The lithophysal tuffs at the DOE repository are designated as Tptpll and Tptpul for lower and upper levels, and have macro porosities from 10 to 30 percent (Chawla, 2007). The lower zone, Tptpll, has lithophysae from 1 cm to 180 cm in diameter, and the upper zone, Tptpul, has lithophysae from 1 cm to 30 cm in diameter (Avar and Hudyma, 2006). The walls of the lithophysal cavities are either smooth or jagged. The shapes of the cavities are either spherical or irregular.

Tuff has been described as a poorly interlocked and heavily broken rock mass with a mixture of angular and rounded rock pieces with poor fillings of angular fragments (Hoek and Brown, 1997). Bedded tuff can have a porosity of 40%, and welded tuff, which has been pressed together over a long period of time, can have a porosity of 14% (Goodman, 1989). Tuff has also been described as a fine grained polyminerallic igneous rock, such as rhyolite (Brady and Brown, 1993).

2.2 Tensile and Compressive Strength of Tuff Rock

Rock strength, for the purposes of engineering design, is related to the peak stress of the stress-strain curve. Nevada Test Site tuff has an unconfined compressive strength of 1.65 ksi and an indirect tensile strength of 10% of the compressive strength. Also, Nevada Test Site tuff has a modulus of elasticity/unconfined compressive strength ratio of 323 and a Poisson's ratio of 0.29 (Goodman, 1989).

Tensile strength of Topopah Spring Tuff can be obtained by:

1. Direct tensile testing by uniaxial tests, and
2. Indirect tensile testing by the Brazilian tests.

Test results from the direct uniaxial tests showed a tensile strength from 1.9 MPa to 11.5 MPa. Test results from the indirect tensile tests showed a tensile strength from 16.0 MPa to 26.3 MPa (Teufel and McNamee, 1990). The compressive strength of Nevada Tuff was found to be 11.3 MPa and the tensile strength was found to be 1.17 MPa. ASTM has specifications for the indirect

Brazilian tensile test (ASTM C496/C 496M, 2004). The ancient Greeks, 2500 years ago, used iron brackets underneath rock beams to increase the tensile strength of their rock structures (Rahn, 1996).

Pyroclastic rocks, such as tuffs, have a variety of strength, permeability and behaviors under conditions of exposure. Also, pyroclastic tuff rocks undergo rapid deterioration upon wetting and drying (Abramson, Lee, Sharma and Boyce, 2002).

Previous experimental studies of lithophysae-rich tuff rock showed a significant reduction in the elastic modulus with increasing porosity. Also, the test data was scattered and exhibited large variations in elastic modulus and strength (Avar, Hudyma and Karakouzian, 2003).

It is difficult to core cylindrical specimens of tuff rock, due to large cavities. Cubic specimens were made and tested (Hudyma, Avar and Karakouzian, 2004). Porosities ranged from 17 % to 49 %. Sizes of cubic specimens had average dimensions of 10 cm to 15 cm. There was a rapid decrease in compressive strength for increased porosity with a wide spread of data. The best-fit regression curve for compressive strength versus porosity had an R^2 value of 0.62.

Uniaxial compressive strength versus porosity for small cored rocks, less than 51 mm in size, showed very low strengths for porosities above 20 % (Rigby, 2004, Figure 6.3-1). Uniaxial compressive strengths ranged from about 330 MPa for 12 % porosity to about 5 MPa for 40 % porosity. These low

strengths are attributed to the tuff rocks containing large amounts of lithophysae and to poor recovery in the field from the drill holes.

2.3 Tests on Analog Materials

Experimental photo elastic tests showed stresses in a circular disk, that have equal and opposite forces applied to the disk, can be compared with the stress patterns that exist in a Brazilian test (Timoshenko and Goodier, 1970).

Experimental tests on plaster of Paris as an analog material to simulate the properties of tuff rock showed an exponential decrease in the elastic modulus for increasing porosity (Avar, Hudyma and Karakouzian, 2003). Tests on the tuff specimens showed a more linear decrease in the modulus. The analog testing showed that the elastic modulus is dependant on both porosity and cavity shape.

Tests on plaster of Paris were also made to assess the effect of macro porosity on both uniaxial compressive strength and failure modes of specimens that simulated porous tuff rock (Hudyma, Avar and Karakouzian, 2004). Tests showed that compressive strength decreased with increasing porosity. Failure modes consisted of spalling, axial splitting, shear failure, and web failure. Failure modes transited from spalling through web failure as porosity increased. Specimens were made using two parts of plaster and one part of water. Both cubic and cylindrical specimens were made as follows:

Fourteen cubic specimens were made with sides about 6” that contained porosities between 5% and 35% using Styrofoam spheres ranging from 1” to 4”. Twenty cylindrical specimens had diameters of 2” and lengths of 4”.

Ten specimens had Styrofoam inclusions to simulate porosity, and ten specimens had air injected into the plaster to create pores which were approximately elliptical in shape and at varying orientations.

Several solid specimens were tested to obtain a zero porosity compressive strength value. The porosity of each specimen was determined by weight and volume measurements. Uniaxial tests were made as follows:

Cubic specimens were made and tested at the Nevada Test Site, and cylindrical specimens were tested at the University of North Florida using a 50 kN test frame. Axial strain was measured with an electronic dial indicator. The strain rate was $5x10^{-4}$.

The four types of failure modes were identified for the cylindrical plaster specimens. They were:

1 Spalling, less than 5% porosity,

2 Axial splitting, from 5% to 10% porosity,

3 Shear failure, from 10% to 20 % porosity, and

4 Web failure, above 20% porosity.

For both spalling and axial splitting, fracture and failure occurred parallel to the maximum principal stress orientation (vertical). Shear failure occurred between the Styrofoam balls on an inclined plane. For the web failure, it is assumed that the webs between the Styrofoam balls crumble and deform plastically. This type of failure is similar to pore collapse failure that is often seen in highly porous sedimentary rocks such as chalk.

The failure modes of the cubic specimens did not show relationships between failure modes and porosity. It was concluded that the relationships between compressive strength and macro porosity can be established for both cubical and cylindrical plaster of Paris specimens (Hudyma, Avar and Karakouzian, 2004).

2.4 Numerical Computer Modeling

A numerical model using circular holes was made using the two dimensional plane strain finite difference, FLAC program (Avar, Hudyma and Karakouzian, 2003). Porosities between 5 and 40 percent were used, which is typical of the amount of lithophysal cavities observed in 10 tuff specimens that were tested. Results of the analyses of FLAC are shown for:

1. Elastic modulus versus porosity,
2. Poisson's ratio versus porosity,
3. Elastic moduli in both directions, and
4. Normalized elastic modulus versus porosity.

In this study, 10,000 cycles were required to cause a maximum axial deformation of 5 mm.

A list of qualified software supporting the lithophysal rock mass calculations was made (Rigby, 2004). Microsoft Excel 2000 was used to determine parameter statistics, data plots, and linear and exponential fits to data. Simulations of compression tests were made using PFC2D and UDEC. These results represent the best available, simulated, mechanical behavior of lithophysal rock. PFC2D lithophysal simulations were made from an actual

lithophysal Tpt photograph. The PFC and UDEC computer programs provide a method for simulating the mechanical behavior of lithophysal tuff rock that is loaded by it's own weight and external forces.

Six-inch cubical Hydro-Stone test specimens were analyzed using the Microsoft Excel 2003 program (Chawla, 2007). The study investigated the effect of porosity on the mechanical properties of cubes of analog lithophysal tuff, namely Hydro-Stone. The mechanical properties studied were compressive strength and elastic modulus.

A presentation was made to summarize the test programs made by Rigby and Chawla at UNLV (Karakouzian and Rigby, 2007). The numerical rock criterion for the Hoek-Brown criterion was shown. It was recommended that future research work should include:

1. Failure criterion for lithophysal rock, and
2. Tensile tests of an analog material of lithophysal tuff rock.

2.5 Rock Failure Criteria

There are five failure criteria that are considered acceptable in rock mechanics (Jumikis, 1983). The five criteria are:

1. Maximum tensile stress,
2. Tresca's maximum shear stress,
3. Coulomb's shear strength line,
4. Mohr, and
5. Griffith's brittle tension.

The maximum tensile stress criterion assumes the rock fails by brittle fracture in tension when the applied least principal stress in the rock is equal to the uniaxial tensile strength.

Tresca's criterion assumes the rock fails when the maximum shear stress is equal to the shear strength of the material, which is at the apex of Mohr's circle.

Coulomb's criterion, which is known as Coulomb's classical law, states that the shear stress of the rock varies with the normal stress, friction angle and the cohesion, which forms a rupture line. When this rupture line is exceeded, failure in the rock occurs. Coulomb's criterion is a straight line.

Mohr's criterion postulates that the rock will fail above the rupture line, the same as Coulomb's criterion. However, Mohr's line may be curved, which is formed from the experimental triaxial tests on the rock. Also, Mohr's criterion says that failure can occur when the largest principal stress has reached a limiting tensile strength of the material (Obert and Duvall, 1967).

Griffith's criterion of tensile failure assumes the existence of thin, flat narrow, elliptical micro cracks in the rock, and that stress concentrations exist at the ends of these cracks. As load is applied to the rock, the cracks become macros is size and ultimately cause macroscopic tensile failure in the rock. Griffith's criterion is an explanation of the mechanism that occurs in the maximum tensile criteria. In 1924 Griffith expanded on his theory, which incorporated a parabolic equation.

Another criterion is a power curve determined from the Mohr's circles of the tensile strengths and compressive strengths. A power curve is determined from a series of tangent points on the Mohr's circles of a plot of the shear stresses versus normal stresses, as shown by Goodman, Figure 3.19 (Goodman, 1989).

A series of ten equations are shown in "Empirical Rock Failure Criteria," (Sheorey, 1997), that are in terms of σ_1 and σ_3, which are stresses determined from the compressive triaxial testing of rock. Sheorey states that a failure criterion should exist in both tensile and compressive regions. This research project discusses failure criteria that are suitable for both the tensile and compressive capacity of rock.

CHAPTER 3

TESTS ON ANALOG MATERIAL

3.1 General

Recent tests using Hydro-Stone TB, as an analog material for tuff, were successfully made to determine the ultimate compressive strength and elastic modulus of 6-inch cubical specimens with various porosities (Rigby, 2007). For this reason, Hydro-Stone TB was used in this research project. Hydro-Stone TB is a trade name of Gypsum Cement. It is a mixture of plaster of Paris, Portland cement, sand and water.

3.2 4-inch Dog Bone Direct Tensile Tests

The 4-inch dog bone specimens are 4-inch cubical specimens with enlarged end sections for attachment to a test machine. Figure 2 shows a photograph of the fabricated Dog Bone 1.

Figure 2 Hydro-Stone TB Specimen Dog Bone 1

The central section is a 4-inch cube, and each end is extended eight inches in length and widened to eight inches in width. A 2-inch standard pipe was used at each end as a connecting member for the test machine. Figure 3 shows the pipes in the wooden mold before the Hydro-Stone TB pour.

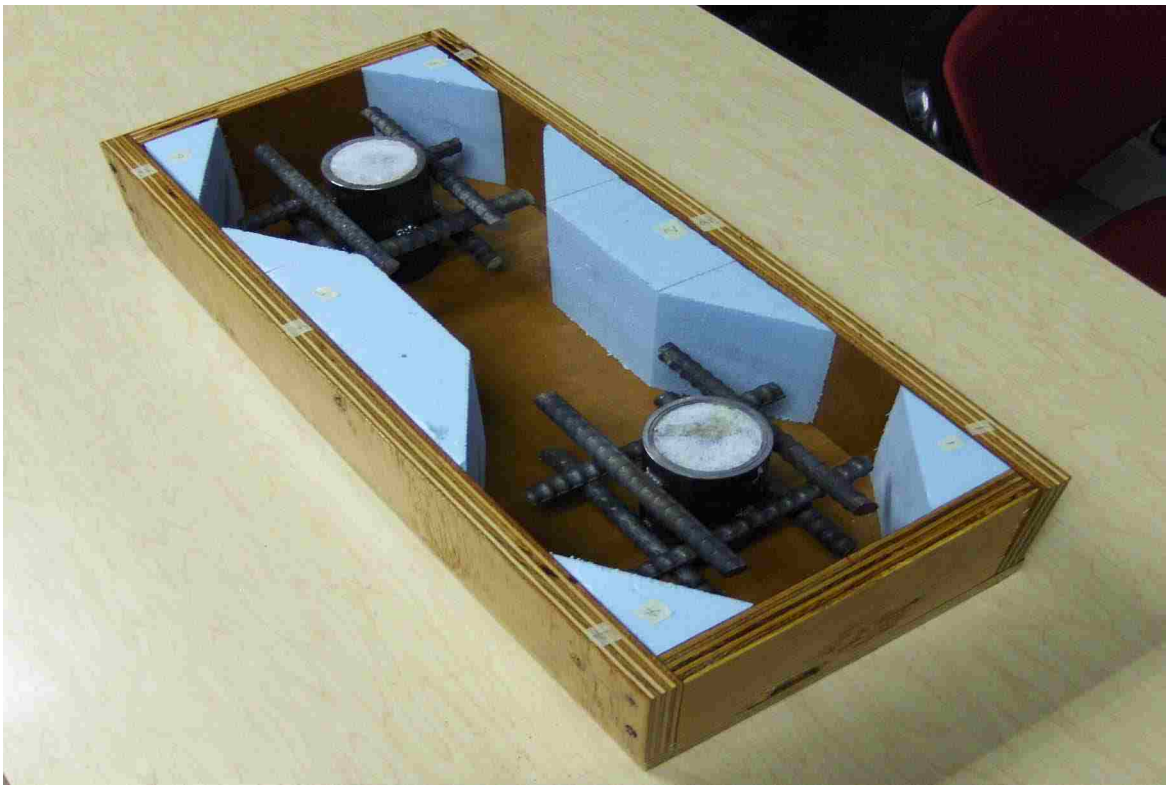

Figure 3 Wooden Mold, Pipe Inserts, Reinforcing Bars and Styrofoam Forms

The wooden mold was fabricated with 7/8-inch plywood and 1/4-inch wood screws. 6-inch long, #4 steel reinforcing bars were attached to the pipes with Super Glue Gel. Styrofoam blocks were cut to form the desired shape of the specimen.

The Hydro-Stone TB, which is a powdered mixture of 90 percent plaster of Paris, 5 percent Portland cement and 5 percent sand, was mixed with water. The weight of the water was 1/3 of the weight of the Hydro-Stone TB. The liquid mix was then poured into the mold. After one hour the Hydro-Stone TB reached a compressive strength of about 4,000 psi and the top surface was smoothed using files. Figure 4 shows Dog Bone 1 in the mold after being filed smooth.

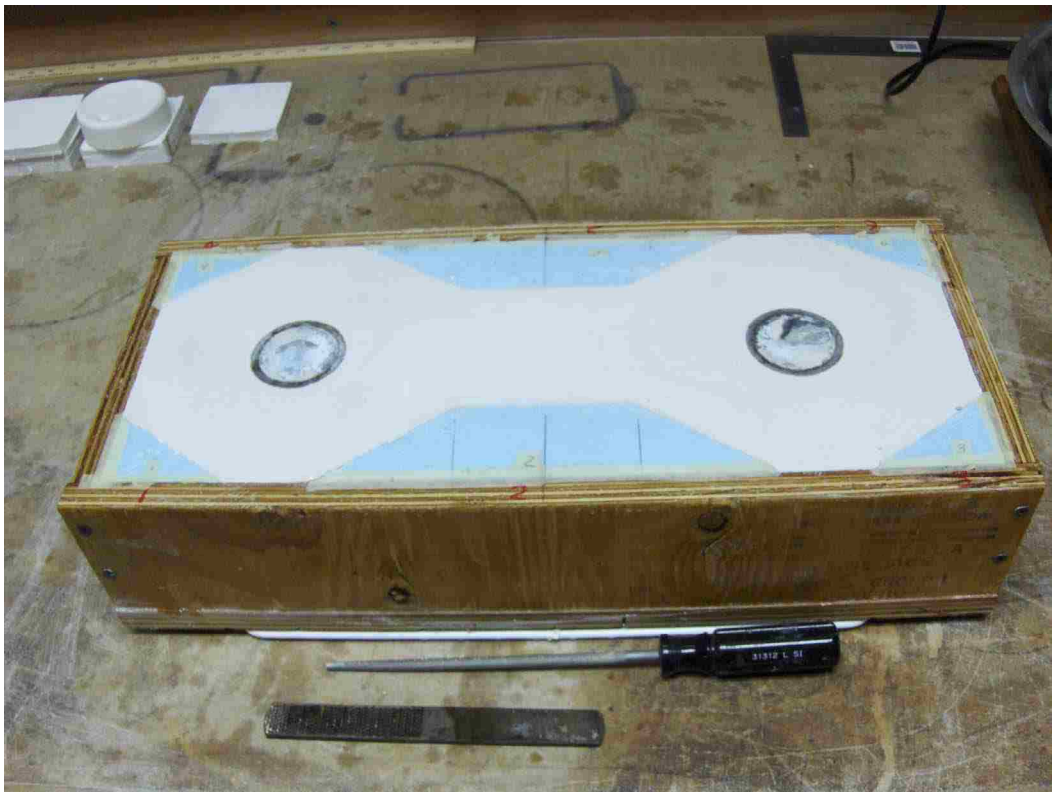

Figure 4 Dog Bone 1 after Hydro-Stone TB Pour

After one day the wooden mold was removed and the specimen was allowed to cure for 28 days. Four SR-4 strain gages and four Linear Variable

Differential Transformer (LVDT) displacement gages were attached to the specimen. These measurements were made so that a value of the elastic tensile modulus could be determined. End attachments were fabricated to attach the specimen to the Minnesota testing machine (MTS), which is located in the UNLV Engineering laboratory. Figure 5 shows the test set up in the MTS machine.

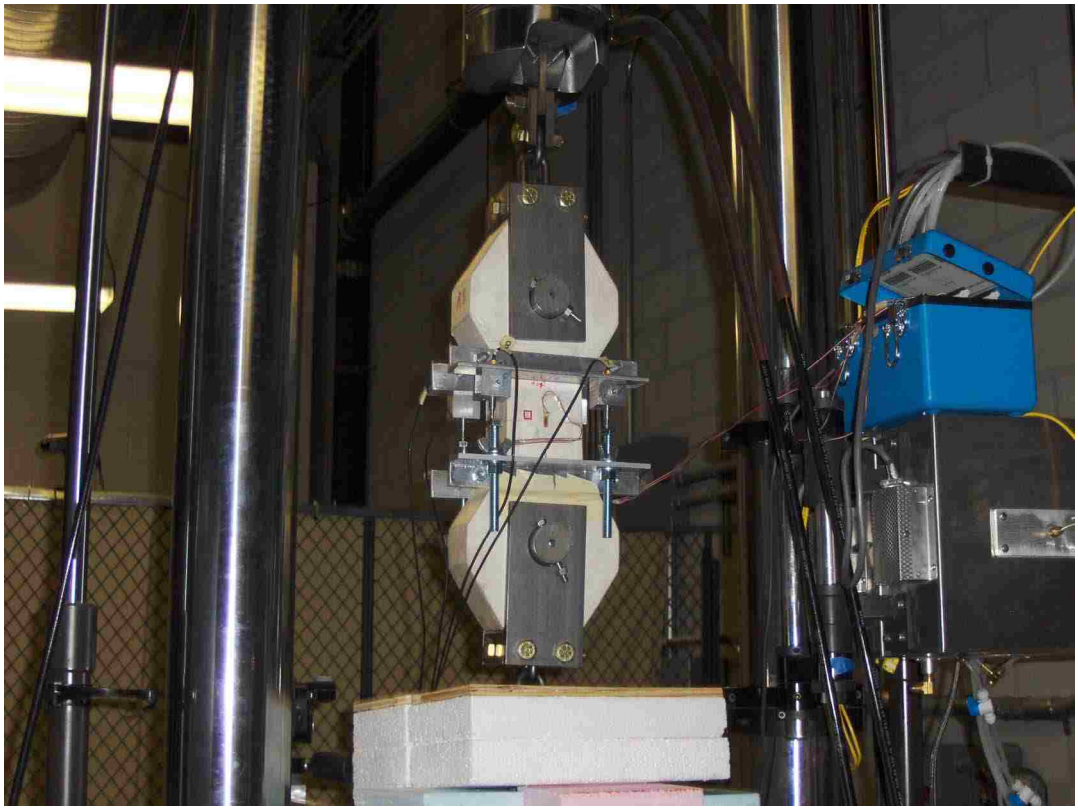

Figure 5 Test Set Up in MTS Machine for Dog Bone 1

As the tensile load was applied to Dog Bone 1, measurements from the SR-4 and LVDT gages were recorded. Stresses were determined from the recorded load readings as the quotient of the load and cross-sectional area of the

specimen. Strains were determined from the recorded LVDT readings as the quotient of the displacement and the distance between the two fixed points on the specimen. Figure 6 shows the results of these stress-strain values.

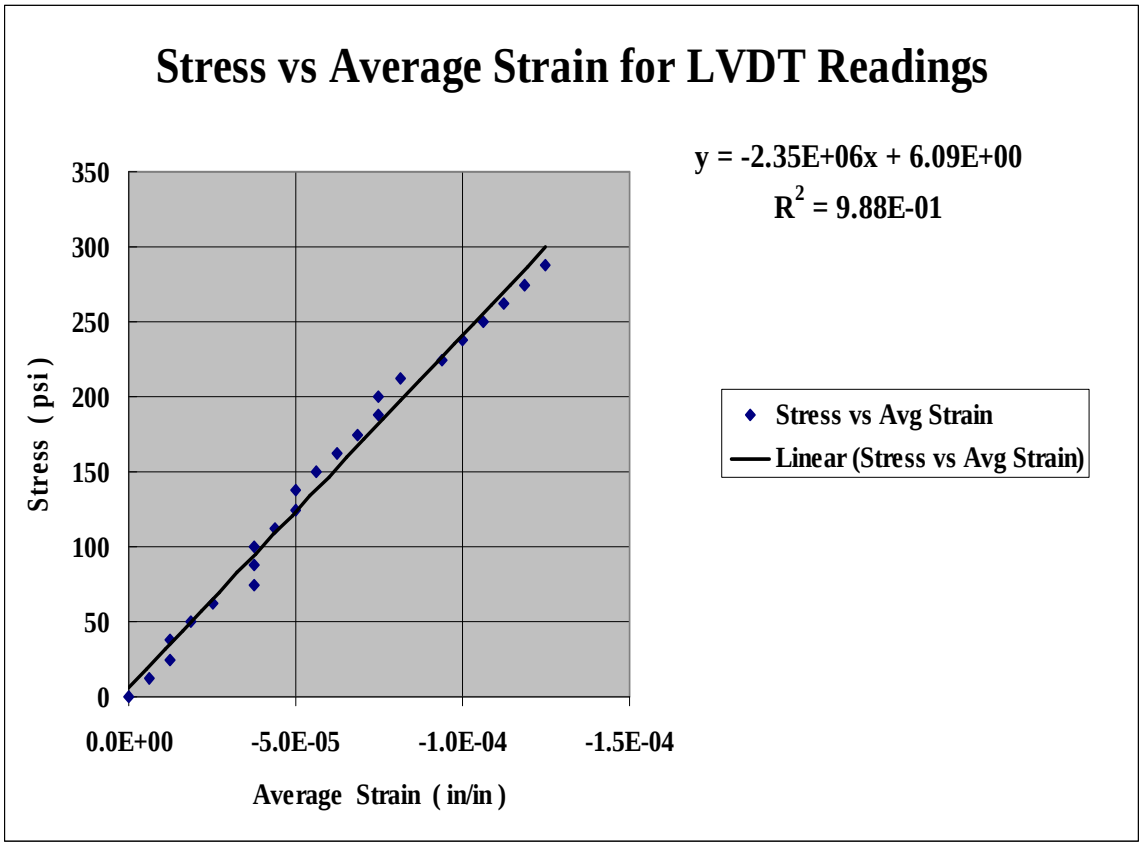

Figure 6 Stress versus Strain for Dog Bone 1

Data was plotted in the Microsoft Excel program using an average of the four LVDT gages, and a linear trendline was made for the average of points. The slope of the trendline is the elastic modulus, 2.35 x 10^6 psi (16.2 GPa).

As the load was increased, the Hydro-Stone TB in Dog Bone 1 eventually yielded in tension. The ultimate failure load in Dog Bone 1 was 5957 lbs (26.5 kN). The specimen failed near the connection at the ends of the longitudinal reinforcing bars. The test was considered a failure for determining the tensile strength of the Hydro-Stone TB 4-inch by 4-inch specimen. Figure 7 shows the parts of Dog Bone 1 after testing. Also, strain recordings from the SR-4 were lost due to a broken connection that occurred when the specimen failed.

Figure 7 Dog Bone 1 after Tensile Test

Failure was not expected at this location, as the area of Hydro-Stone TB was approximately 50 percent greater than the area at the narrow mid section. Also, a UDEC stress analysis showed lesser stresses at the failed location, compared with stresses at the mid section (see Chapter 4). It is possible that failure was caused by stress concentrations at the ends of the steel reinforcing rods. Although the test was a failure for determining the tensile strength, the test was considered a success for determining the elastic modulus.

Dog Bone 2 was designed and fabricated with only lateral reinforcing bars to help distribute the load from the test machine to the Hydro-Stone TB. Figure 8 shows the mold, pipes, welds and reinforcing bars for Dog Bone 2.

Figure 8 Mold for Dog Bone 2 with Pipes and Reinforcing Bars

The reinforcing bars for Dog Bone 2 were #3 bars and 4-inches long. Also, the steel bars were welded to the steel pipes. The Hydro-Stone TB was mixed and poured into the mold. After one day the mold was removed and Dog Bone 2 was allowed to cure for 28 days. Dog Bone 2 was then tested in the MTS machine, the same as Dog Bone 1 was tested. Dog Bone 2 failed at the minimum cross sectional area along the pipe connection at a load of 2809 lbs (12.5 kN). Figure 9 shows Dog Bone 2 in the MTS machine after failure.

Figure 9 Dog Bone 2 in MTS Testing Machine after Failure

Possible reasons for failure of Dog Bone 2 were stress concentrations around the steel pipe and lack of reinforcing bars in the longitudinal direction.

Dog Bone 3 was designed to have a 7.52 percent porosity using 2 wooden dowels that had a diameter of 7/8 inch. The 2 dowels decreased the area in the narrow 4-inch section by 44 percent. The area of Hydro-StoneTB at the steel pipe connection was 2.5 times more that the area at the 2 dowels, which was expected to be enough to initiate tensile failure in the narrow, 4-inch section. Figure 10 shows the mold for Dog Bone 3 with the steel pipes, steel reinforcing bars and wooden dowels in place before the Hydro-Stone TB pour.

Figure 10 Mold for Dog Bone 3 with Pipes, Bars and Porosity Dowels

The Hydro-Stone TB was mixed and poured into the mold. On the first day after the pour, a crack formed in the Hydro-Stone TB at the location of the

wooden porosity dowels. A possible explanation of the formation of this crack was that when the specimen cooled after the heat of hydration dissipated, the specimen started to shrink and tensile stresses were introduced into the specimen. These tensile stresses were greatest at the location of least area in the specimen, which was at the porosity dowels. Figure 11 shows the crack in Dog Bone 3.

Figure 11 Crack in Dog Bone 3

As the mold was being removed, the crack was seen to be completely through the specimen, as is shown in Figure 12.

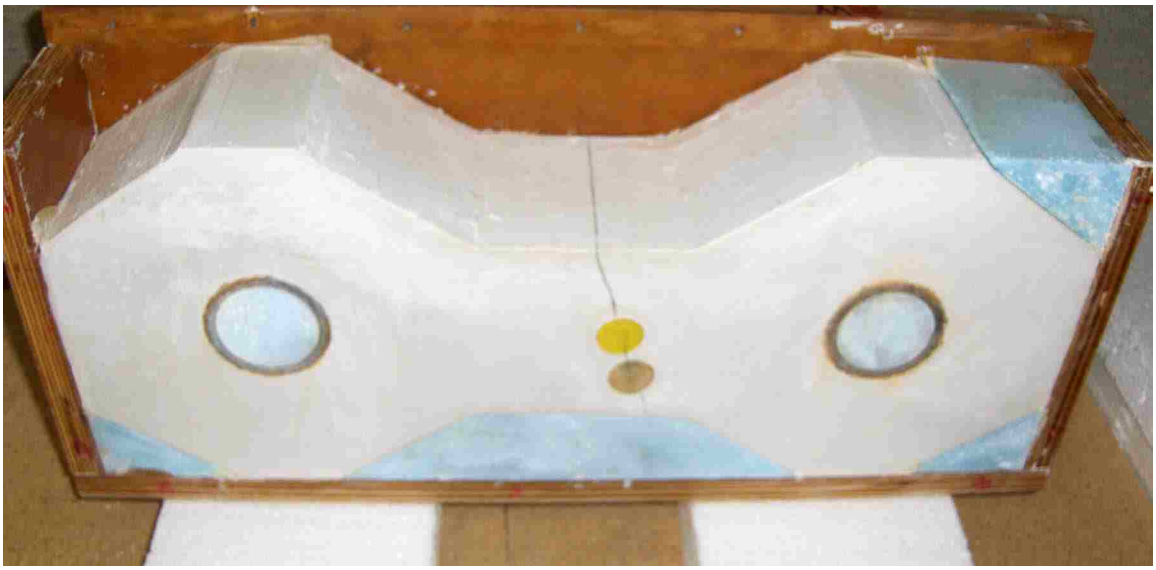

Figure 12 Mold Removal of Dog Bone 3 Showing Crack

Dog Bone 3 was considered a failure.

Dog Bone 4 was designed and poured similar to Dog Bone 3, except that the mold was removed one hour after the pour. Also, eight #3 steel reinforcing bars, 4-inches long, were welded to the steel pipe connectors. The bars were also welded to each other at their intersections near their ends. The ends of the bars were also tapered to reduce stress concentrations. The two 7/8-inch diameter wooden dowels were placed further apart, as compared with Dog Bone 3. The wooden dowels were painted with two coats of polyurethane to prevent moisture from penetrating into the wood. Also, the wooden dowels were coated with Vaseline grease before the pour, and the inside bottom and sides of the mold were sprayed with oil to facilitate removal of the dowels and mold. Figure 13 shows the mold for Dog Bone 4.

Figure 13 Mold for Dog Bone 4 with Pipes, Bars and Porosity Dowels

The mold for Dog Bone 4 was successfully removed one hour after the pour without any cracks forming in the Hydro-Stone TB. Figure 14 shows Dog Bone 4 after the mold removal.

Figure 14 Dog Bone 4 after Mold Removal

Four days after the pour, when the estimated compressive strength of the Hydro-Stone TB was over 5,000 psi (34.5 MPa), the wooden dowels were tapped with a steel rod and hammer for removal. The Hydro-Stone TB cracked during the tapping. Figure 15 shows the crack that formed.

Figure 15 Crack in Dog Bone 4

Dog Bone 4 was also considered a failure.

Dog Bone 5 was designed similar to Dog Bone 4 except that the wooden dowels were replaced with aluminum rods that could be twisted for removal. The aluminum rods also had a smoother surface, which aids in their removal with no damage to the Hydro-Stone TB. The steel reinforcing bars were 4-inches long, which was 2-inches shorter than the bars of Dog Bone 1. Also, the bars were tapered at the ends to reduce any stress concentrations that might develop. With the shorter tapered bars, voids in the 4-inch section, and 2.5 times more area of Hydro-Stone TB at the connections, failure in tension was expected to occur at the void part of the 4-inch section of the specimen.

A preliminary test was made on two aluminum rods to test their removal capabilities from the Hydro-Stone TB. The two rods were positioned in a plastic

Figure 16 Aluminum Rod Removal Test

cup and Hydro-Stone TB was poured into the cup. One rod had wax paper wrapped around it, and the other rod had Vaseline grease spread over it. The specimen was removed from the plastic cup one hour after the Hydro-Stone TB was poured. Figure 16 shows the Hydro-Stone TB specimen and rods. The rods were then twisted with a wrench and successfully removed without cracking the Hydro-Stone TB.

A mold was then prepared for Dog Bone 5 using aluminum rods instead of wooden rods. Diameters of the aluminum rods were 0.870 inches. The rods were removed one hour after the pour without cracking the Hydro-Stone TB.

Figure 17 shows Dog Bone 5 after the removal of the rods and wooden mold.

Figure 17 Dog Bone 5 after Aluminum Rods and Mold Removals

Dog Bone 5 was cured for 28 days and then placed into the MTS testing machine. The specimen failed in tension at the ends of the reinforcing bars at a load of 4193 lbs (18.7 kN). The crack was similar to the crack in Dog Bone 1.

Figure 18 shows the crack in Dog Bone 5 after failure.

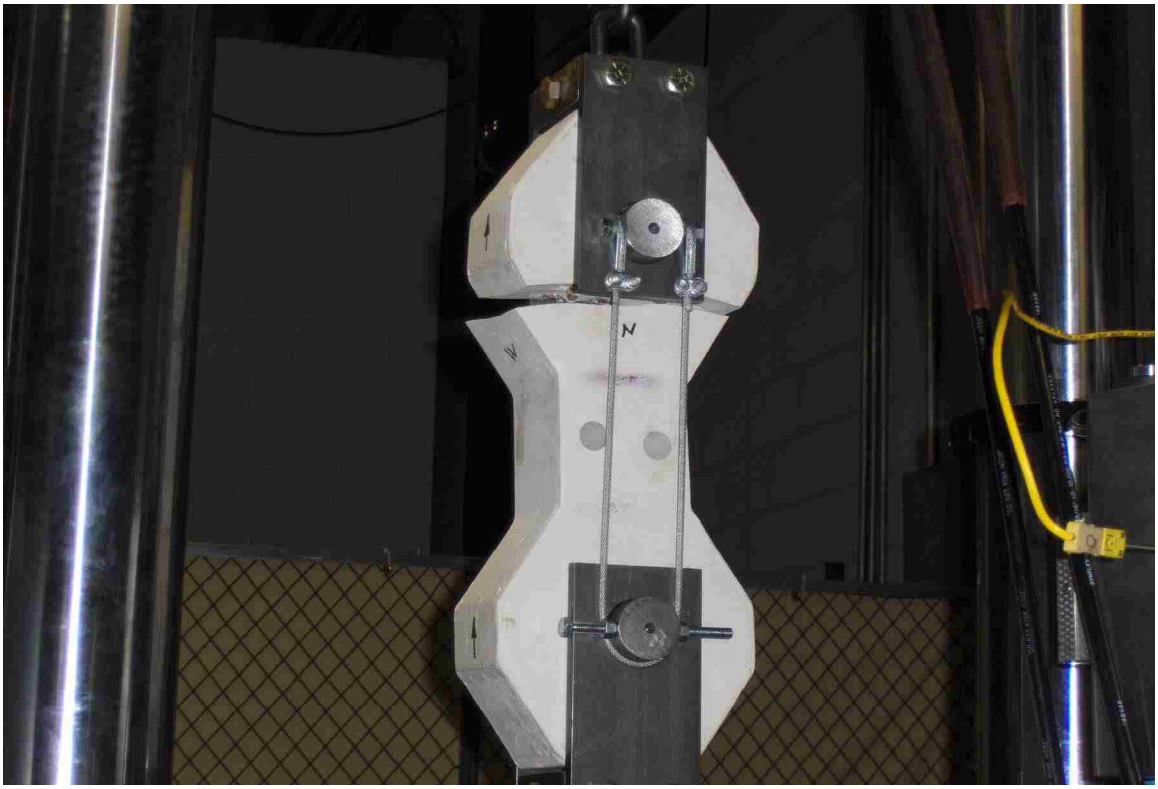

Figure 18 Dog Bone 5 in MTS Testing Machine after Failure

At a meeting with Dr. Karakouzian, it was decided to abandon the dog bone approach of testing. Plans were made to test specimens of 6-inch rectangular direct tensile tests. Also, plans were made to test 4-inch diameter Brazilian indirect tensile specimens.

3.3 6-inch Rectangular Direct Tensile Tests

Plans were made to make wooden molds to cast 6” x 6” x 2” Hydro-Stone TB specimens of various porosities and connect them to steel tee sections that could be attached to the UNLV testing MTS machine. A cost estimate was made by a

local steel fabricating company and the cost of fabricating two test set ups was $1,100.00. Also, a UDEC stress analysis showed high stresses at the corners of the models (see Chapter 4). Another meeting was held with Dr. Karakouzian and the decision was made to only proceed with the Brazilian indirect tests.

3.4 4-inch Brazilian Indirect Tensile Tests

3.4.1 General

A series of twenty Brazilian indirect tensile tests were planned and tested in the UNLV Tinus-Olsen testing machine. Both solid and voided specimens were tested. Specimen dimensions and test data are shown in Appendixes II and III. Table 1 summarizes the number, size, shape and percent porosities of the specimens. The material of the specimens was Hydro-Stone TB.

Table 1 Number, Size, Shape and Porosity of Brazilian Test Specimens

Number of Specimens for Brazilian Tests					
Geometry	Percent of Porosity				
	0	6.18	6.25	12.5	18.75
Solid (No Voids)	4				
Small Circular Holes		8			
Large Circular Holes			4	2	2
Total Number of Specimens = 20					

The diameter of the small circular holes was 45/64 inch (0.7031”) and the diameter of the large circular holes was one inch (1.0000”). Four specimens were weighed for 29 days to determine weight loss, see Appendix I.

3.4.2 Solid Specimens

Figure 19 shows the test set up and testing in the Tinus-Olsen test machine for the specimen, Solid_3. Also shown in Figure 19 are the four solid specimens, Solid_1, Solid_2, Solid_3 and Solid_4 after testing.

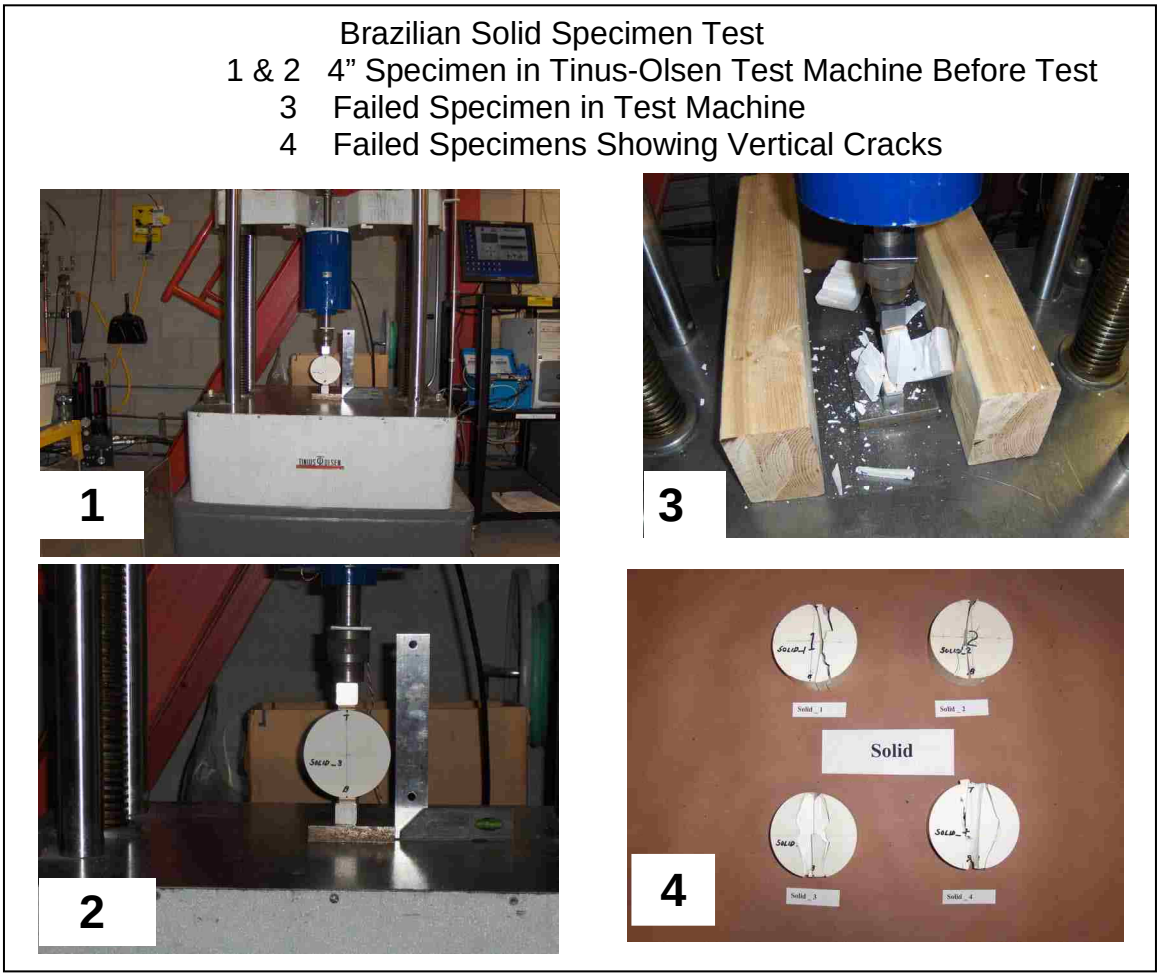

Figure 19 Test in Tinus-Olsen Machine for Solid Specimens

Figure 20 shows an expanded view of the four solid specimens after testing.

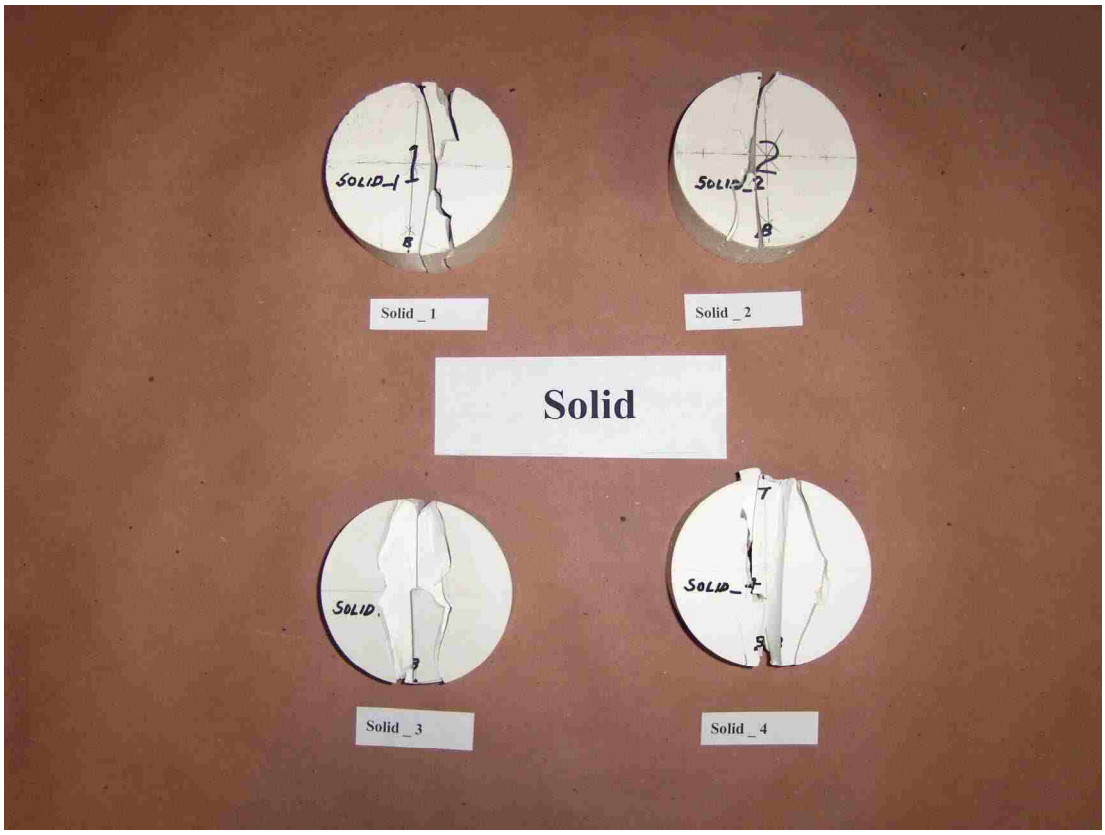

Figure 20 Solid Specimens after Testing

Initially, 2 solid specimens and 6 voided specimens with 1-inch diameter holes were tested. These tests were considered a success and 12 additional specimens were fabricated and tested. 2 of the additional specimens were solid, 2 were voided specimens with 1-inch diameter holes and 8 were voided specimens with 45/64-inch (0.7031") holes.

3.4.3 6.18 and 6.25 Percent Specimens

Figure 21 shows the two small hole specimens with 6.18 percent voids after testing. Diameter of the small holes is 0.7031 inches.

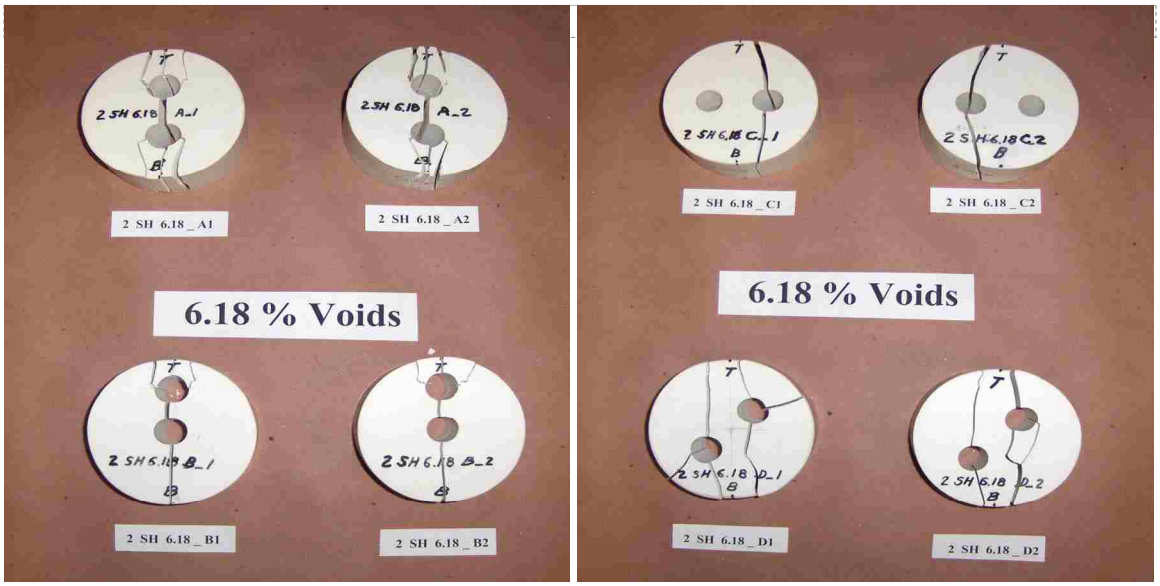

Figure 21 Small Hole 6.18 % Voided Specimens after Testing

Failure loads are shown in Table 5 and locations of the holes are shown in Table 9.

Most of the cracks in the test specimens formed at the same locations that were shown to be locations of failure in the UDEC analyses. Refer to Chapter 4 for the UDEC analyses and photographs.

Figure 22 shows the one large hole specimens with 6.25 percent voids after testing. Diameter of the large holes is 1.0000 inches.

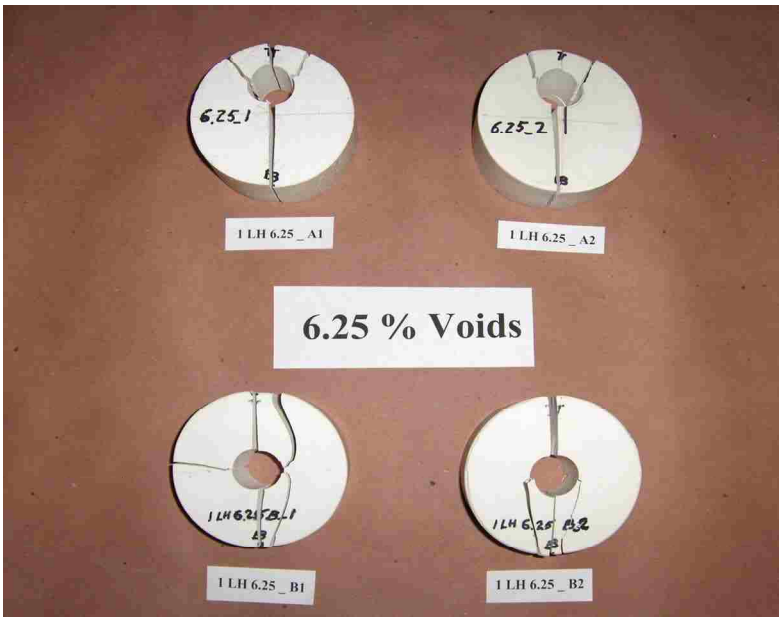

Figure 22 Large Hole 6.25 % Voided Specimens after Testing

3.4.4 12.50 and 18.75 Percent Specimens.

Figure 23 shows the two and three large hole specimens after testing.

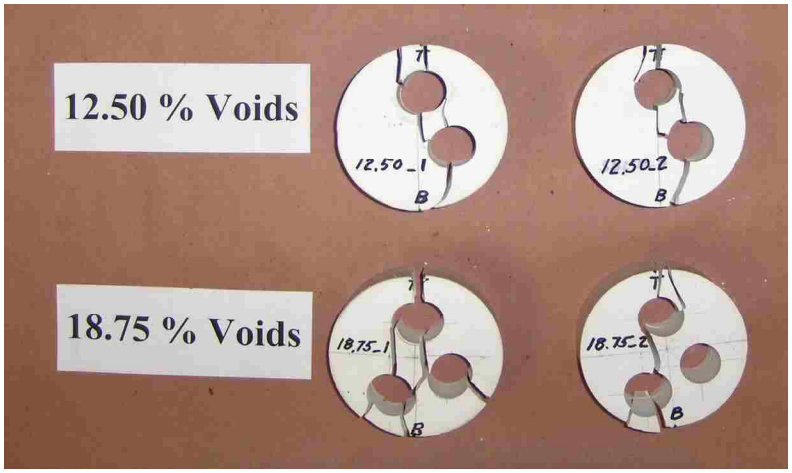

Figure 23 Large Hole 12.50% and 18.75% Voided Specimens after Testing

3.4.5 Test Results

Figure 24 shows the results of the Ultimate Tensile Strengths versus porosities for the 20 test specimens, as determined in Appendix II.

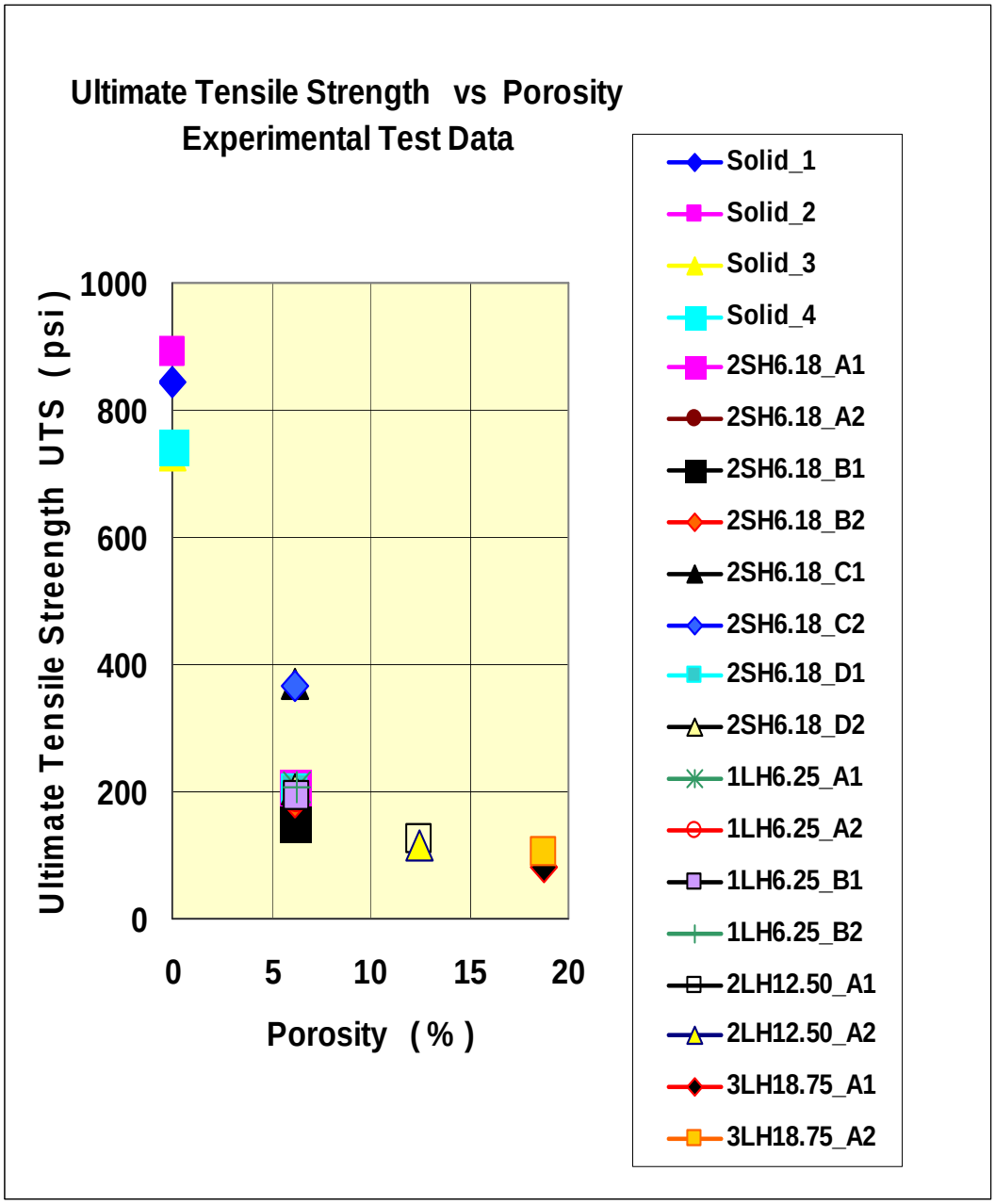

Figure 24 Ultimate Tensile Strength versus Porosity

An average of the Ultimate Tensile Strengths at each of the porosities of 0, 6.2, 12.5 and 18.7 percent was determined. Each of these averages was plotted as a function of porosity, as shown in Figure 25. The trendline for a power curve is also shown for the porosities between 6.2 and 18.7 percent.

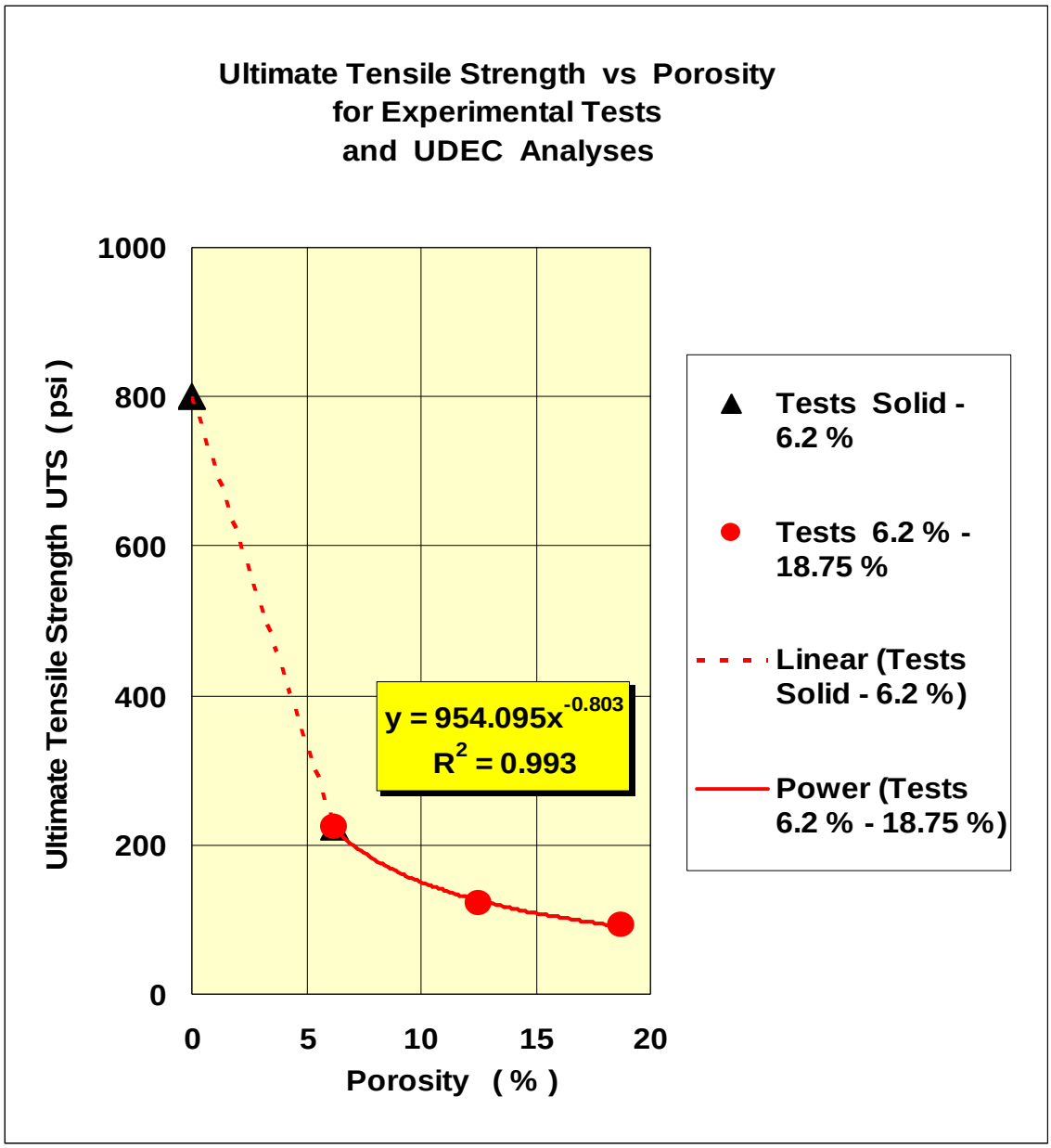

Figure 25 Averages of Ultimate Tensile Strengths versus Porosity

CHAPTER 4

COMPUTER SIMULATIONS

4.1 4-inch Dog Bone Model

Itasca's UDEC 3.1 program (Itasca, 2000) is used to analyze Dog Bone 1. Two types of model analyses are used in this project: namely, the elastic model and the Mohr-Coulomb model. The elastic model makes an analysis based on a linear stress-strain relationship.

Input into the program consists of the density, bulk modulus and shear modulus. These input values and equations for the bulk and shear modulus are described and shown in Appendix IV.

The Mohr-Coulomb model utilizes the plasticity of the material and requires the additional properties of the friction angle, cohesion, tensile strength, joint normal stiffness and joint shear stiffness. These properties are described in Appendix IV. The Mohr-Coulomb equation for Hydro-Stone TB is shown on Figure 50 of Chapter 5. In the case of a tensile failure, the UDEC 2D program shows failure, when the tensile stress in the model reaches the tensile strength of the material, as shown on Figure 30.

UDEC 2D is a two-dimensional, finite-difference program. The rock is simulated in the computer as a model that is subdivided into a mesh of finite-difference elements. The basic formulation of UDEC uses a two-dimensional plane-strain state, which is one of the inaccuracies when applied to a test specimen, which has a finite length, since the plane strain assumes an infinite length. If a long prismatical body is loaded perpendicular to the longitudinal

elements and are constant along the length, it can be assumed that all cross sections act in the same manner, as described by Timoshenko on page 15 and shown on Figures 8-10 (Timoshenko and Goodier, 1970). Results of a UDEC 2D elastic analysis of the vertical stresses in Dog Bone 1, which is loaded top and bottom with a uniform load of 1000 psi, are shown in Figure 26.

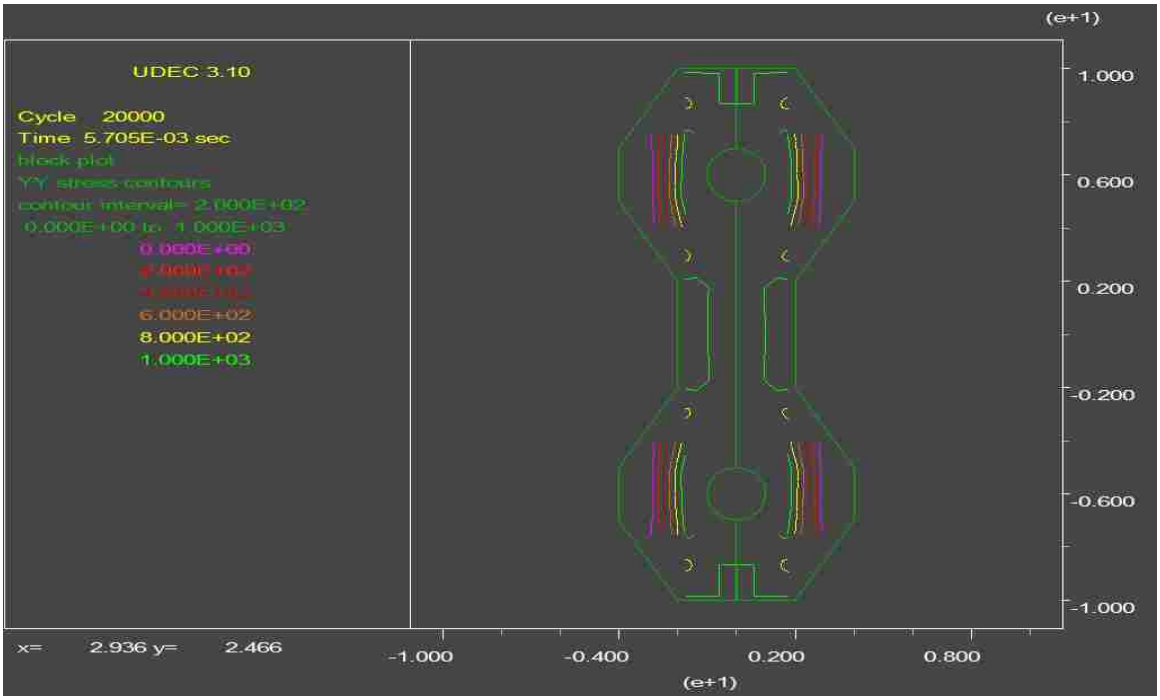

Figure 26 Dog Bone 1 Stresses in the Vertical Direction

A load of 1,000 psi was applied to the top and bottom of the model. Figure 26 shows the stress in the narrow 4-inch section of the model is 1,000 psi. The stresses at the opening are 1,000 psi or less. It was expected that the reinforcing bars would reduce the stresses around the opening, but this was not the case, and the Dog Bone specimens failed by the connections and at the ends of the reinforcing bars. Input data for Dog Bone 1 is shown in Appendix IV.

4.2 6-inch x 6-inch Model

UDEC was also used to make an elastic analysis of the stresses in a square, 6-inch by 6-inch, model that was loaded in tension. Results for the analysis of the vertical stresses in the UDEC computer model are shown in Figure 27.

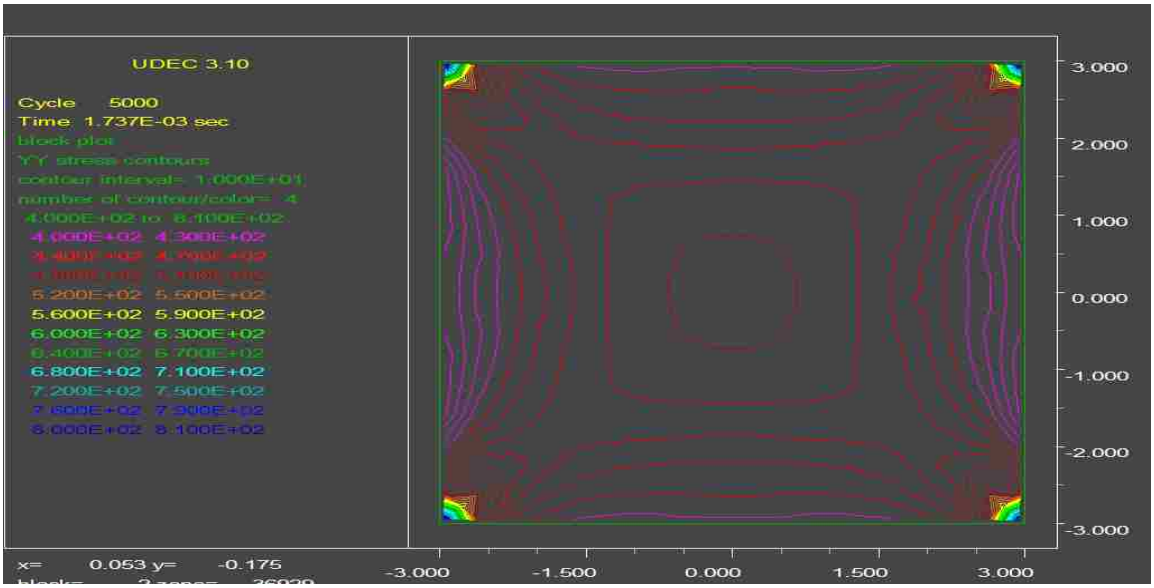

Figure 27 6-inch by 6-inch Model Stresses in the Vertical Direction

The model was loaded in tension using a uniform velocity displacement along the top and bottom surfaces. Figure 27 shows that a tensile stress of 810 psi will exist at the outer corners of the top and bottom surfaces, while a stress of 430 psi will exist in the central portions of the top and bottom surfaces. This stress distribution shows that failure would first be initiated at the outer corners.

4.3 4-inch Brazilian Models

4.3.1 Solid Specimens

UDEC was used to make failure analyses of 4-inch Brazilian test models. Figure 28 shows the results of the UDEC model for the Solid_3 specimen.

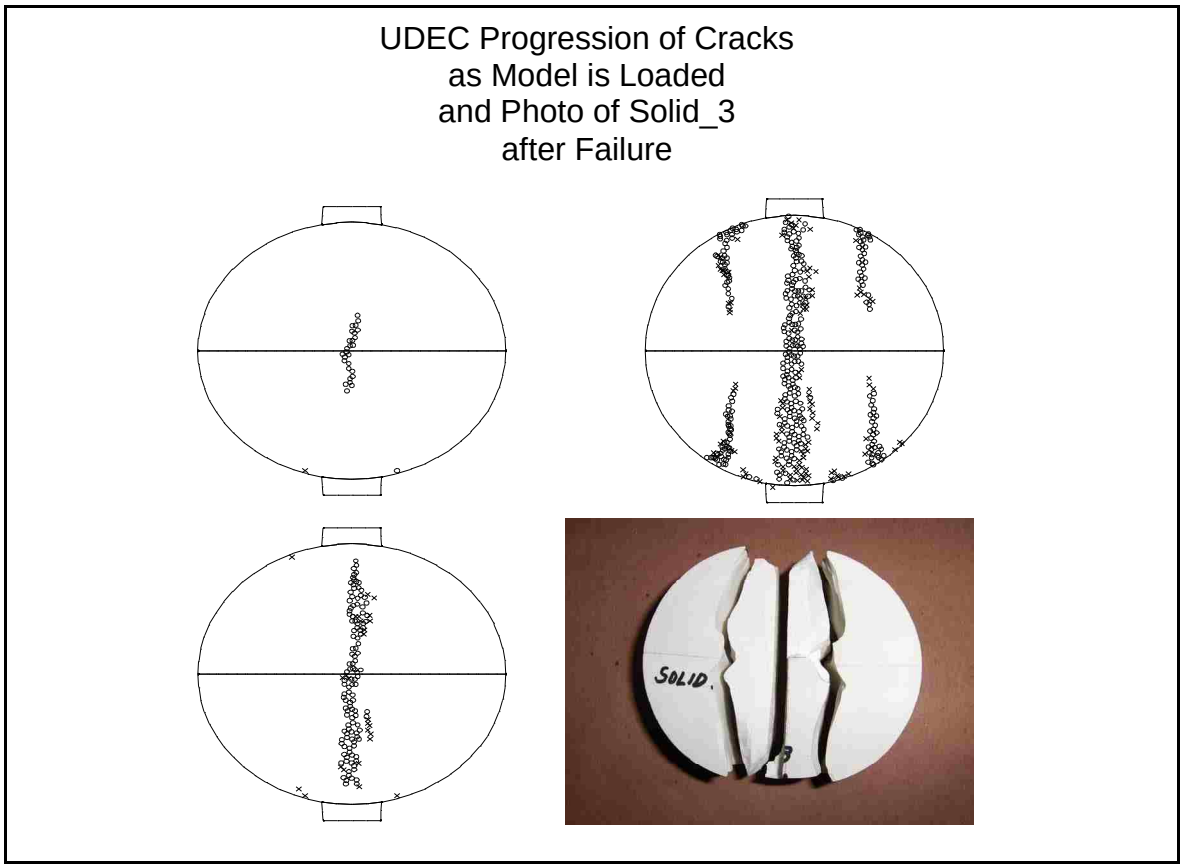

Figure 28 UDEC Solid Models and Test Specimen Solid_3

The cracks first formed at the center. As the load increased, more cracks formed. The photograph of Solid_3 shows that the failed locations on the test specimen matched closely the cracks on the UDEC analysis. Mesh size in the UDEC programs was 0.20 inches, as shown in Appendix V.

Figure 29 shows the horizontal stresses at the initiation of failure. The maximum horizontal stress at the center of the model is 800 psi, which was the calibrated value of jten for the input value of the maximum allowable tensile stress in the Mohr-Coulomb failure criteria that is used by UDEC.

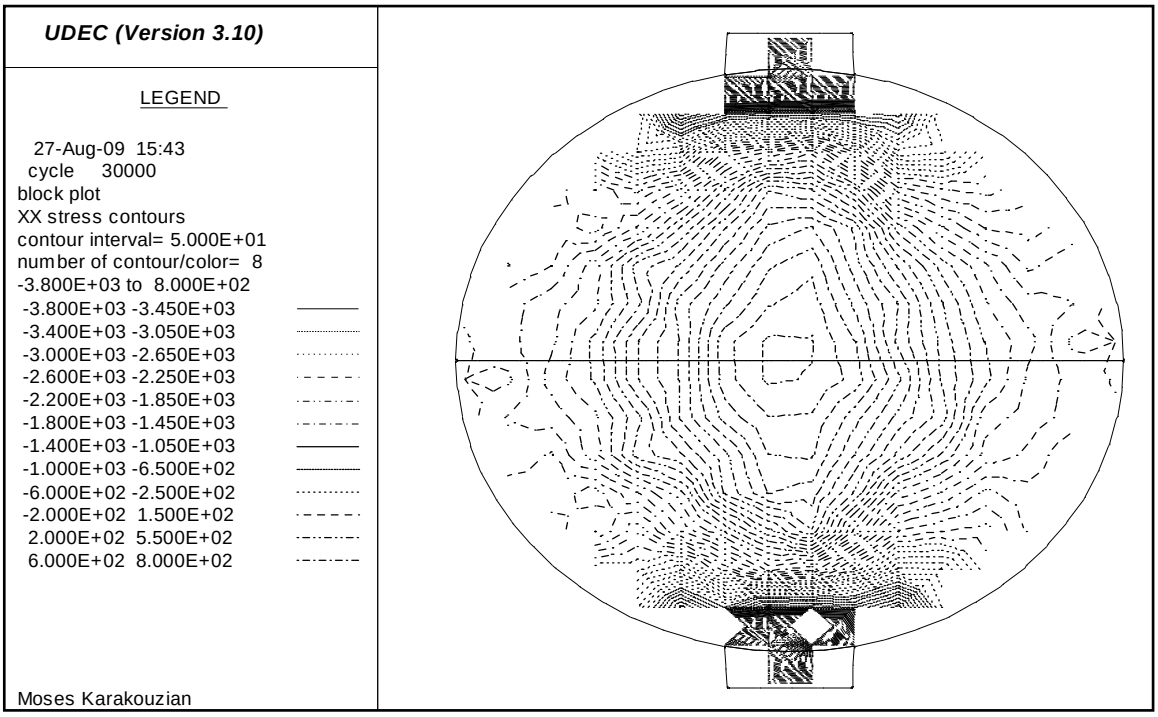

Figure 29 Horizontal Stresses in Solid Model at Failure

Data inputs for the Brazilian UDEC models are shown in Appendix V.

Figure 30 shows the stress versus displacement curve for the UDEC solid model as the load is increased from zero to failure. Stresses are for the center location (0, 0) and displacements are offset to show the stress at the point of failure (horizontal displacements at the center location are zero). The UDEC Mohr-Coulomb equations for failure are shown in Appendix VI

Figure 30 also shows that the horizontal stress at failure is 800 psi, which was the calibrated input value of the tensile strength of the Hydro-Stone TB.

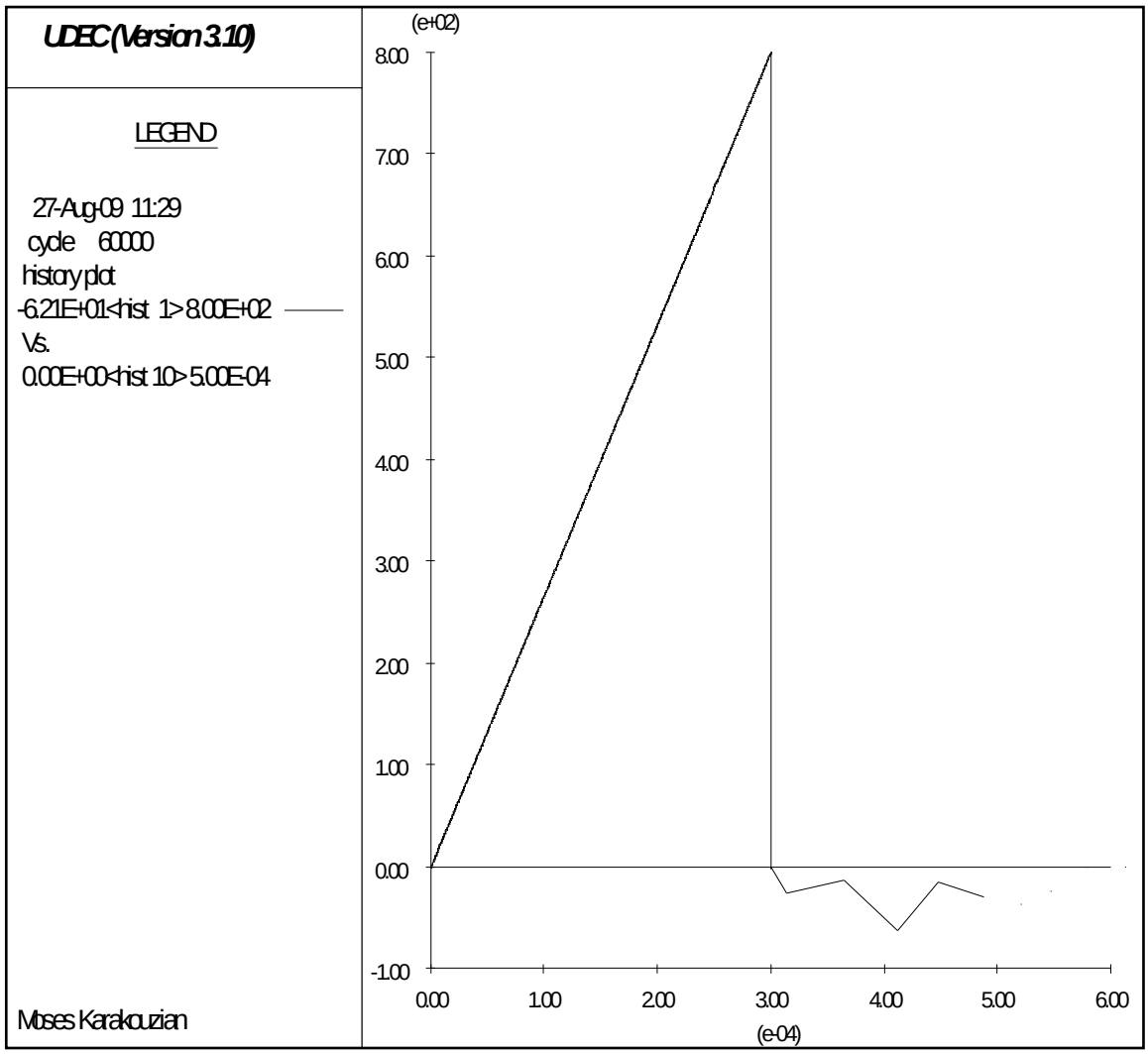

Figure 30 Horizontal UDEC Stress versus Displacement for Solid Model

Figure 31 shows the horizontal tensile stresses along the central horizontal axis of the model. The maximum tensile stress was 800 psi at the center and zero at the far sides. Figure 32 shows the deflected shape of the solid model that is magnified by a factor of 50.

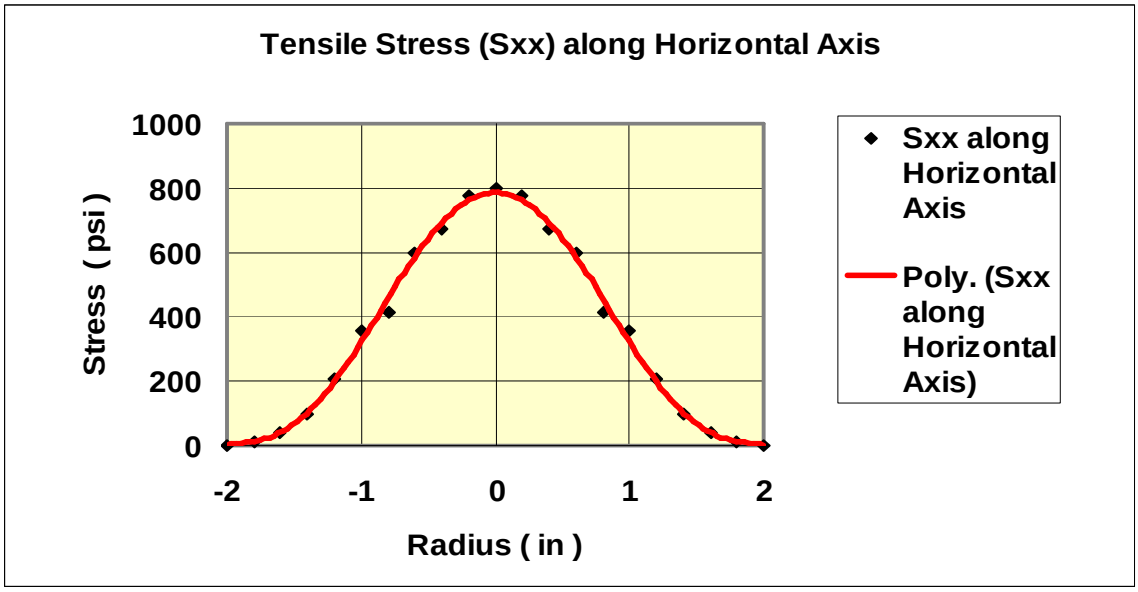

Figure 31 Horizontal UDEC Stress versus Radius for Solid Model

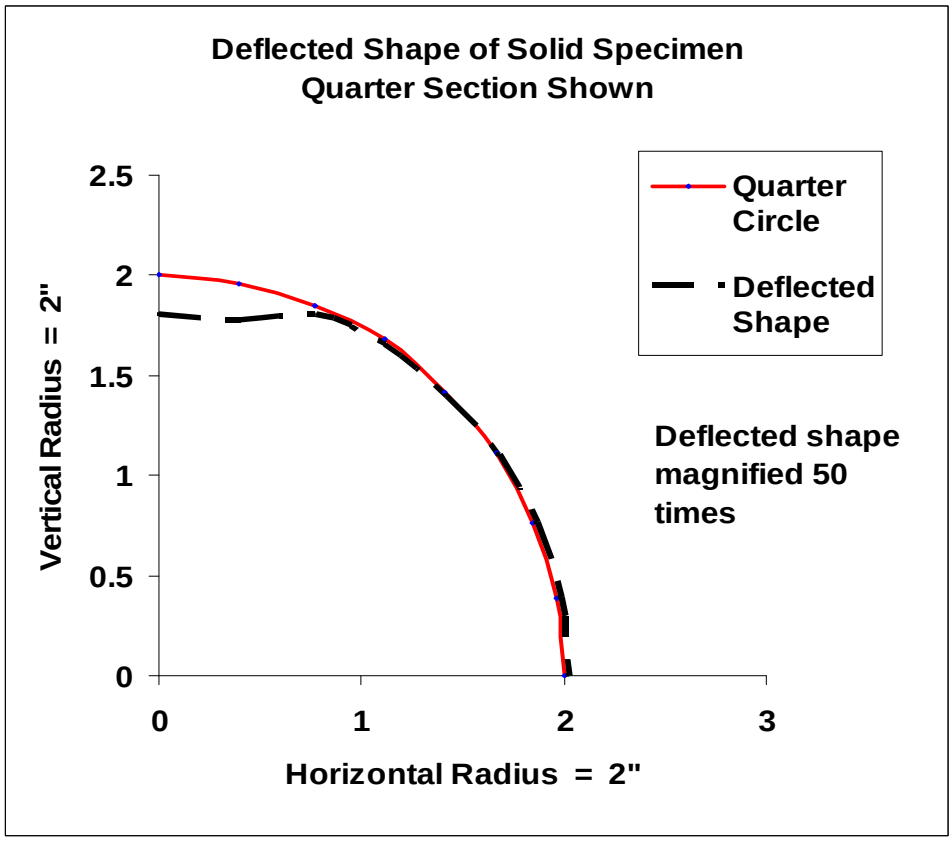

Figure 32 Deflected Shape of Solid Model

4.3.2 6.18 Percent Specimens

Figure 33 shows the results of the UDEC model for the two small hole specimens, 2SH6.18_A1 and 2SH6.18_A2. The failure cracks first formed at the top hole. As the load was increased, more cracks formed at the bottom hole, and then the cracks formed completely through the model. The photograph of the specimens after failure shows that the cracked locations in the actual test specimens were similar to the crack formations in the UDEC analysis.

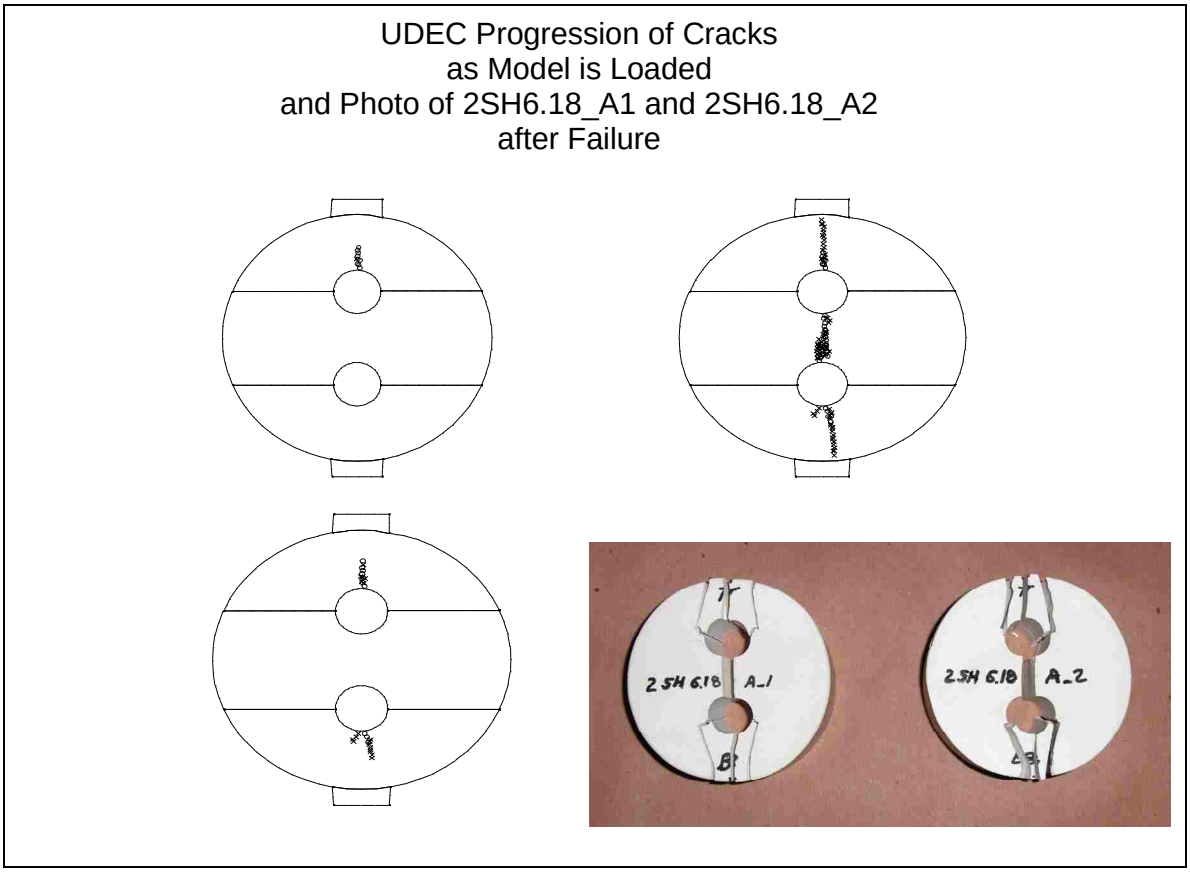

Figure 33 UDEC Model and Test Specimens 2SH6.18_A1 and 2SH6.18_A2

Figure 34 shows the vertical stress at the top (0, 2") of the two small hole UDEC model versus displacement for the 2SH6.18_A models.

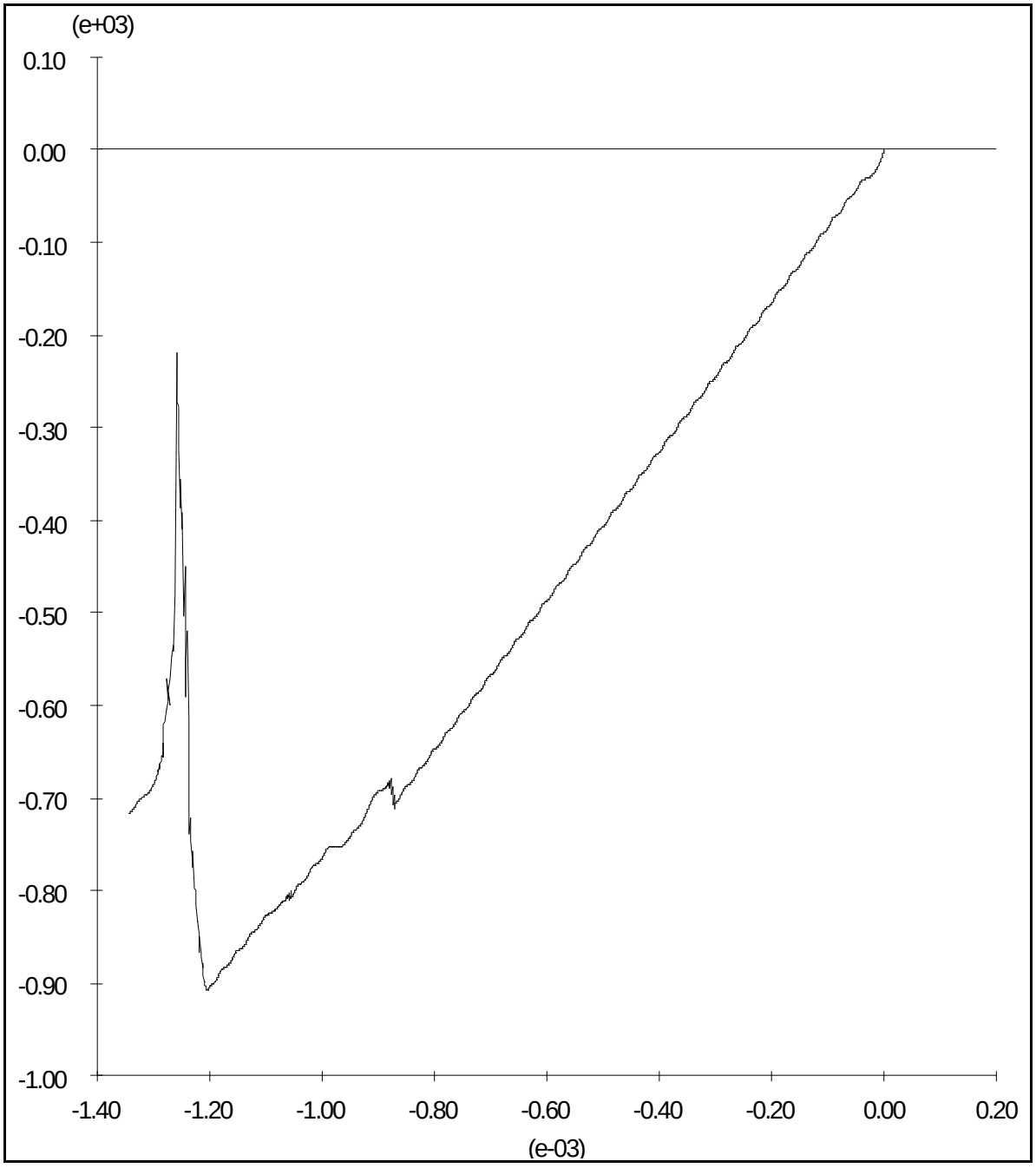

Figure 34 Vertical Stress versus Displacement at Top of 2SH6.18_A Models

Figure 35 shows the results of the UDEC model for the two small hole specimens, 2SH6.18_B1 and 2SH6.18_B2. The failure cracks first formed at the top hole. As the load was increased, more cracks progressed to the bottom hole, and then the cracks formed completely through the model. The photograph of the specimens after failure shows that the cracked failure locations in the actual test specimens were similar to the crack formations in the UDEC analysis.

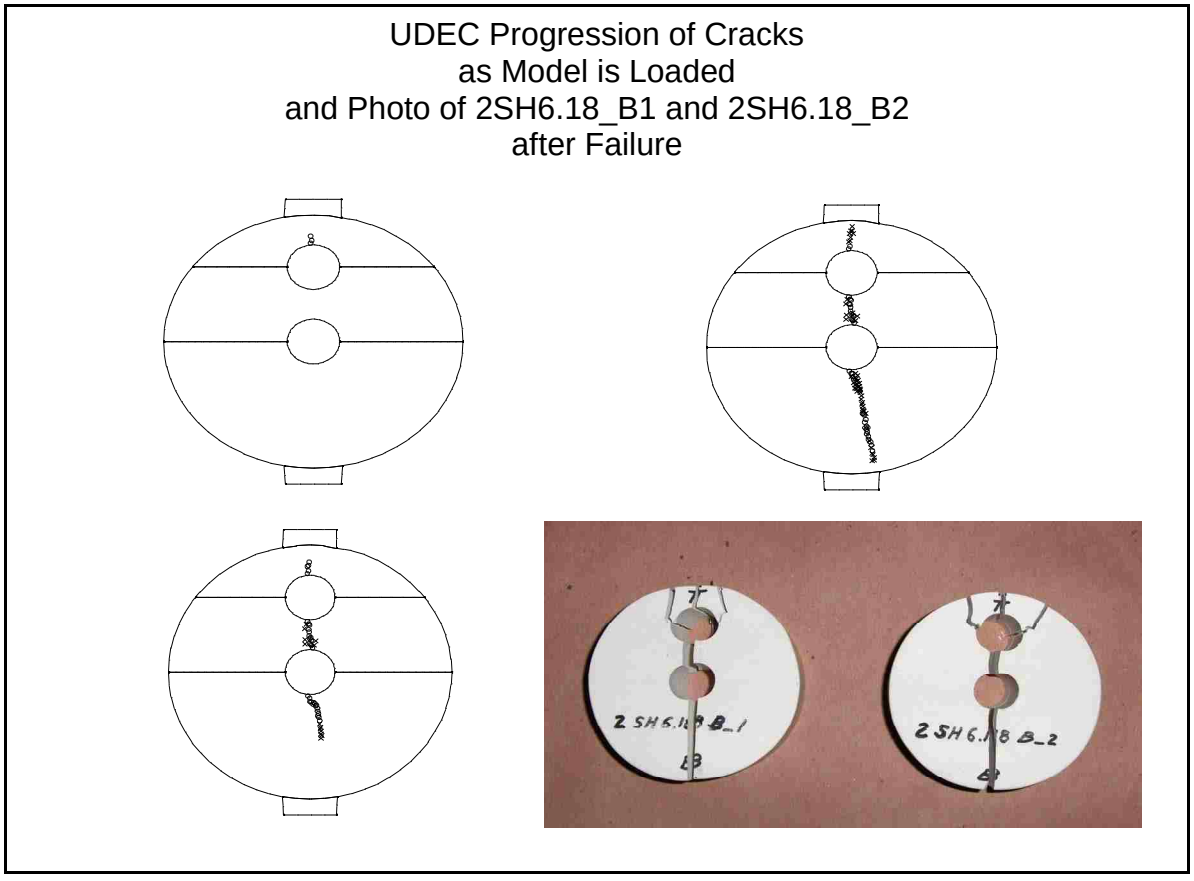

Figure 35 UDEC Model and Test Specimens 2SH6.18_B1 and 2SH6.18_B2

Figure 36 shows the vertical stress at the top (0, 2") of the two small hole UDEC model versus displacement for the 2SH6.18_B models.

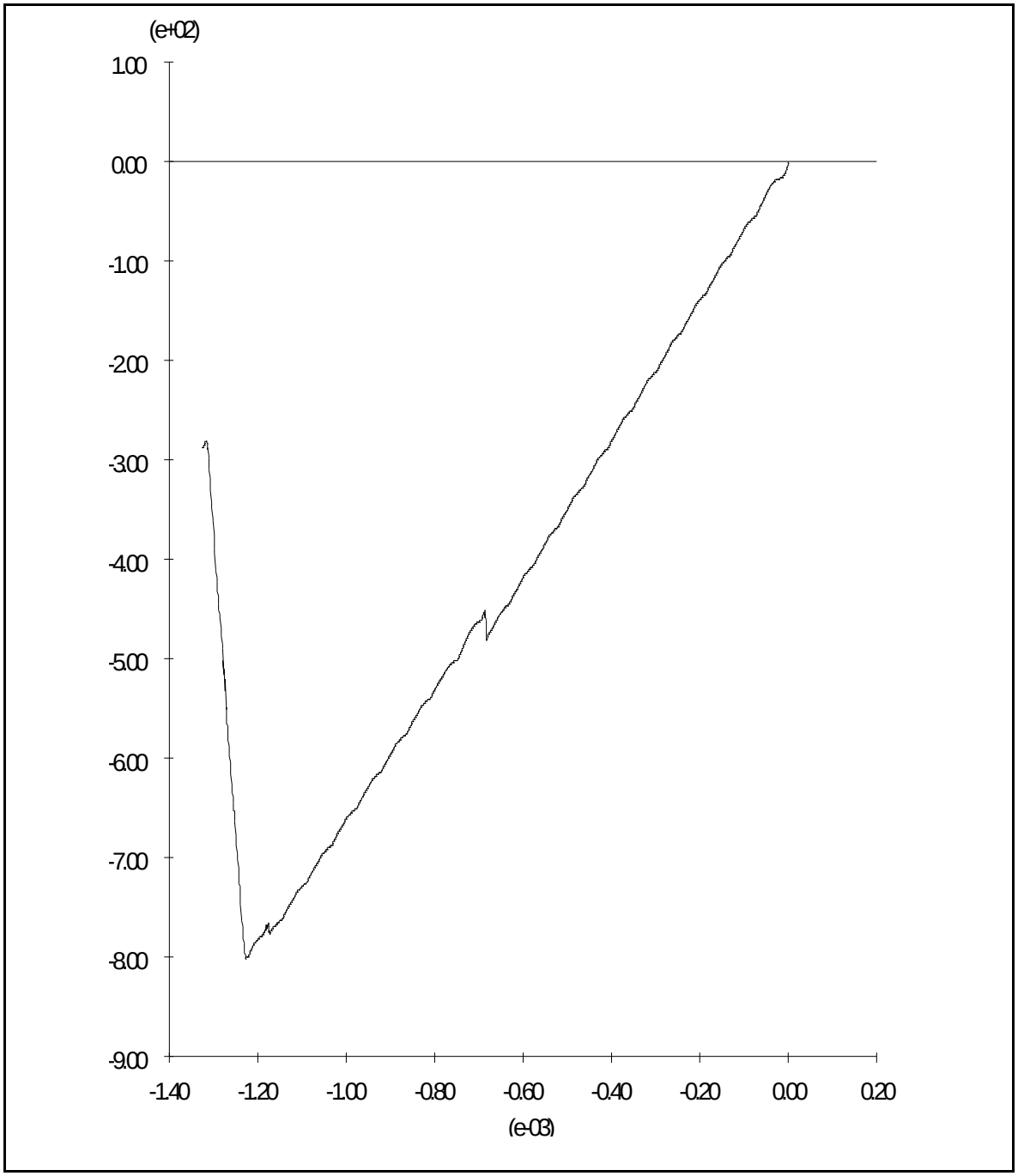

Figure 36 Vertical Stress versus Displacement at Top of 2SH6.18_B Models

Figure 37 shows the results of the UDEC model for the two small hole specimens, 2SH6.18_C1 and 2SH6.18_C2. The failure cracks first formed at the bottom of one of the holes. As the load was increased, more cracks progressed at the bottom and top of the hole. Then, the cracks progressed to the outside surfaces of the model. The photograph of the specimens after failure shows that the cracked locations in the actual test specimens were almost exactly the same as the crack formations in the UDEC analysis.

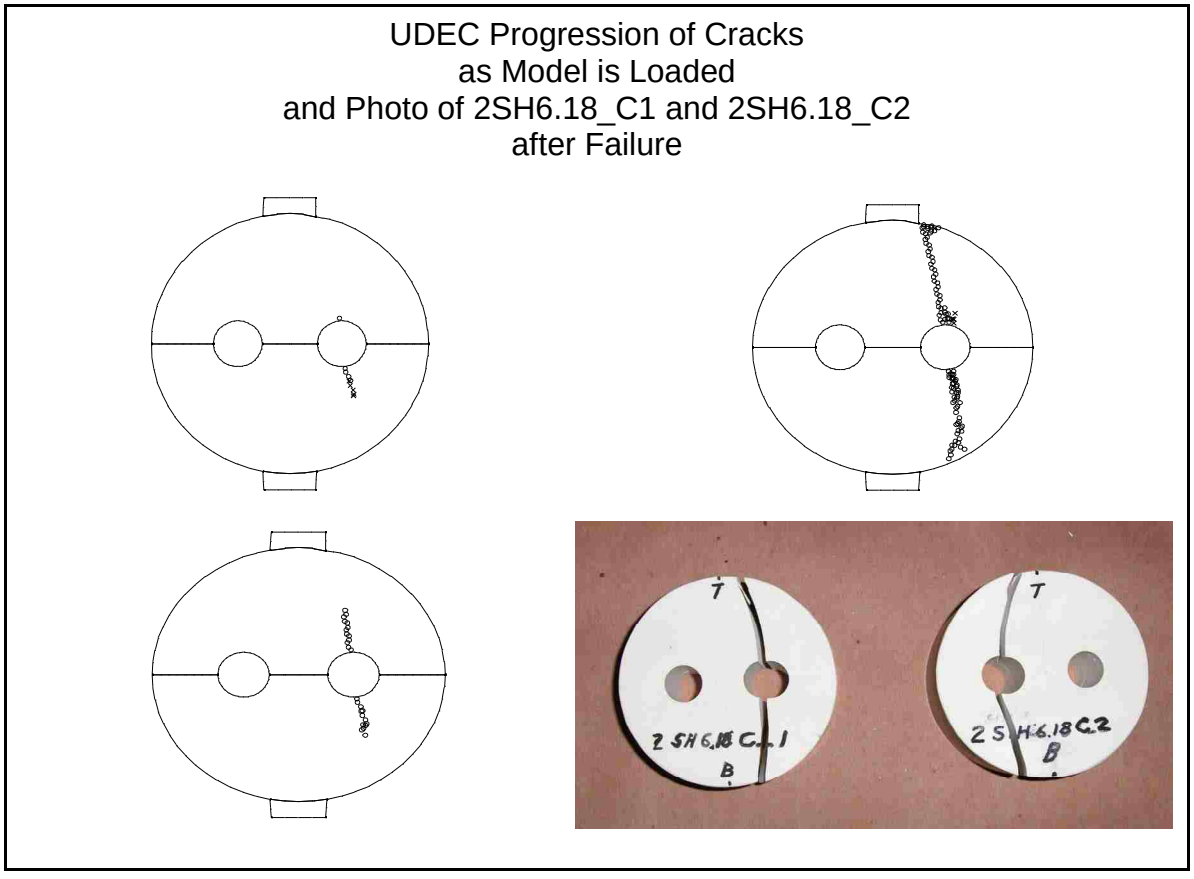

Figure 37 UDEC Model and Test Specimens 2SH6.18_C1 and 2SH6.18_C2

Figure 38 shows the vertical stress at the top (0, 2") of the two small hole UDEC model versus displacement for the 2SH6.18_C models. The UDEC model did not show failure, since only the side spalled off and the model continued to act, as being partially solid.

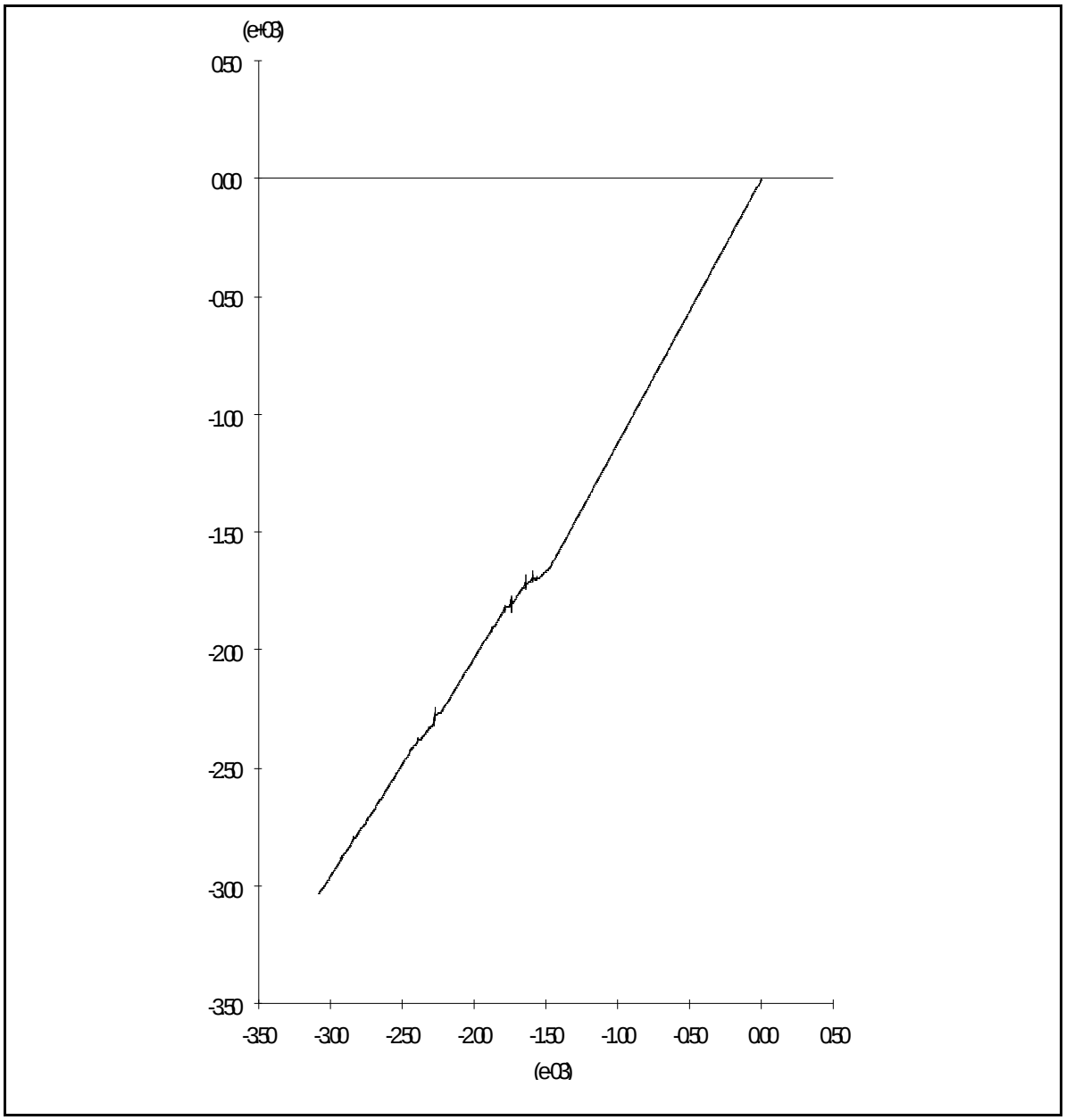

Figure 38 Vertical Stress versus Displacement at Top of 2SH6.18_C Models

Figure 39 shows the results of the UDEC model for the two small hole specimens, 2SH6.18_D1 and 2SH6.18_D2. The failure cracks first formed at the top of the top hole and then, at the bottom of the bottom hole. The photograph of the specimens after failure shows that these cracked failure locations in the actual test specimens were the same as the crack formations in the UDEC analysis. However, as the load was further applied, cracks formed in the UDEC model that were dissimilar to the actual specimen tests.

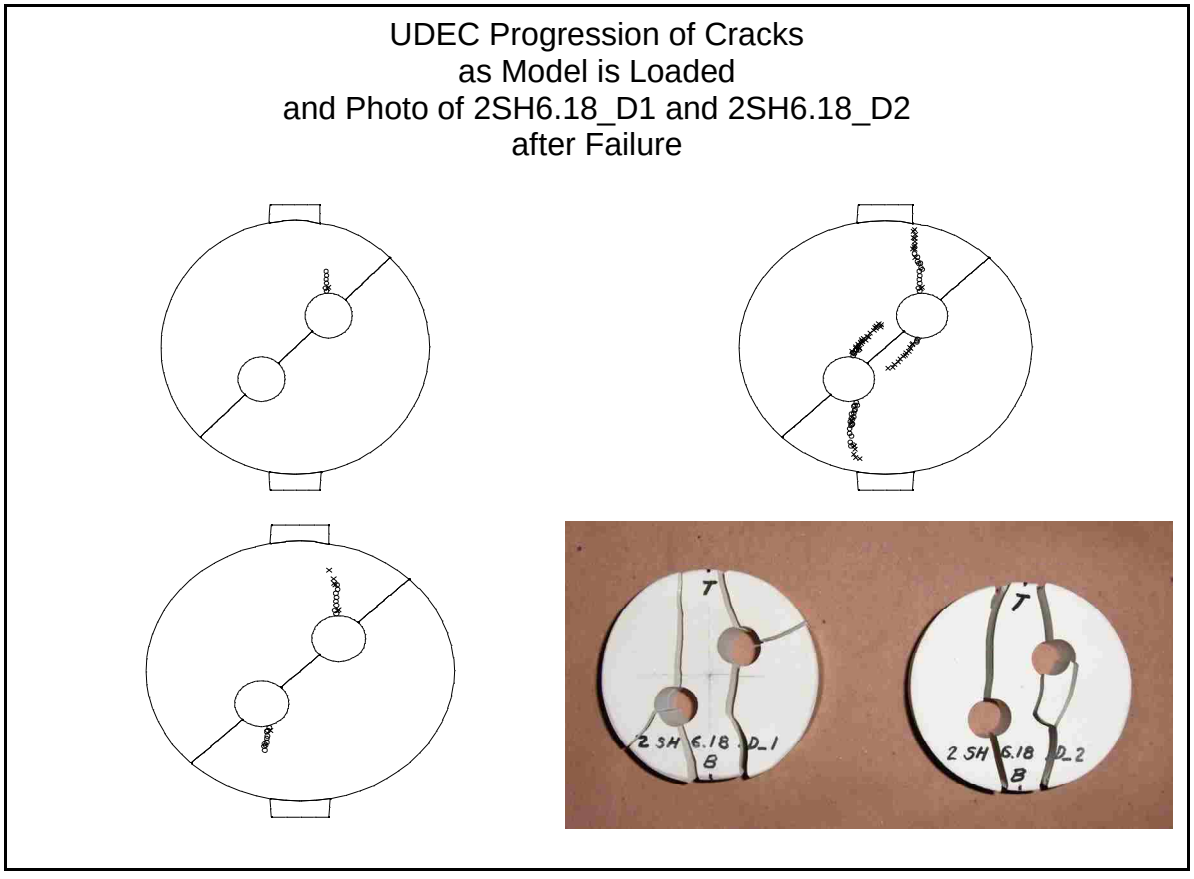

Figure 39 UDEC Model and Test Specimens 2SH6.18_D1 and 2SH6.18_D2

Figure 40 shows the vertical stress at the top (0, 2") of the two small hole UDEC model versus displacement for the 2SH6.18_D models. The UDEC model showed a first failure at 980 psi, and this value was used as the model failure stress.

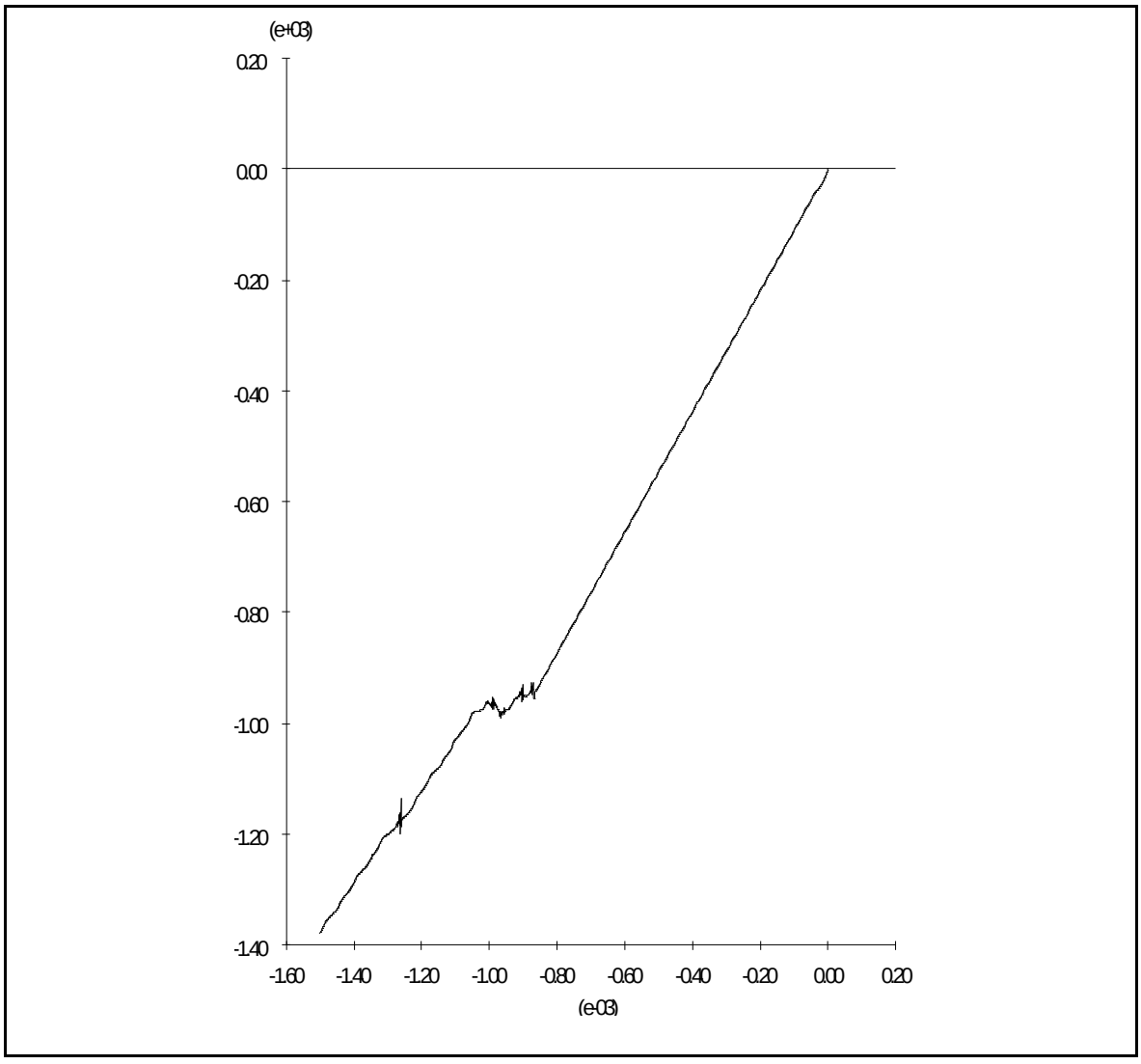

Figure 40 Vertical Stress versus Displacement at Top of 2SH6.18_D Models

4.3.3 6.25 Percent Specimens

Figure 41 shows the results of the UDEC model for the one large hole specimens, 1LH6.25_A1 and 1LH6.25_A2. The failure cracks first formed at the top of the hole. As the load was increased, more cracks formed. The photograph of the specimens after failure shows that the failed locations on the actual test specimen matched closely the crack formations in the UDEC analysis.

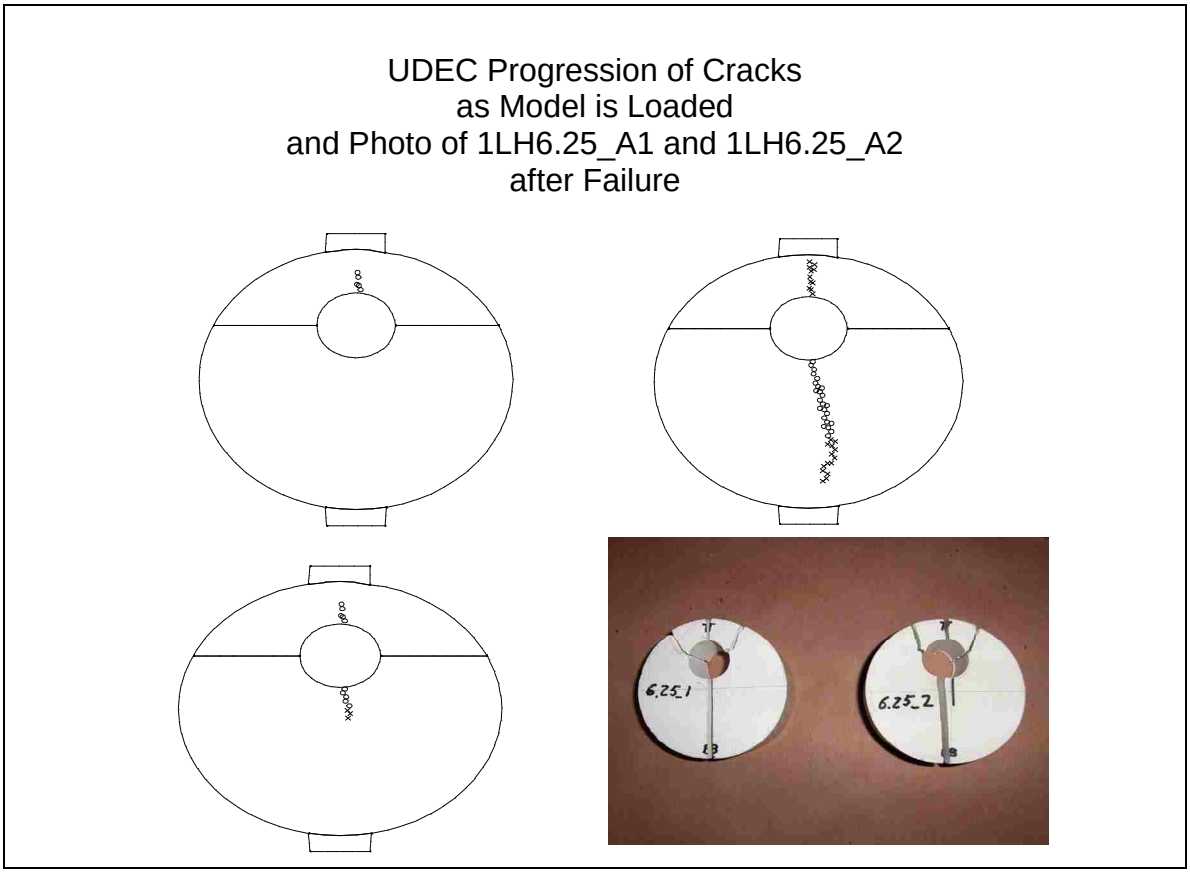

Figure 41 UDEC Model and Test Specimens 1LH6.25_A1 and 1LH6.25_A2

Figure 42 shows the vertical stress at the top (0, 2") of the UDEC model versus displacement for the 1LH6.25_A models. The peak of the curve, where the stress starts to decrease was considered the failure of the model. This stress was used to compute the failure load at the top of the model. The failure load was then used in the Brazilian equation (Goodman, 1989) to compute the Ultimate Tensile Strength (UTS).

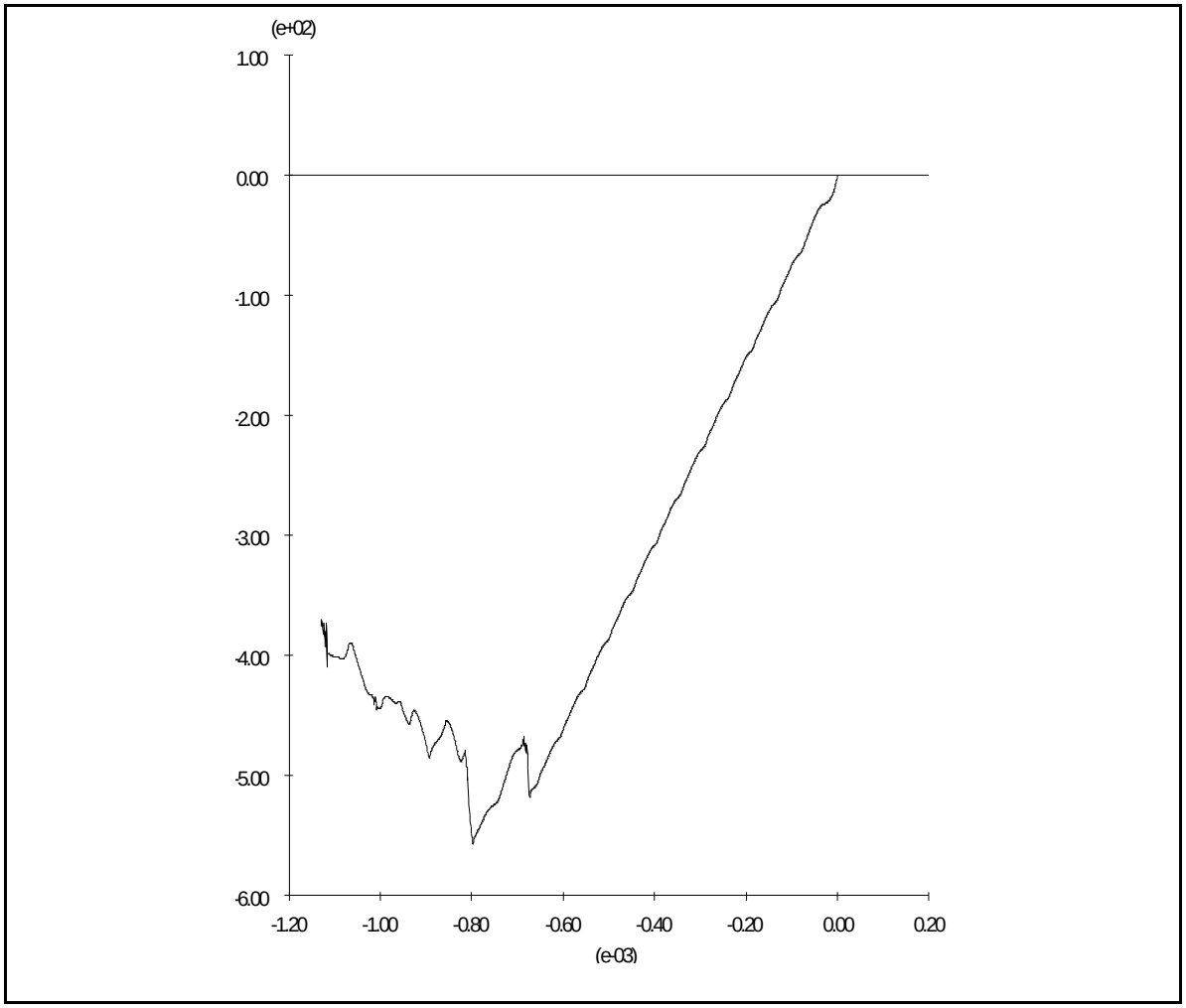

Figure 42 Vertical Stress versus Displacement at Top of 1LH6.25_A Models

Data for the test models are shown in Appendix V.

Figure 43 shows the results of the UDEC model for the one large hole specimens, 1LH6.25_B1 and 1LH6.25_B2. The failure crack first formed at the bottom of the hole. As the load was increased, more cracks formed. The photograph of the specimens after failure shows that the cracked locations in the center of the actual test specimens were similar to the crack formations in the UDEC analysis.

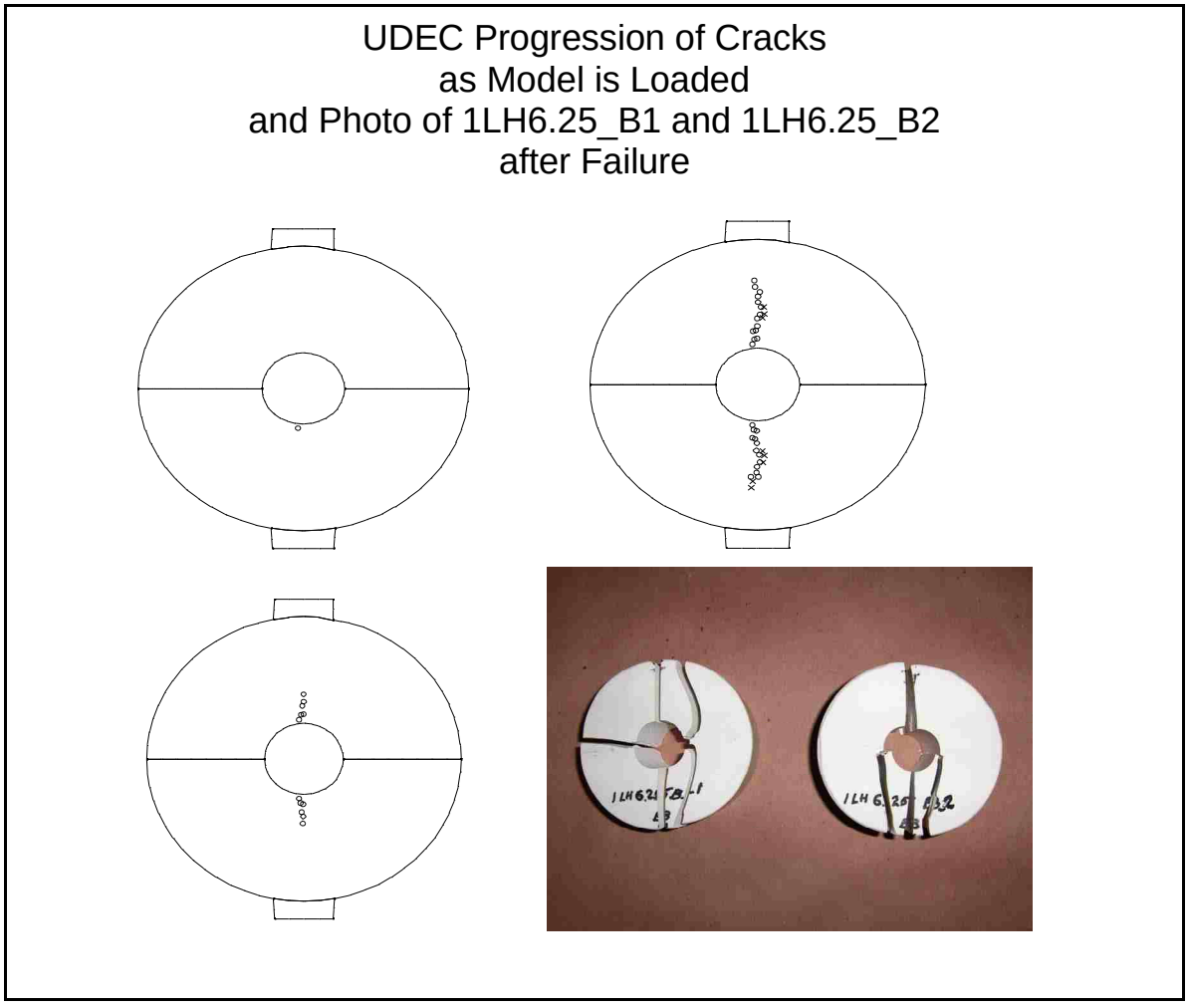

Figure 43 UDEC Model and Test Specimens 1LH6.25_B1 and 1LH6.25_B2

Figure 44 shows the vertical stress at the top (0, 2") of the UDEC model versus displacement for the 1LH6.25_B models.

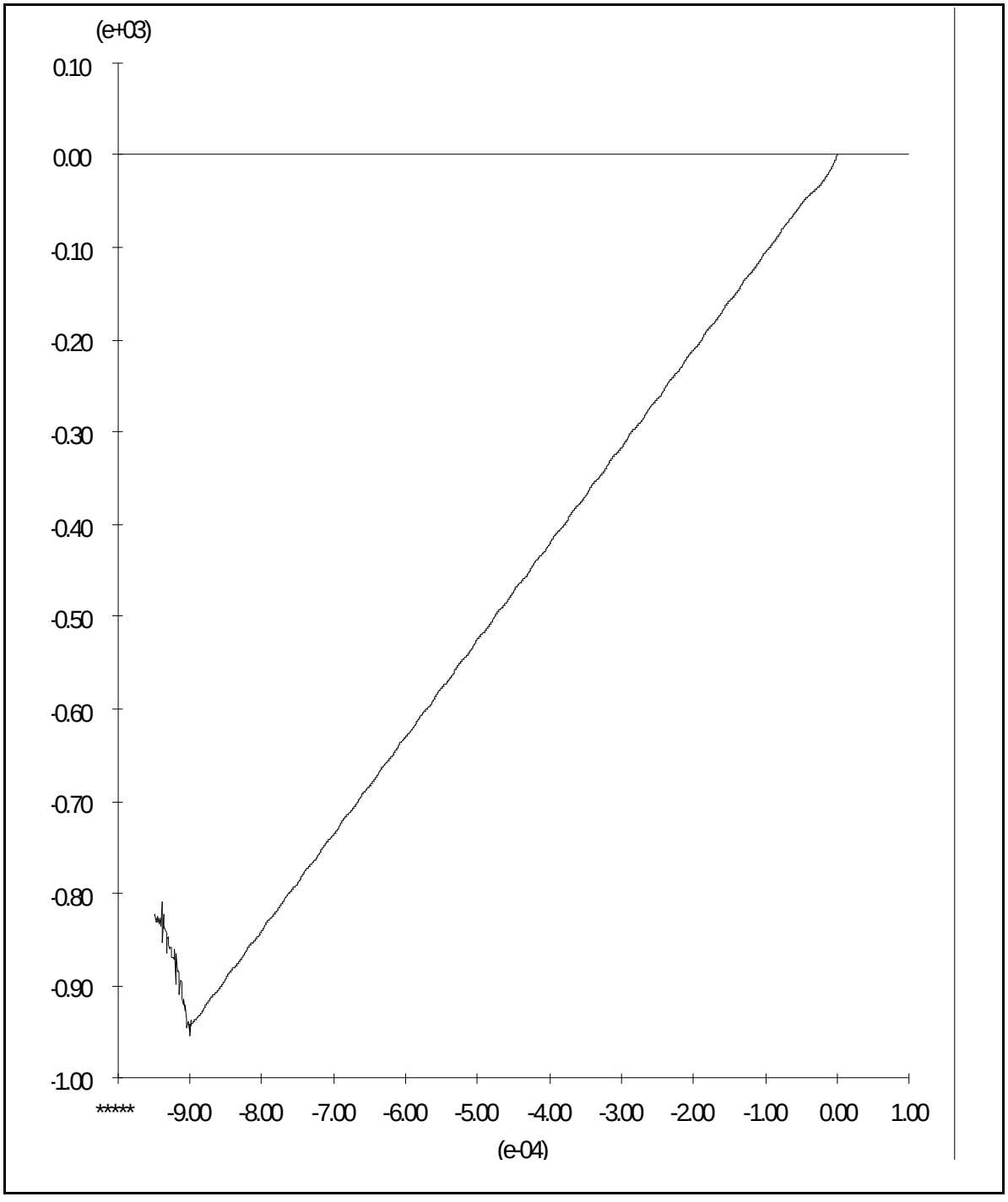

Figure 44 Vertical Stress versus Displacement at Top of 1LH6.25_B Models

4.3.4 12.50 Percent Specimens

Figure 45 shows the results of the UDEC model for the two large hole specimens, 2LH12.50_A1 and 2LH12.50_A2. The failure cracks first formed at the top hole. As the load was increased, more cracks formed. The photograph of the specimens after failure shows that the cracked locations in the actual test specimens were similar to the crack formations in the UDEC analysis.

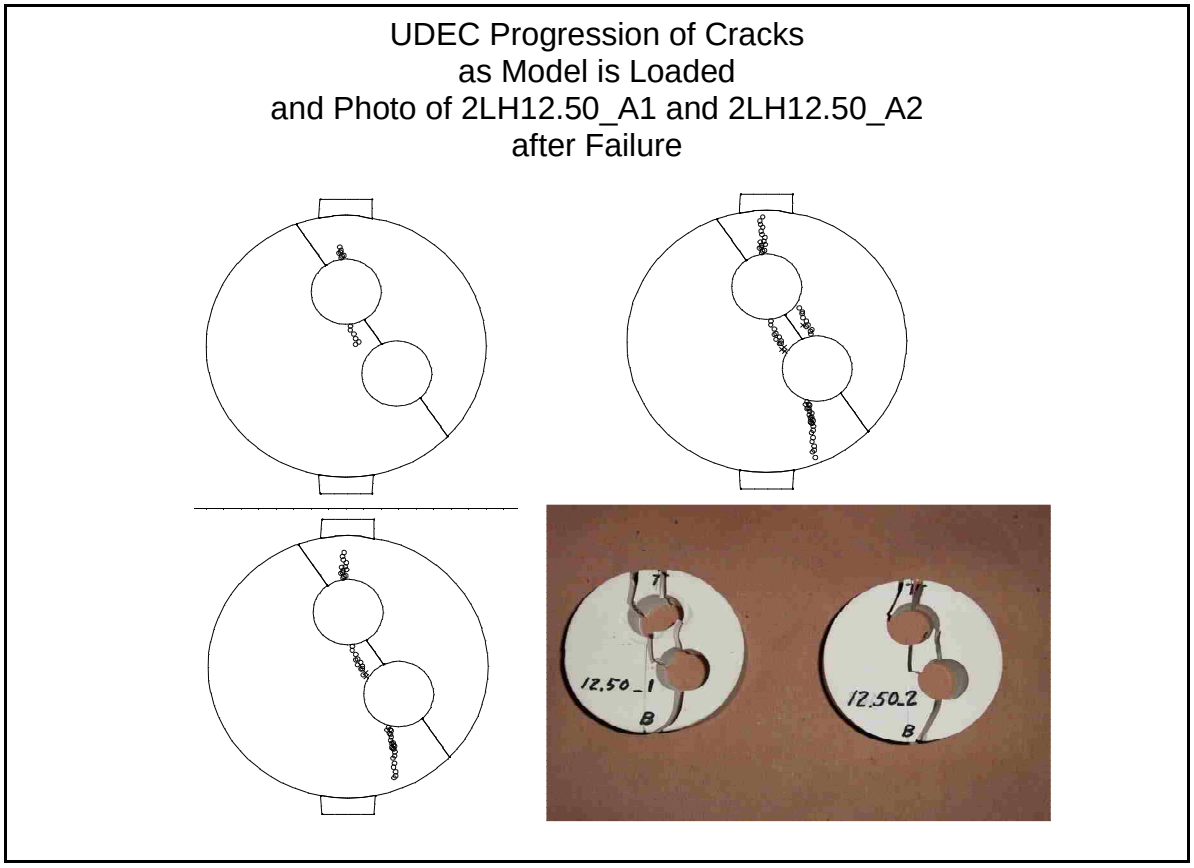

Figure 45 UDEC Model and Test Specimens 2LH12.50_A1 and 2LH12.50_A2

Figure 46 shows the vertical stress at the top (0, 2”) of the two hole UDEC model versus displacement for the 2LH12.50_A models.

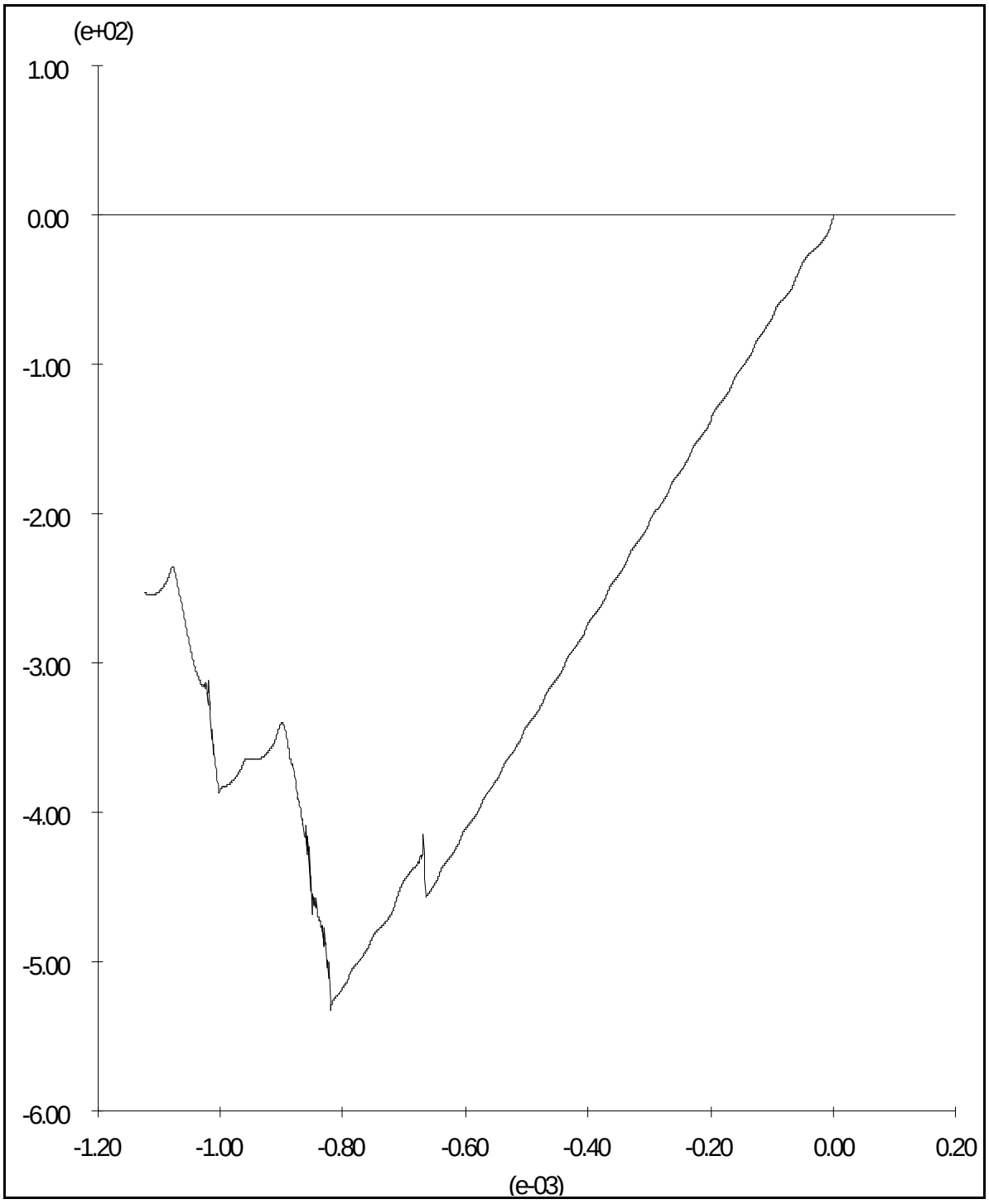

Figure 46 Vertical Stress versus Displacement at Top of 2LH12.50_A Models

4.3.5 18.75 Percent Specimens

Figure 47 shows the results of the UDEC model for the three large hole specimens, 3LH18.75_A1 and 3LH18.75_A2. The failure cracks first formed at the bottom hole. As the load was increased, more cracks formed. The photograph of the specimens after failure shows that the cracked locations in the actual test specimens were similar to the crack formations in the UDEC analysis.

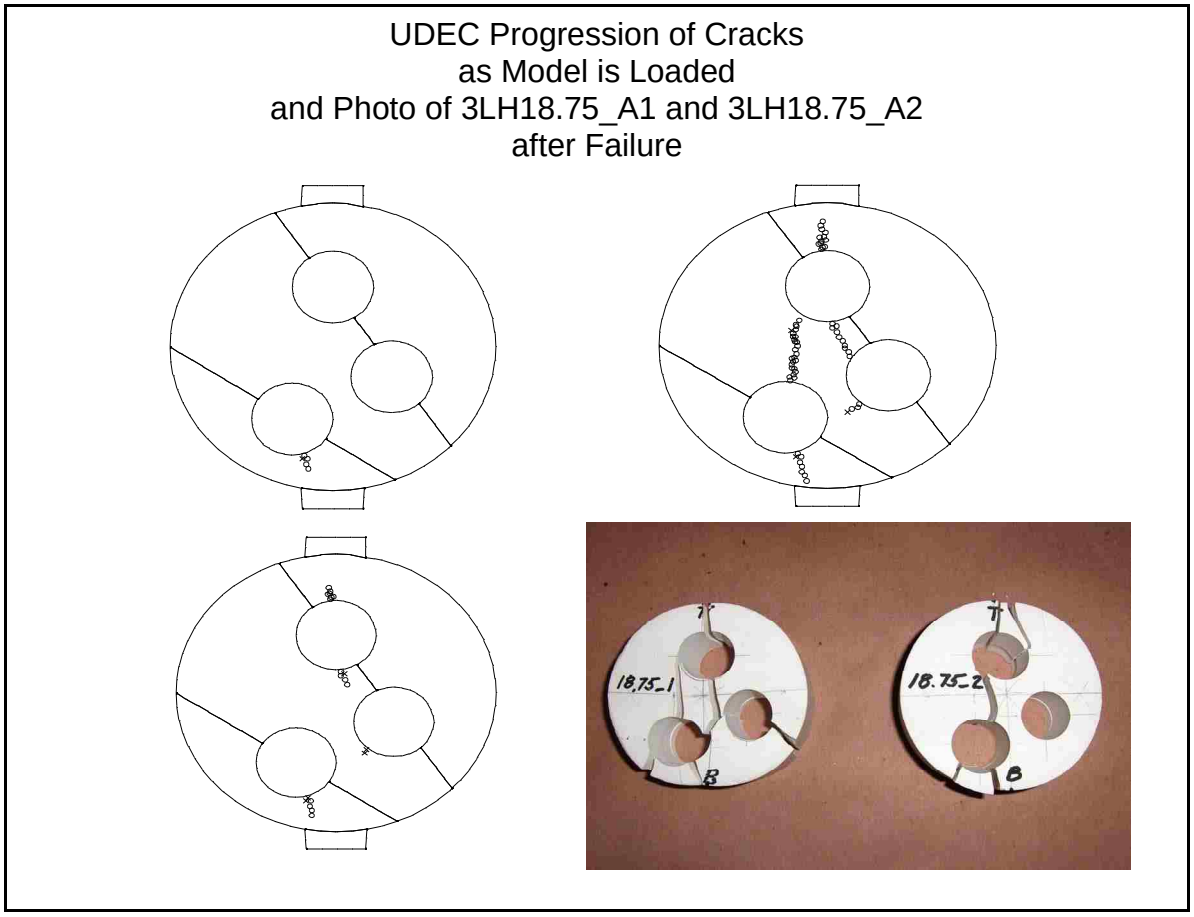

Figure 47 UDEC Model and Test Specimens 3LH18.75_A1 and 3LH18.75_A2

Figure 48 shows the vertical stress at the top (0, 2”) of the three hole UDEC model versus displacement for the 3LH18.75_A models.

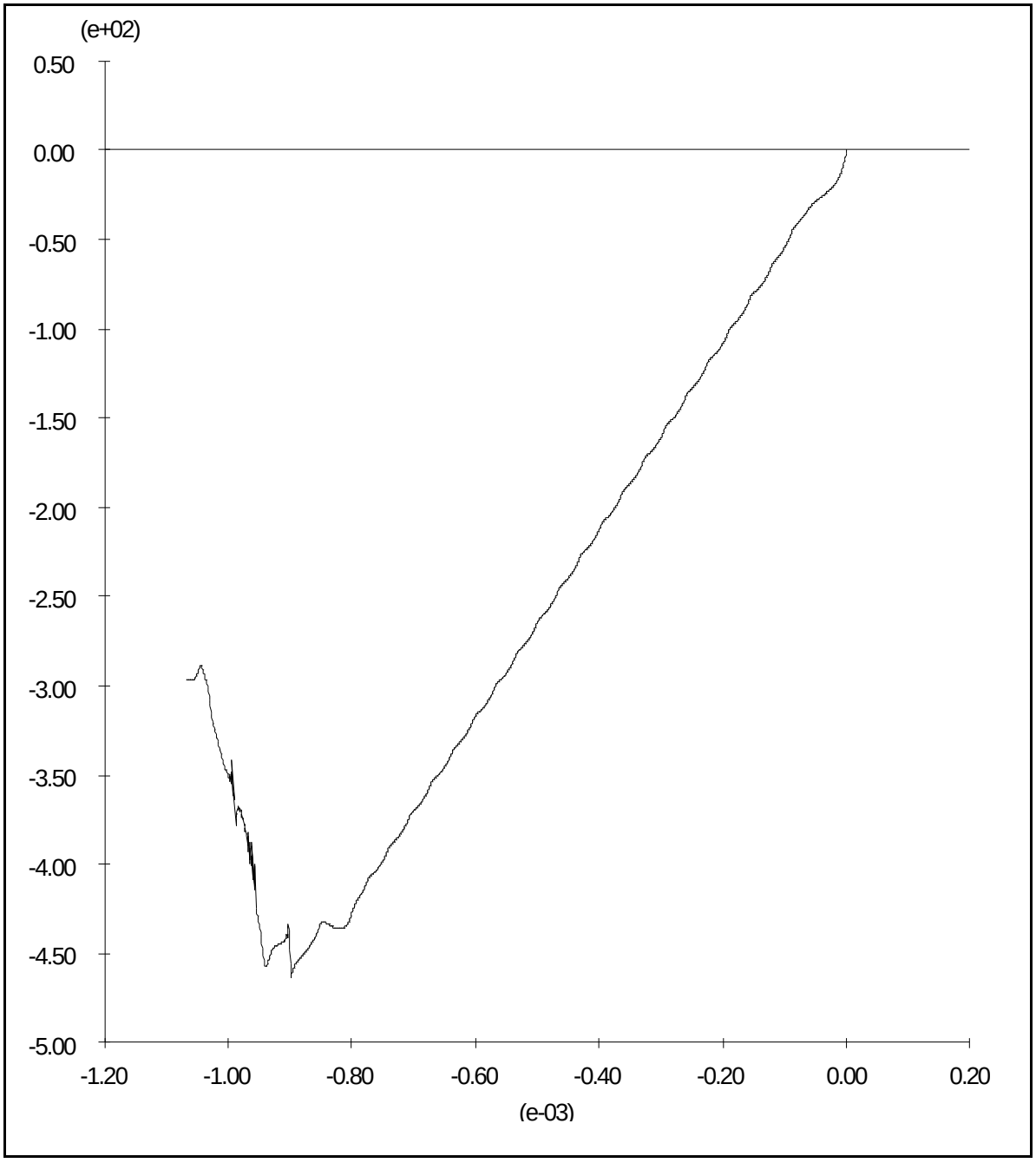

Figure 48 Vertical Stress versus Displacement at Top of 3LH18.75_A Models

4.3.6 Brazilian Specimen Summary

Calculations for the Ultimate Tensile Strength, UTS, as determined by the UDEC analyses are shown in Appendix V. Figure 49 shows tensile strengths versus porosities for both the experimental test results and the UDEC analyses.

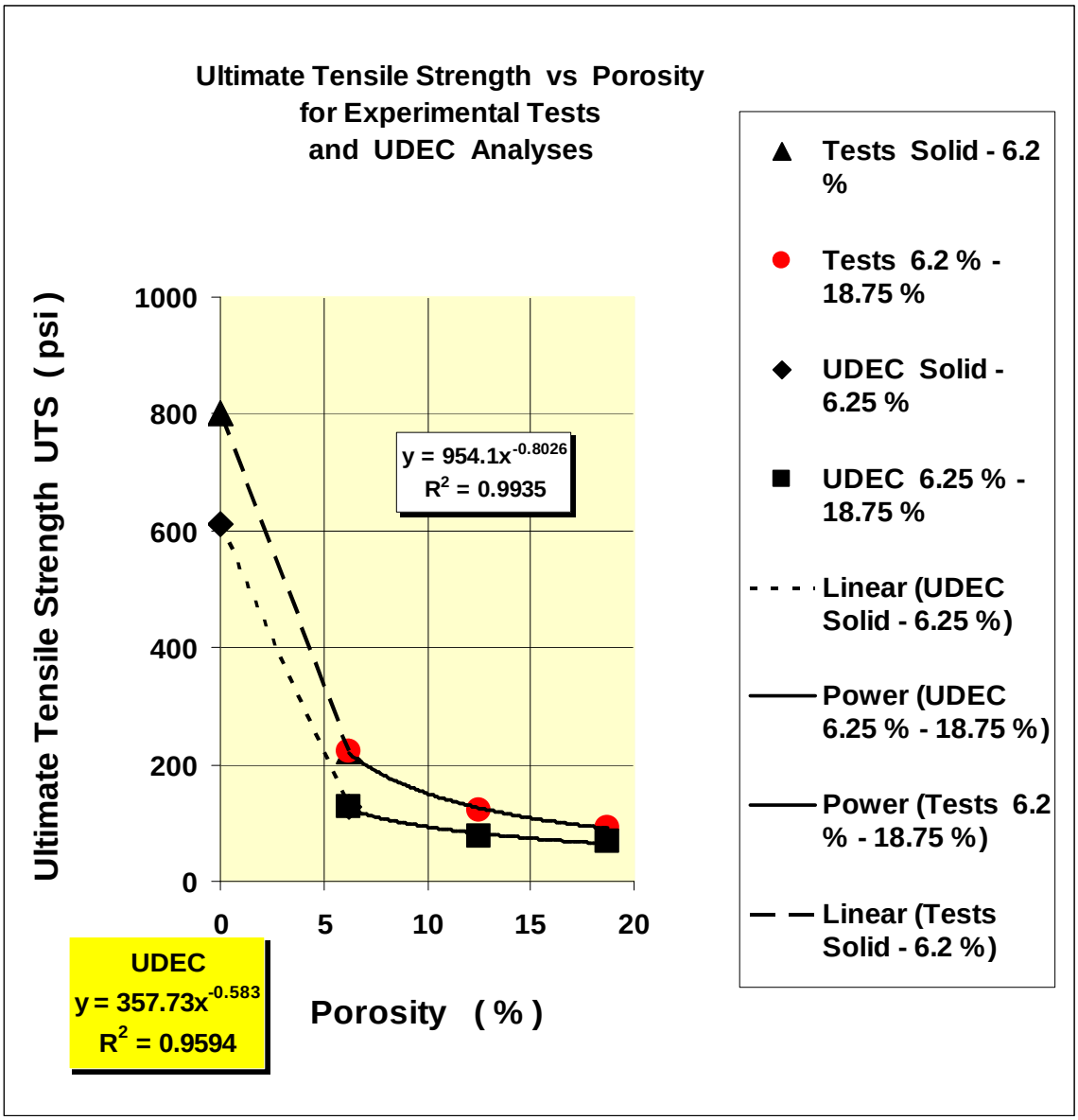

Figure 49 Ultimate Tensile Strengths versus Porosity for TESTS and UDEC

CHAPTER 5

FAILURE CRITERIA

5.1 General

Failure in rock has been defined as the mechanical condition in the rock whereby the rock deforms permanently or fractures (Jumikis, 1983). Failure criteria are established for various rocks so that geotechnical engineers can ascertain whether a structure in rock can support itself, or if additional structural supports are required. A failure criterion is usually represented by a line in a two dimensional, shear stress versus normal stress, coordinate system.

The first criterion was established by Coulomb in 1776, which is a straight line, and is a function of the strength of the rock and the friction angle (Jumikis, 1983). If the stresses in the rock of a structure are below the line, then the structure is safe without extra support. If the stresses are on or above the line, then the structure is not safe and extra structural support is required.

Another criterion was stated by Tresca in 1864, which assumes that failure occurs at the maximum shear stress, which is at the apex of Mohr's circle (Jumikis, 1983). A line can be drawn between a series of apexes of Mohr's circles for various stress conditions of tensile and compressive stresses in a particular rock. The resulting failure line has been termed the Mohr-Coulomb in s-t space (Bardet 1997).

The maximum tensile stress criterion states that when the maximum principal normal stress reaches the ultimate tensile strength, failure will occur. This is the condition that can exist at the crown of an underground tunnel. The maximum

tensile strength criterion has often been added to the Coulomb theory as a limiting cut off value for the tensile strength of the rock. Coulomb's theory was expanded upon in 1900 by Mohr, who said that Coulomb's straight line could be a curved line, as determined by triaxial experimental compressive tests. Various equations have been introduced to represent this curved line. The power equation is an example of the failure criterion being represented by a curved line (Goodman, 1989). Various other power equations have been used (Hoek and Brown, 1997). Also, the Griffith criterion, 1924, is a parabolic power equation for rock failure (Jumikis, 1983).

Five basic failure criteria were discussed in Chapter 2. Ten forms of these criteria are shown in "Empirical Rock Failure Criteria," pages 14 & 15 (Sheorey, 1997). This text also shows that the failure criteria can be expressed in terms of the principal stresses or the shear and normal stresses, page 10. For this project, the failure criteria are all expressed in terms of the shear and normal stresses, so that comparisons can be made for all of the criteria discussed. The shear stress was used as the independent variable in the equations, so that when a power equation is transformed from zero along the normal stress axis, the limiting point on the curve is at the tensile strength of the rock.

The following are analyses of the Mohr-Coulomb, Mohr-Coulomb in s-t space, Griffith and Power failure criteria, as it applies to the Hydro-Stone TB analog material for tuff rock.

5.2 Mohr-Coulomb Criterion

The classical Coulomb's law states that the normal stress is a linear function of the shear stress, and is dependent on angle of friction and tangent point of Mohr's circle. The Mohr-Coulomb criterion can have either a straight or curved line. The straight line is used in this case, as no data are available for the triaxial testing of the Hydro-Stone TB. Also, the maximum tensile strength is used as a cut off point on the Coulomb line. Refer to the UDEC Users Manual, Figure 3.50, page 3-113, for a detailed description and figure of the Mohr-Coulomb failure criterion (Itasca, 2000). The Mohr-Coulomb failure criterion for Hydro-Stone TB with zero porosity is shown by the equation in Figure 50.

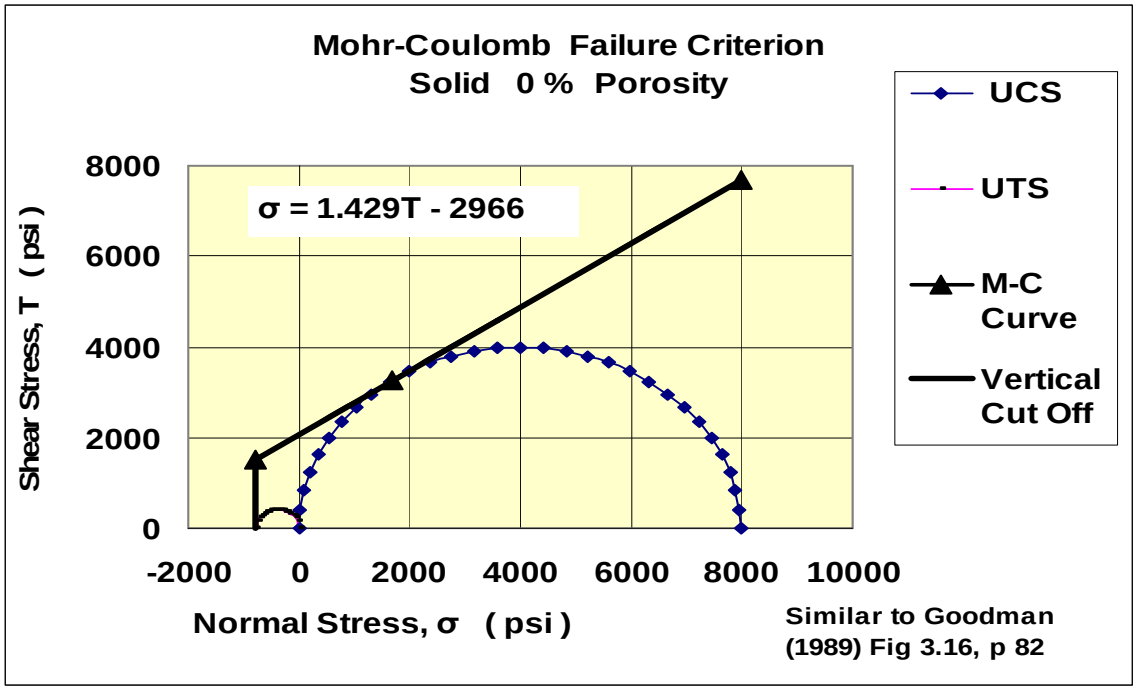

Figure 50 Mohr-Coulomb Failure Criterion

The intersection point of the equation and Mohr's circle for the uniaxial compressive strength was determined from geometry by knowing the uniaxial compressive strength (Rigby, 2007) and a friction angle of 35 degrees.

Several authors have said that the direct tensile strength of rock should be 90 percent of the Brazilian tensile test (Arioglu, et. al., 2006). Other authors have said that the Brazilian test underestimates the tensile strength of concrete (Lin and Wood, 2003). The Brazilian tensile strength was considered to be the tensile strength of the material for this project, since there is no data available on the direct tensile strength of Hydro-Stone TB.

5.3 Mohr-Coulomb in s-t Space Failure Criterion

The Mohr-Coulomb in s-t Space Failure Criterion assumes that failure will occur at the maximum shear stress, which is at the apex of Mohr's circle for a particular state of stress. A detailed explanation of the Mohr-Coulomb in s-t Space Failure Criterion is shown in Bardet's text in Figure 5 on page 365 (Bardet 1997). The s-t space is the notation adapted by the Massachusetts Institute of Technology, and it refers to the apexes of Mohr's circles that are plotted in the Sigma-Tau space. Mohr's circles for the Brazilian tensile strength, Brazilian compressive strength and the uniaxial compressive strength were used to determine the maximum shear stresses. The Mohr's circles and their maximum apexes are shown in Figure 51 for the Hydro-Stone TB material with zero porosity. Also shown is the equation of the trendline for the Mohr-Coulomb in s-t Space Failure Criterion.

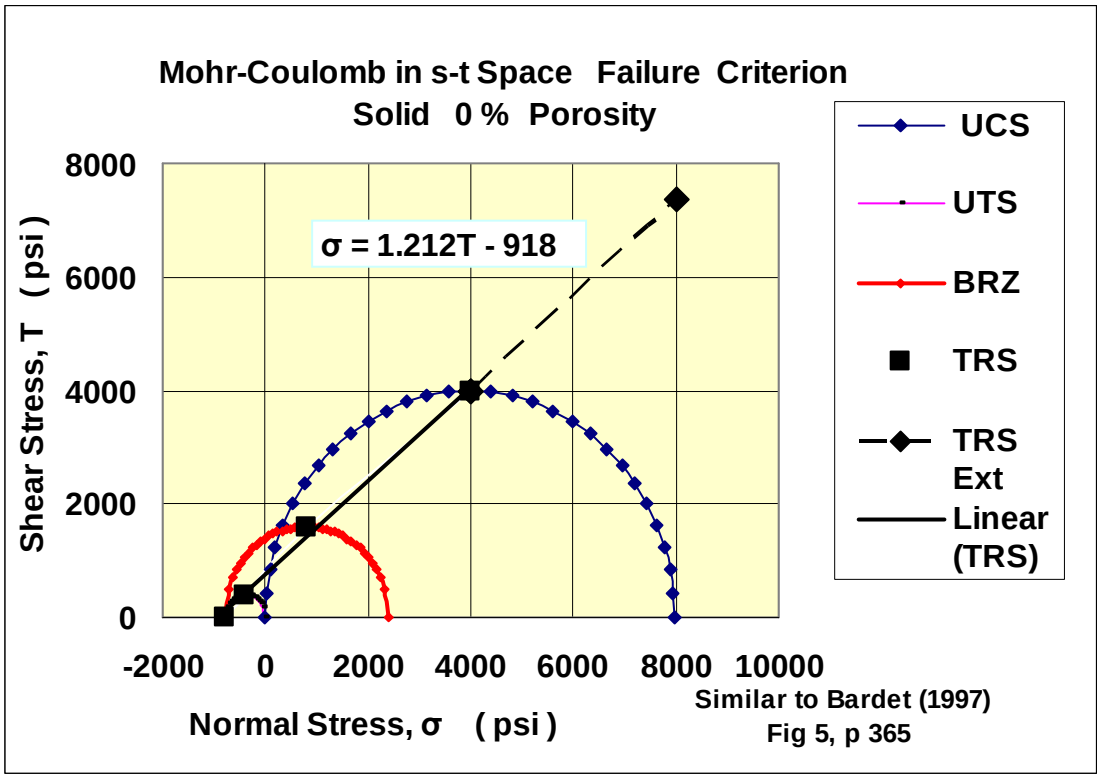

Figure 51 Mohr-Coulomb in s-t Space Failure Criterion

5.4 Griffith Failure Criterion

In 1921 Griffith postulated that fracture of rock is initiated at tensile stress concentrations at the tips of small cracks. In 1924 Griffith extended his theory by representing the shear stress as a function of the normal stress and ultimate tensile stress with a parabolic equation (Brady and Brown, 1993). Figure 52 shows the Griffith Failure Criterion with the parabolic equation for the Hydro-Stone TB with zero porosity.

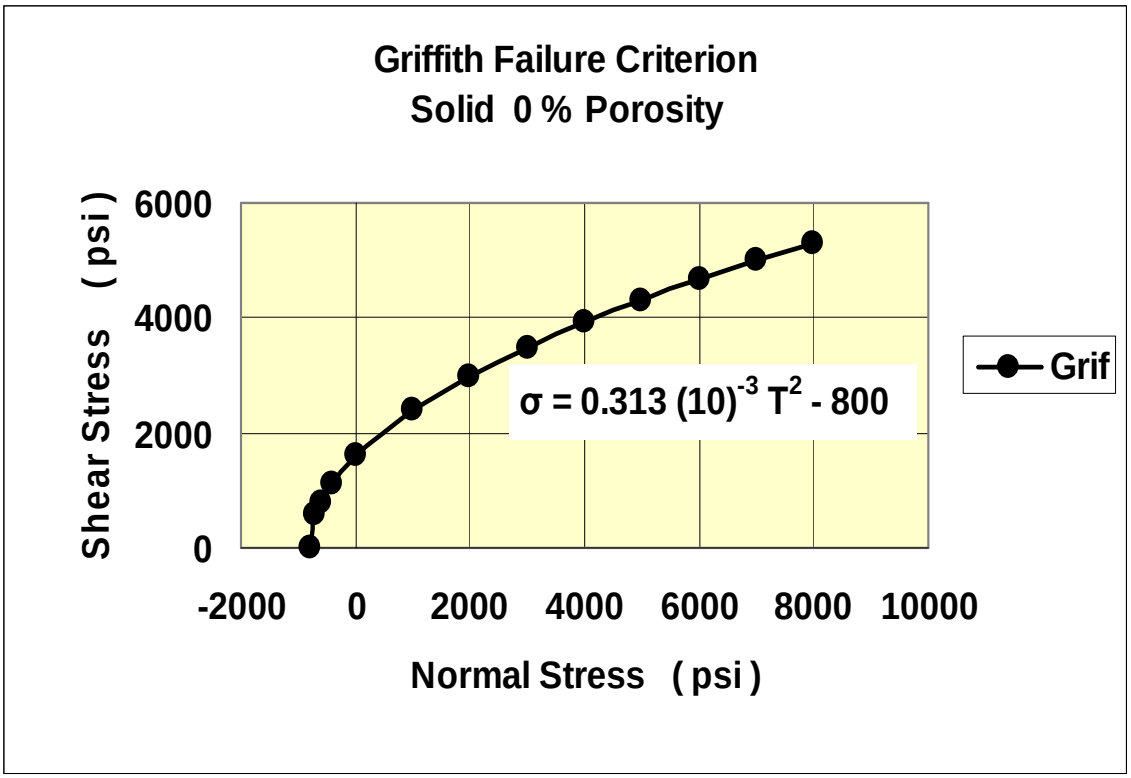

Figure 52 Griffith Failure Criterion

5.5 Power Failure Criterion

Another way to write a failure criterion is to use the Griffith form of the equation and make the exponent a variable instead of using an exponent of two (2). By using this method, a power curve can closely fit the tangents of Mohr's circles that are drawn from the results of experimental data. When there is a tensile strength of the rock, the power equation is $\sigma = A\,\tau^{B} + T_o$, where T_o is the tensile strength of the rock. A and B are constants that can be found from matching the tangent points of the curve to Mohr's circles.

One method is to use the tensile strength, Brazilian compressive strength and unconfined compressive strength to draw three Mohr's circles, which can be

used to locate the tangent points on the three Mohr's circles. The procedure for developing this curve is shown by Goodman, Fig. 3.19, p 88, (Goodman, 1989).

Figure 53 shows the power equation for Hydro-Stone TB with zero porosity. Mohr's circle for the unconfined compressive strength was determined from the results of previous tests (Rigby, 2007). Mohr's circle for the Brazilian compressive strength was determined from the equation, $\sigma = 3\ T_o$ (Timoshenko and Goodier, 1970). Mohr's circle for the tensile strength was determined from test results of this project.

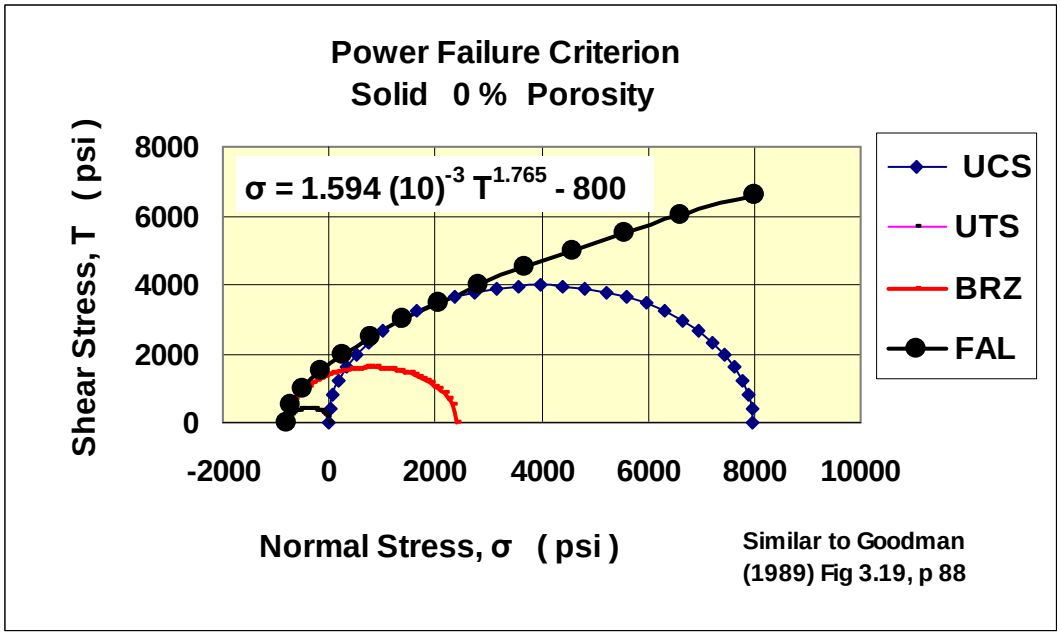

Figure 53 Power Failure Criterion

5.6 Summary of Criteria

For a comparison of the four criteria, each of the curves in Figures 50 through 53 is plotted on Figure 54.

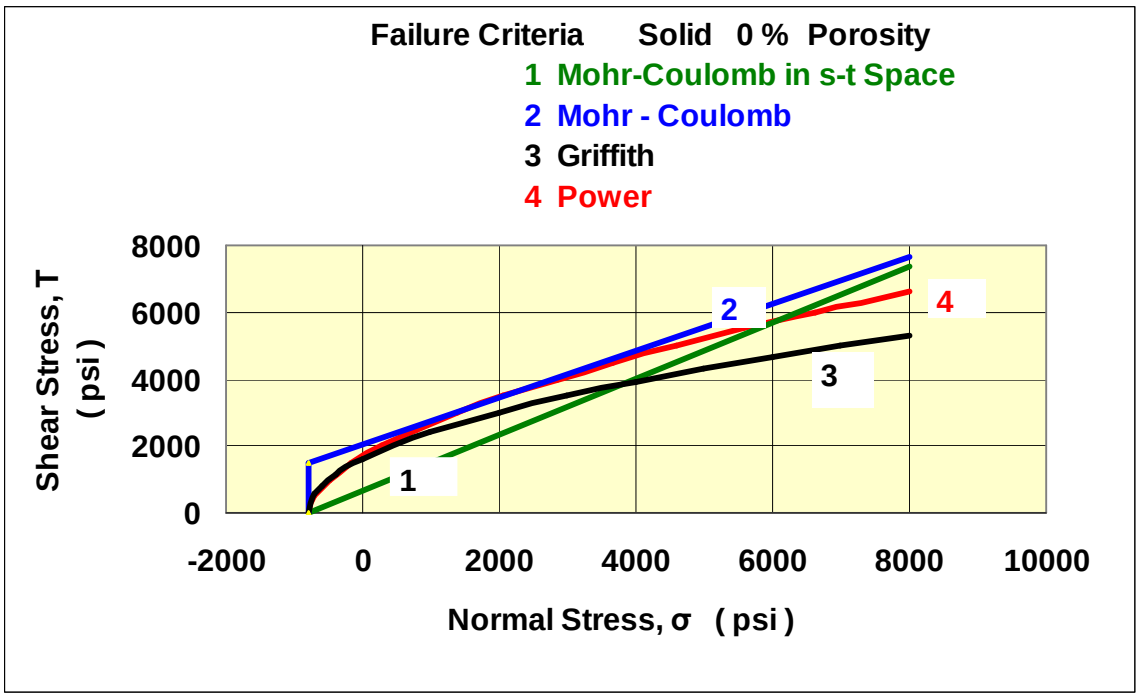

Figure 54 Comparisons of Failure Criteria

Figure 54 shows that the linear Mohr-Coulomb in s-t Space Failure Criterion gives the lowest shear stresses for normal stresses between a tensile stress of 800 psi and a compressive stress of 4,000 psi. The parabolic Griffith Criterion gives the lowest shear stresses between compressive stresses of 4,000 psi to 8,000 psi. These Failure Criteria show the lower bounds of normal and shear stresses. Also, the Mohr-Coulomb Criterion shows the upper bound of stresses.

5.7 Failure Criteria for Various Porosities

Figure 55 shows the effect of porosity on the Mohr-Coulomb Failure Criterion for 0, 6, 12 and 18 percent porosities. The tensile test data were determined from the experimental tests made in this project, as shown in Chapter 3, and the compressive test data were from previous tests (Rigby, 2007).

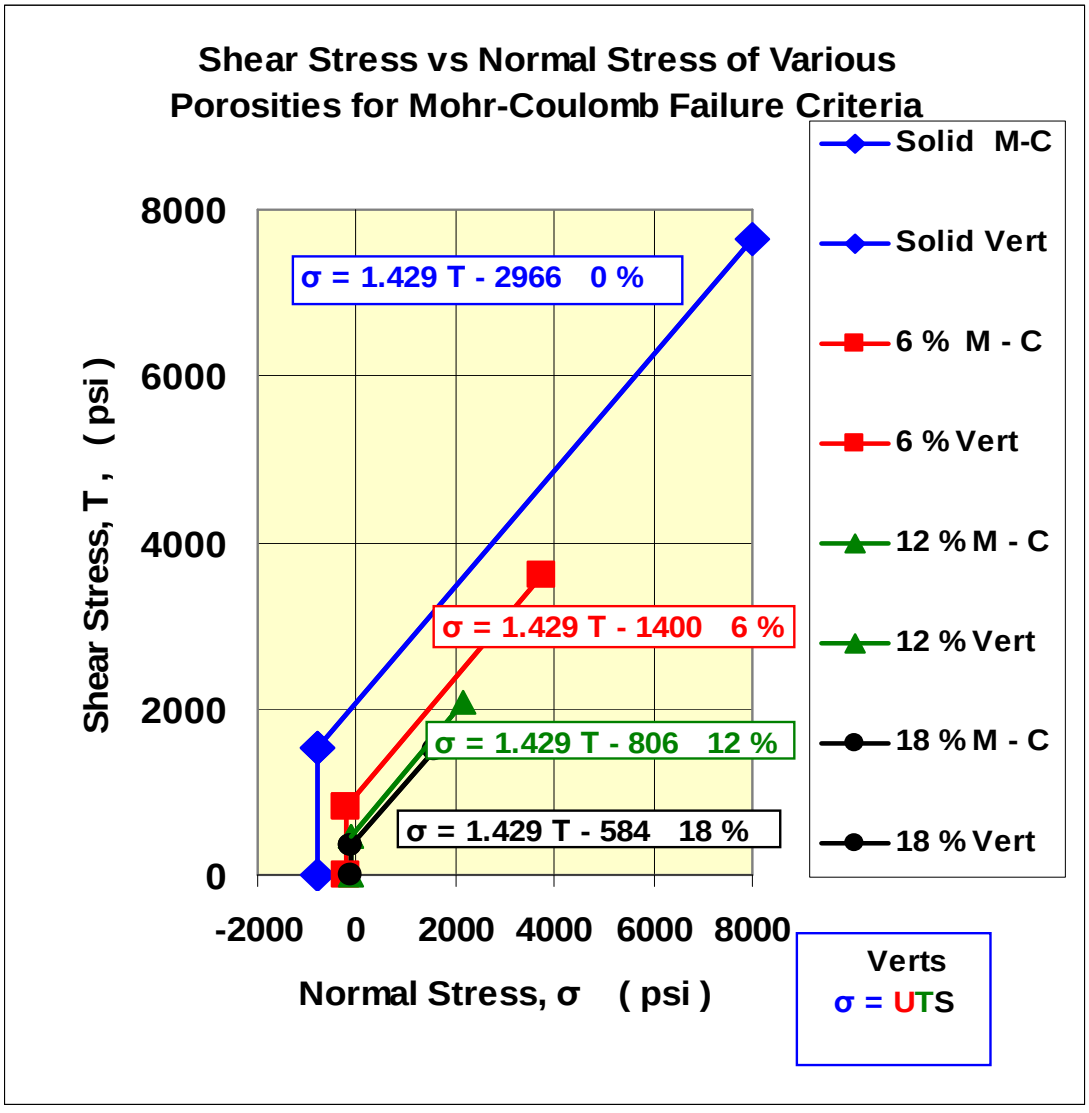

Figure 55 Effect of Porosity on the Mohr-Coulomb Failure Criteria

Figure 56 shows the effect of porosity on the Mohr-Coulomb in s-t Space Failure Criterion for 0, 6, 12 and 18 percent porosities.

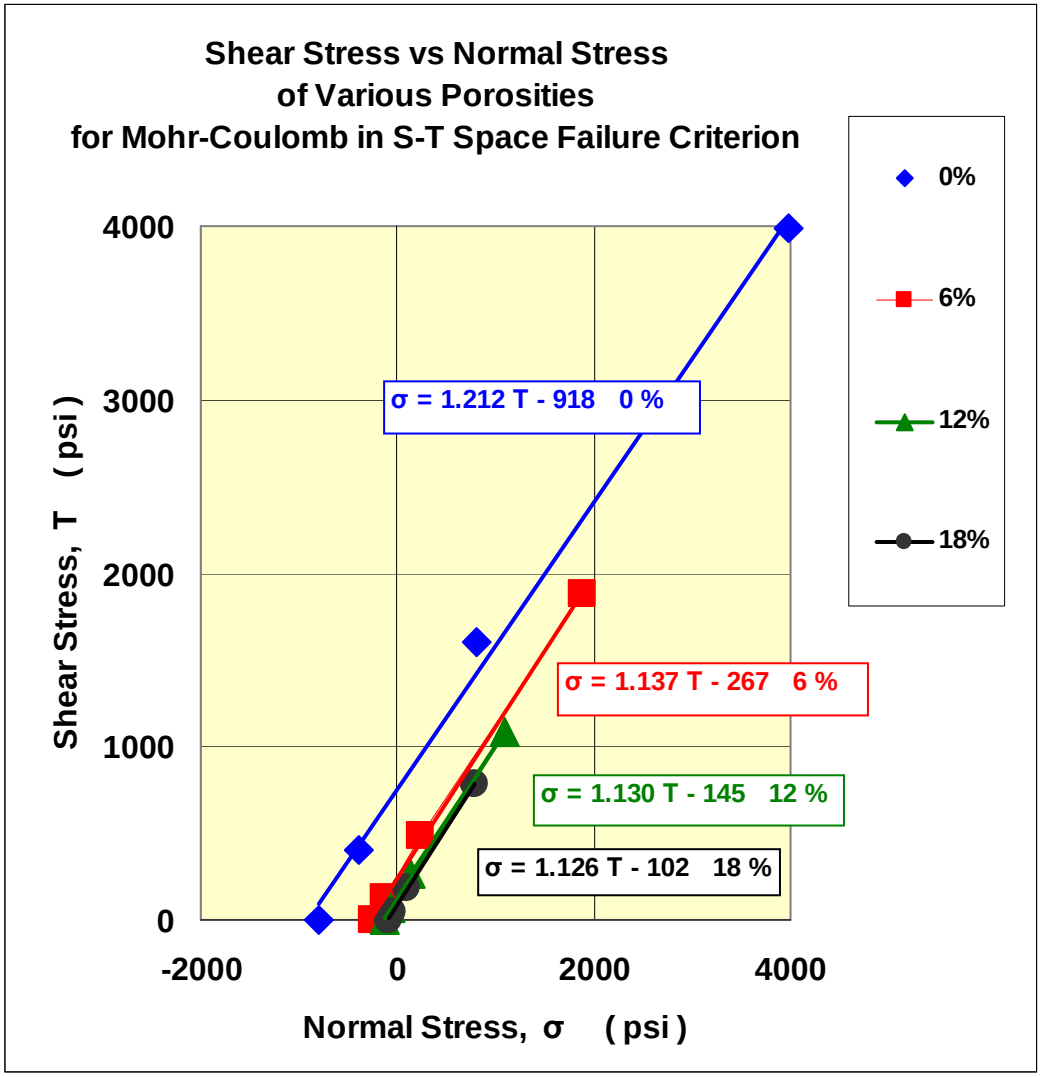

Figure 56 Effect of Porosity on the Mohr-Coulomb in s-t Space Failure Criterion

The slopes of the curves of the Mohr-Coulomb in s-t Space Failure Criteria in Figure 56 are slightly greater than the slopes of the curves of the Mohr-Coulomb Failure Criteria.

Figure 57 shows the effect of porosity on the Griffith Failure Criterion for 0, 6, 12 and 18 percent porosities.

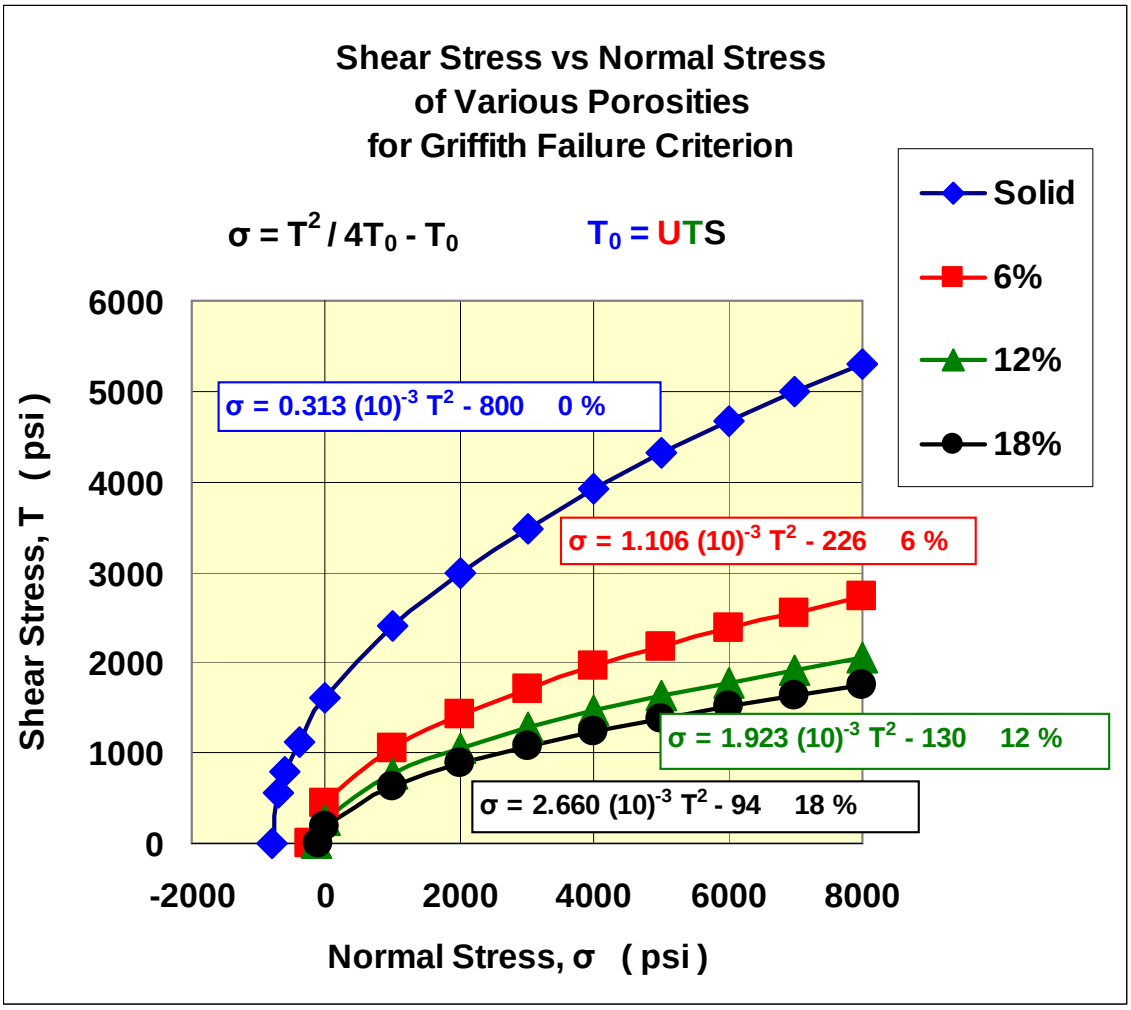

Figure 57 Effect of Porosity on the Griffith Failure Criterion

The Griffith Criterion is a parabolic equation that assumes the shear stress is two times the tensile strength when the normal stress is equal to zero. For example, for zero porosity and a shear stress of 1600 psi, the normal stress is equal to zero, as shown on the top curve in Figure 57.

Figure 58 shows the effect of porosity on the Power Failure Criterion for 0, 6, 12 and 18 percent porosities.

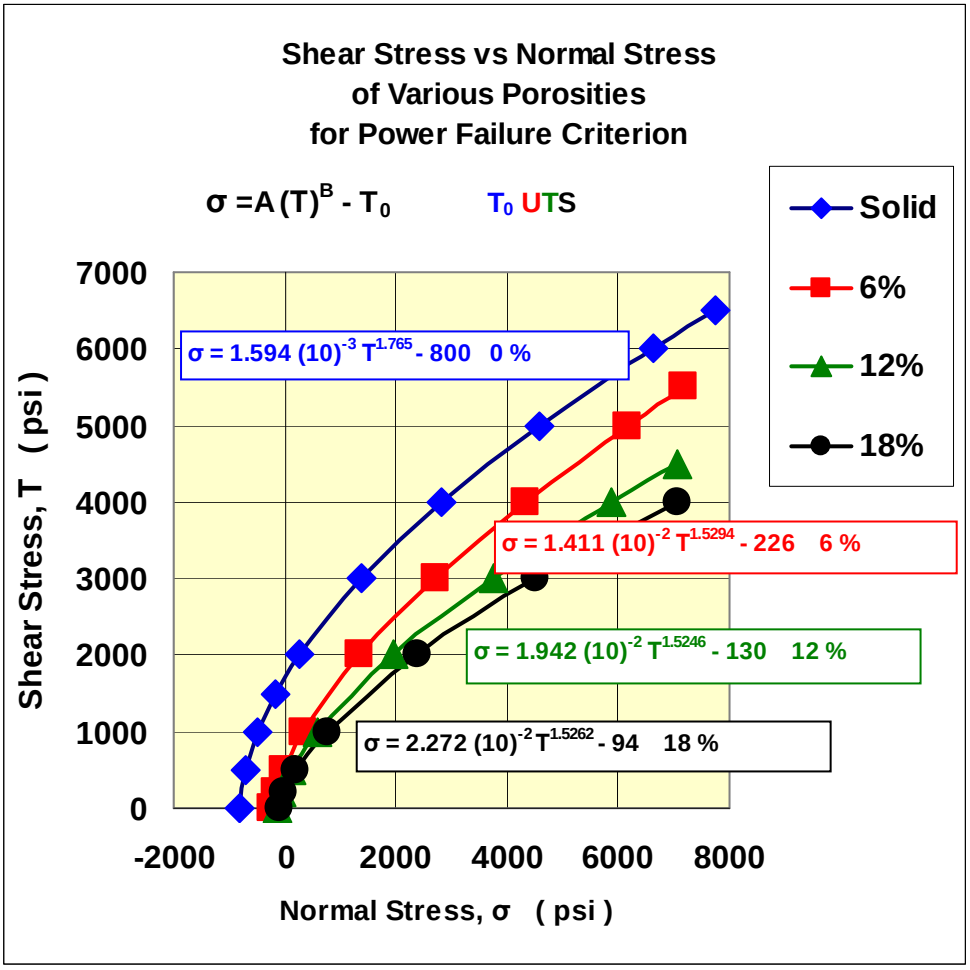

Figure 58 Effect of Porosity on the Power Failure Criterion

The Power Failure Criterion in Figure 54 shows higher shear stresses than the Griffith Failure Criterion. The Griffith Failure Criterion assumes an exponent of 2, while the Exponential Failure Criterion determines an exponent by matching points on Mohr's circles. The exponents of the Power Failure Criterion varied from approximately 1.5 to 1.6.

Figure 59 shows the percent changes in the UCS and UTS values for porosities between 0% and 19 %, which shows that the changes between compression and tension are very similar to each other.

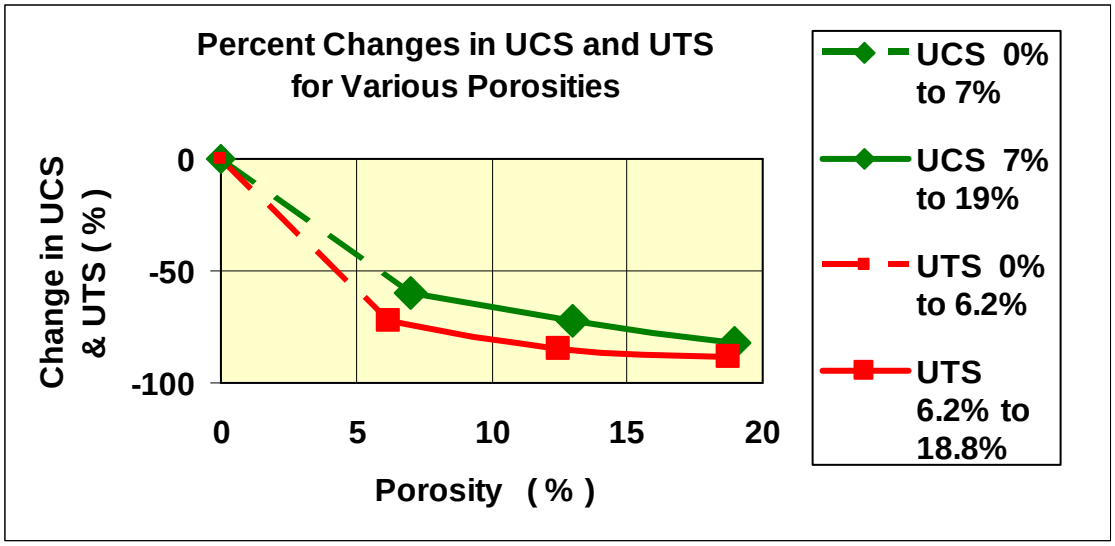

Figure 59 Percent Changes in UCS & UTS

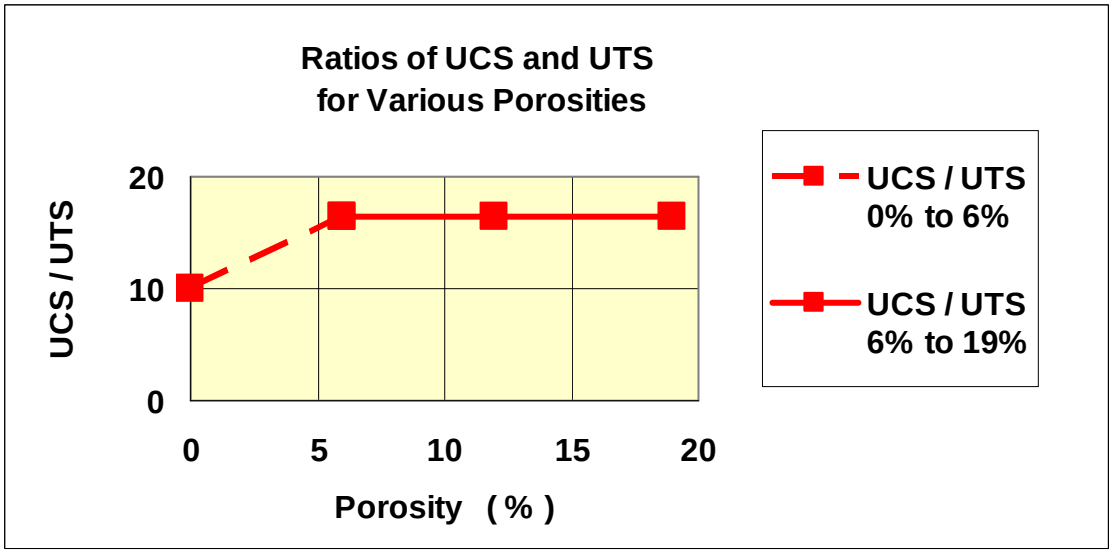

Figure 60 Ratios of UCS and UTS

Figure 60 shows the ratios of the UCS (Rigby, 2007) and UTS values for porosities between 0% and 19 %. For zero percent porosity, the ratio of UCS and UTS was 10.0, which is the same that was shown by Goodman on page 61, Table 3.1, for Nevada Test Site tuff (Goodman 1989). For porosities from 6% to 19%, the ratio of UCS and UTS was a constant 16.5 %.

The 6% specimens that were investigated had different configurations in hole sizes and hole locations for a better generalization of failure criteria. The 12.5% and 18.75% specimens had only one hole size and configuration. However, Figures 59 and 60 show a consistent trend for all porosities from 6% to 19%.

5.8 Stress Concentrations

Table 2 shows stress concentration factors for the Brazilian test specimens as determined from four references.

Table 2 Stress Concentration Factors

Stress Concentration Factors at Edge of Hole						
Hole Diameter	1.0000”			0.7031”		Reference
Number of Holes	1	2	3	1	2	
Theoretical	3.2 C			3.1 C		Peterson, 1974
Experimental	3.9 E	6.0 E	7.0 E		3.4 E	**Timoshenko, 1970
UDEC Models	*4.5	*8.9	*10.0		*5.2	Itasca, 2000
Infinite Plate	3.0			3.0		Pilkey, 1994

* UDEC Models assume plain strain conditions
** Cylinder splitting Brazilian equation

The factors for the theoretical model were determined from the text, “Stress Concentration Factors,” Figure 96, page 161 (Peterson, 1974). The letter ‘C’ after the number refers to the stress concentration factor being obtained from a curve, which assumed plain stress in the analysis.

The factors for the experimental test specimens were determined from the Brazilian stress equation (Timoshenko and Goodier, 1970), as shown in Appendix II. The letter ‘E’ after the number refers to the stress concentration factor being determined from the quotient of the experimental Ultimate Tensile Strength (UTS) of the solid specimens and the experimental UTS of the voided specimens. The UTS in each case was determined from the Brazilian equation using the net diameter, which is equal to the total diameter of the disk minus the diameter of the hole, as shown in appendix II. The experimental test specimens had a plane stress condition.

The factors for the UDEC models were determined by dividing the UTS of the solid model by the UTS of the voided models, as determined by UDEC. The UDEC models had a plane strain condition. The stresses in UDEC are 30 percent higher (1+v) for plane strain conditions, as compared with the plane stress conditions, which explains why the load for the UDEC model is 30 percent less than the loads that were observed for the experimental test specimens, which had a plane stress condition.

The factors for the infinite plate were determined from the text “Stress, Strain, and Structural Matrixes,” Table 6-1, page 271 (Pilkey, 1994).

CHAPTER 6

SUMMARIES

6.1 Discussions

The tensile modulus of elasticity was determined to be 2.35 x 10^6 psi (16.2 GPa) from the Hydro-Stone TB Dog Bone 1 test specimen. The compressive modulus of elasticity from previous tests was 2.31 x 10^6 psi (15.9 GPa), that was determined from an average of twenty, 6-inch cubical Hydro-Stone TB test specimens (Rigby, 2007). The close comparison of the tensile and compressive modulus of elasticity shows that the dog bone approach can be used to measure mechanical properties. It may be possible that with longer and wider end sections, failure could be initiated in the narrow middle section. The dog bone tests made in the MTS test machine were already at their limit of length to fit into the test machine.

The UDEC analysis of the direct tensile tests of a 6” x 6” test model showed high stresses at the corners of the model, which means that failure would probably be initiated at these locations in a test specimen instead of in the center, and that the experimental results may not be representative of the central geometry of the specimen.

If funds are ever available for extending this project, the direct tensile tests of Hydro-Stone TB specimens would be a worthwhile project. End connections for the dog bone tests have already been fabricated, which worked successfully in the previous tests. Also, a wooden mold has been made for fabricating 6” x 6” x 2” Hydro-Stone TB specimens.

Twenty Hydro-Stone TB specimens were successfully tested in the UNLV Tinus-Olsen testing machine, as shown in Chapters 3 through 5. Also, the UDEC computer models showed crack initiations at similar locations to those observed in the test specimens, as shown in Chapter 4.

The average ultimate indirect tensile strength of the four solid Hydro-Stone TB Brazilian specimens was 800 psi (5.52 MPa), which is 10 percent of the ultimate unconfined compressive strength of 7976 psi (55 MPa), as determined from previous tests (Rigby, 2007). This matches results shown for Nevada Test Site tuff, which was found to have an indirect tensile strength of 10 percent of the unconfined compressive strength, as shown in the rock mechanics text by Goodman, Table 3.1, page 61 (Goodman 1989).

The ultimate tensile stress of 800 psi that was determined from the Brazilian test specimens was specified in the UDEC input. The applied loads that caused failure in the UDEC analyses were approximately 32 percent less than the applied loads that were determined from the experimental failure loads, as computed in the elasticity text by Timoshenko for the splitting equation that is shown on page 167 (Timoshenko and Goodier, 1970). The boundary conditions of the loaded surfaces in the UDEC analysis are probably not an actual match of what occurs in a test specimen.

Another possible explanation for the difference between the experimental and UDEC results is that the Brazilian equation, as derived by Timoshenko, uses a concentrated load, which is specified by the ASTM specifications (ASTM 496, 2004), but then specifies the use of a plywood strip to distribute the load, which

places part of the applied load to each side, which is recommended in order to prevent compression failure at the point of loading. Figure 28 shows that there are vertical failure zones on each side of the center which are not shown in the Brazilian equation analyses. Therefore, the Brazilian equation that is used to calculate the ultimate stress may not be entirely correct, since the Brazilian equation uses a concentrated load. Future research should include investigation into this condition.

Another source of error is that UDEC uses a plane strain analysis, which assumes an infinite length, while the actual specimens are a disc of finite length. For a Poisson's ratio of 0.28, as shown in Appendix IV, the stresses in the UDEC equations are 28 percent higher (1+u) for the plane strain conditions as compared with the plane stress conditions that existed in the test specimens. These higher stresses in the UDEC plane strain condition produced a lower collapse load and a lower ultimate tensile strength for the UDEC analysis, which was observed by the test results shown in Figure 49.

Also, the UDEC 2D program uses a two-dimensional state of stress, and the actual test specimens are three dimensional, which might explain the reasons for some of the differences.

Both UDEC and the experimental test results show a large drop in tensile strength from the solid to the 6.2 percent porosity condition. The experimental ultimate tensile stress for the solid condition is 800 psi (5.52 MPa), and for the 6.2 percent condition is 224 psi (1.54 MPa). This shows a 72 percent drop in tensile strength for only an increase of 6.2 percent in porosity. From 6.2 percent

porosity to 18.5 percent porosity there is a smaller reduction in the tensile strength, as shown on Figures 49.

A review of the two small hole specimens that had a porosity of 6.18 percent showed that the _A specimens had an average ultimate tensile strength, UTS, of 205 psi (1.41 MPa) and the _B specimens had an UTS of 168 psi (1.16 MPa). Figures 33 and 35 show that failure is first initiated at the top of the openings. The _B specimens had a smaller distance between the load point and the opening, so that higher stress first occurred in the _B specimens as compared with the _A specimens. Calculations for the UTS are shown in Appendix II.

The _D specimens and _A specimens had a similar distance between the load points and the openings, as shown in Figures 33 and 39. The _D specimens had an average UTS of 203 psi (1.40 MPa) and the _A specimens had an average UTS of 205 psi (1.41 MPa). The closeness of these two values can be attributed to the similar distances from the load points to the top of the hole.

The _C specimens had a solid portion of the specimen between the load points. The _C specimens had an average UTS of 368 psi (2.54 MPa). This higher UTS, as compared with the _A, _B or _D specimens can be attributed to the solid portion between the load points.

In reviewing the failure criteria, the Mohr-Coulomb in s-t space failure criterion shows the lowest failure line up to a normal stress of 4,000 psi (27.6 MPa) as compared with the Mohr-Coulomb, Griffith and Power criteria. Also, the Griffith criterion shows the lowest failure line for normal stresses over 4,000 psi (27.6

MPa). These two criteria would provide the safest design criteria for structures in rock that have mechanical properties analogous to Hydro-Stone TB, such as tuff rock. The upper bound values, as shown by the Mohr-Coulomb criteria, show the upper limiting stress values for a reasonable structural design.

6.2 Conclusions

From the previous study it can be concluded that:

1. Dog bone type tests can be used to determine elastic modulus of elasticity.
2. Dog bone type tests have the limitation of failures at the end connections.
3. Direct tensile tests have the limitation of failures at the outer corners.
4. Hydro-Stone TB is a suitable material for Brazilian indirect tensile testing.
5. UDEC shows the same failure modes, as observed in actual test specimens.
6. UDEC shows lower tensile stress values than observed in actual tests.
7. Tresca, Mohr-Coulomb, Griffith and Power Failure Criteria can be used to predict failure for various porosities in rock like materials.
8. The Tresca criterion provides the lowest failure line for normal stresses up to 4,000 psi (27.6 MPa).
9. The Griffith criterion provides the lowest failure line for normal stresses over 4,000 psi (27.6 MPa).
10. The Mohr-Coulomb criterion shows the highest failure line for the criteria evaluated in this study.
11. The Brazilian equation may not be an accurate analysis for specimens that have a distributed applied load.

6.3 Recommendations

From the previous study it can be recommended that:

1. The Mohr-Coulomb in s-t Space and Griffith Failure Criteria should be used in the design of tunnels, as they show the lowest limiting stress values.

2. Most of tunnel loads should be carried by additional structural support in porous rock, as the porosity in rock greatly reduces the strength and load carrying capacity of the rock.

3. More research is needed in the area of triaxial testing of rock to widen the scope of knowledge on the strength of porous rock. Also, the Brazilian equation should be evaluated for use with a distributed applied load.

APPENDIX I

DATA FOR WEIGHT LOSS OF SPECIMENS

Before testing the Brazilian specimens, the weights of four specimens were weighed at various time intervals up to 29 days to check the stabilization time of weight loss due to moisture evaporation. Table 3 shows the weight losses that were measured on an Ohaus Explorer scale to the nearest 0.1 gram and converted into ounces.

Table 3 Weight Loss and Time for 4” Diameter x 2” Long Specimens

Time	Weight Loss (oz)			
Day	Specimen_1	Specimen_2	Specimen_3	Specimen_4
1	0.00	0.00	0.00	0.00
2	1.18	1.30	1.32	1.13
3	1.95	2.01	2.01	1.80
4	2.30	2.38	2.36	2.21
6	2.45	2.52	2.51	2.38
8	2.58	2.63	2.62	2.54
14	2.59	2.64	2.63	2.55
21	2.60	2.64	2.64	2.56
29	2.60	2.64	2.64	2.56

Figure 61 shows the weight loss versus time for the 4” diameter by 2” long Hydro-Stone TB specimens. The weights of all four specimens stabilized after eight days.

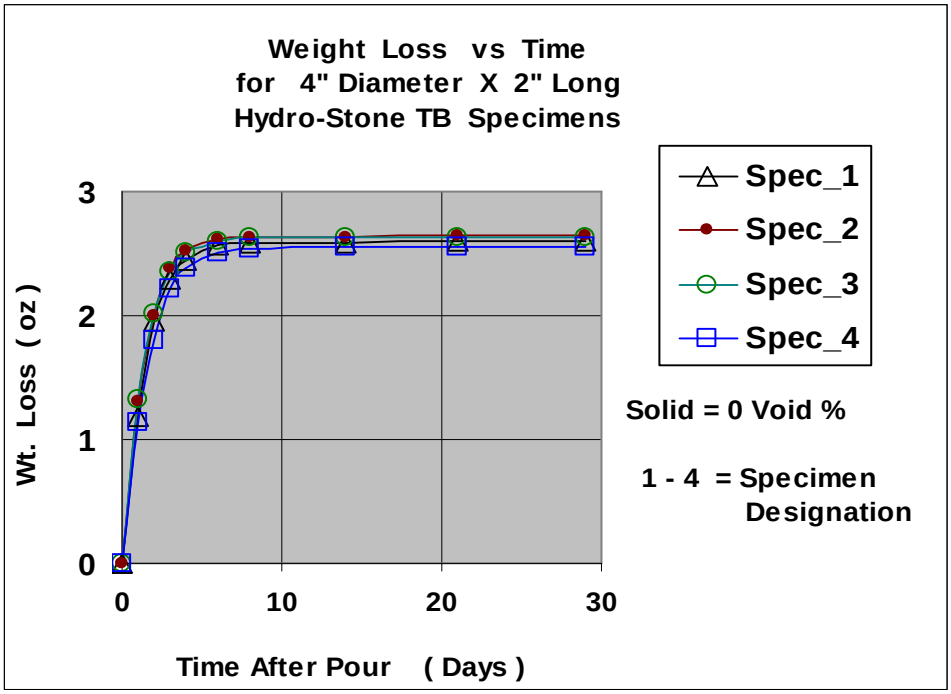

Figure 61 Weight Loss vs Time for 4” Diameter x 2” Long Hydro-Stone TB Specimens

APPENDIX II

EXPERIMENTAL DATA FOR BRAZILIAN SPECIMENS

20 Brazilian test specimens were fabricated and tested at UNLV. Data for these specimens are shown in Table 4. There are 18 columns in the table which show the following:

Column 1 shows Specimen Name. Solid refers to the specimens with no voids. 2SH means 2 small holes in the specimen. The number after 2SH is the porosity in percent. The A1 and A2 refer to duplicate specimens. The letters A, B, C and D refer to different arrangements of the holes in the specimens. See text photographs and Table 9 for specific hole locations. 1LH means 1 large hole in the specimen. 2LH means 2 large holes in the specimen, and 3LH means 3 large holes in the specimen.

Column 2 shows the amount of porosity in each specimen.

Columns 3 thru 6 show diameter measurements made on each specimen. Measurements were made with a Starrett electronic digital caliper. Measurements were made to the nearest 5/10,000 of an inch (0.0005”). Four readings were made on each specimen. A reading was made on the front and back at 0 degrees, and a reading was made at 90 degrees on the front and back.

Column 7 shows the average of the four readings of Columns 3 thru 6.

Column 8 shows the specimen name, which is the same as in Column 1.

Columns 9 thru 12 are digital caliper readings of the lengths of the specimens. Four readings were made on each specimen. A reading was made at 0, 90, 180 and 270 degrees around the specimen.

Column 13 is the average of the four length readings of Columns 9 thru 12.

Column 14 is the name of the specimen, the same as Columns 1 and 8.

Column 15 is the load at which the specimen failed.

Column 16 is the diameter correction equation for the reduced diameter of the specimen for the void space. The maximum stress at failure occurs adjacent to a void, which reduces the failure load, as shown in the UDEC analyses of Chapter 4. To account for this effect in the Brazilian equation, the diameter of the hole was used to reduce the total diameter of the specimen. This is an approximation, but in lieu of a more exact equation, the reduced diameter correction is applied.

Column 17 is the corrected diameter of the specimen, as described for Column 16.

Column 18 is the Ultimate Tensile Stress (UTS), as determined from the Brazilian equation, Eq [1], (Goodman, 1989), which is:

Ultimate Tensile Strength (UTS), $\sigma_t = 2 P / \pi D L$ Eq [1]

where: P is the peak tensile load in Column 15,

D is the corrected diameter in Column 17,

L is the length in Column 13.

For concrete indirect tensile testing, an 8-inch length is required for a 4-inch diameter specimen (ASTM C 496/C, 2004). For asphalt, a 2-inch length is required for a 6-inch diameter (Christensen and Bonaquist, 2004). A 2-inch length and a 4-inch diameter were chosen for this project as reasonable dimensions to study the effect of porosity on the Hydro-Stone TB specimens.

Table 4 Data for Brazilian Test Specimens

Data Column 1 Spec Name	for 2 % Voids	Braz. 3 Diam. (in)	Spec. 4	5	6	7 Diam. (in)
		0^{o} Front	0^{o} Back	90^{o} Front	90^{o} Back	Avg.
Solid_1	0	4.0125	4.006	4.0195	4.019	4.0143
Solid_2	0	4.0115	4.039	4.0185	4.025	4.0235
Solid_3	0	4.0025	4.005	3.985	3.993	3.9964
Solid_4	0	4.0445	4.0265	4.008	4.0005	4.0199
					Avg	4.0135
2SH6.18_A1	6.18	3.986	3.985	4.0025	3.985	3.9896
2SH6.18_A2	6.18	3.986	3.985	4.009	3.9985	3.9946
2SH6.18_B1	6.18	3.998	3.9885	4.006	3.985	3.9944
2SH6.18_B2	6.18	3.98	3.9885	4.0015	3.9905	3.9901
2SH6.18_C1	6.18	4.026	3.9855	3.975	3.985	3.9929
2SH6.18_C2	6.18	3.9995	3.9935	3.9975	3.9845	3.9938
2SH6.18_D1	6.18	4.0605	4.0375	4.0125	4.016	4.0316
2SH6.18_D2	6.18	4.0115	4.0035	4.0465	4.086	4.0369
					Avg	4.0030
1LH6.25_A1	6.25	4.004	3.9955	3.9985	3.999	3.9993
1LH6.25_A2	6.25	4.023	4.0125	4.03	4.006	4.0179
1LH6.25_B1	6.25	3.995	3.992	3.993	3.993	3.9933
1LH6.25_B2	6.25	4.0385	4.026	4.067	4.037	4.0421
					Avg	4.0131
2LH12.50_A1	12.5	4	4.023	4.003	4.0135	4.0099
2LH12.50_A2	12.5	4.0035	4.005	4.03	4.009	4.0119
					Avg	4.0109
3LH18.75_A1	18.75	3.9905	3.993	3.9905	4.0125	3.9966
3LH18.75_A2	18.75	3.9965	4.0005	3.994	3.9985	3.9974
					Avg	3.9970

Table 4 Continued

8 Data Spec Name	9 Length (in) 0°	10 90°	11 180°	12 270°	13 Length (in) Avg.
Solid_1	1.971	1.972	1.976	1.964	1.9708
Solid_2	1.971	1.987	1.982	1.975	1.9788
Solid_3	2.0115	2.0105	2.0125	2.021	2.0139
Solid_4	2.0165	2.017	1.988	2.0085	2.0075
				Avg	1.9927
2SH6.18_A1	2.067	2.059	2.067	2.078	2.0678
2SH6.18_A2	2.016	2.0585	2.022	2.045	2.0354
2SH6.18_B1	2.042	2.056	2.047	2.0585	2.0509
2SH6.18_B2	2.09	2.07	2.0605	2.0775	2.0745
2SH6.18_C1	2.0545	2.042	2.056	2.052	2.0511
2SH6.18_C2	2.0535	2.05	2.036	2.0695	2.0523
2SH6.18_D1	2.043	2.048	2.035	2.0395	2.0414
2SH6.18_D2	2.053	2.054	2.0565	2.042	2.0514
				Avg	2.0531
1LH6.25_A1	1.8905	1.873	1.8795	1.9085	1.8879
1LH6.25_A2	2.0185	2.064	1.9905	2.0335	2.0266
1LH6.25_B1	2.053	2.0345	2.0465	2.05	2.0460
1LH6.25_B2	2.058	2.0265	1.995	2.034	2.0284
				Avg	1.9972
2LH12.50_A1	1.9865	2.0165	2.005	2.041	2.0123
2LH12.50_A2	1.961	1.9875	1.933	1.958	1.9599
				Avg	1.9861
3LH18.75_A1	1.81	1.7945	1.719	1.7845	1.7770
3LH18.75_A2	1.8125	1.85	1.8725	1.824	1.8398
				Avg	1.8084

Table 4 Continued

14 Data Spec Name	15 Measured Load, P (lbs)	16 Corrected D Equation	17 Corrected D (in)	18 Test UTS (psi)
Solid_1	10495	D - 0.0000	4.0143	845
Solid_2	11138	D - 0.0000	4.0235	891
Solid_3	9193	D - 0.0000	3.9964	727
Solid_4	9396	D - 0.0000	4.0199	741
Avg	10056		4.0135	800
2SH6.18_A1	2211	D - 0.7031	3.2865	207
2SH6.18_A2	2142	D - 0.7031	3.2915	204
2SH6.18_B1	1598	D - 0.7031	3.2913	151
2SH6.18_B2	1972	D - 0.7031	3.2870	184
2SH6.18_C1	3931	D - 0.7031	3.2898	371
2SH6.18_C2	3869	D - 0.7031	3.2907	365
2SH6.18_D1	2184	D - 0.7031	3.3285	205
2SH6.18_D2	2174	D - 0.7031	3.3338	202
Avg	2510		3.2999	236
1LH6.25_A1	1825	D - 1.0000	2.9993	205
1LH6.25_A2	1816	D - 1.0000	3.0179	189
1LH6.25_B1	1846	D - 1.0000	2.9933	192
1LH6.25_B2	2081	D - 1.0000	3.0421	215
Avg	1892		3.0131	200
2LH12.50_A1	1191	D - 1.0000	3.0099	125
2LH12.50_A2	1075	D - 1.0000	3.0119	116
Avg	1133		3.0109	121
3LH18.75_A1	684	D - 1.0000	2.9966	82
3LH18.75_A2	906	D - 1.0000	2.9974	105
Avg	795		2.9970	93

APPENDIX III

TEST DATA

Loads were recorded at each second of time interval in the Tinus-Olsen testing machine. Table 5 shows the values for five seconds before and after the failure loads, which are in bold print.

Table 5 Failure loads from Tinus-Olsen Testing Machine

Solid		1LH6.25		2LH12.50		3LH18.75	
_3	_4	_B1	_B2	_A1	_A2	_A1	_A2
-9014	-9243	-1842	-2073	-1129	-1040	-686	-845
-9052	-9268	-1843	-2075	-1141	-1017	-694	-859
-9082	-9304	-1844	-2077	-1153	-1034	-644	-868
-9118	-9333	-1844	-2079	-1164	-1049	-659	-881
-9159	-9358	-1844	-2079	-1177	-1063	-671	-894
-9193	**-9396**	**-1846**	**-2081**	**-1191**	**-1075**	**-684**	**-906**
-572	-2806	-1846	-2079	-11	11	-5	-9
-206	-2740	-1845	-2079	0	-1	0	-1
-184	-2634	-1846	-2079	0	-1	1	-1
-184	-2517	-1846	15	1	0	0	0
-184	-2566	-4	2	1	1	0	-1

2SH6.18		2SH6.18		2SH6.18		2SH6.18	
_A1	_A2	_B1	_B2	_C1	_C2	_D1	_D2
-2204	-2125	-1587	-1958	-3897	-3814	-2167	-2153
-2204	-2128	-1589	-1960	-3905	-3825	-2171	-2158
-2205	-2133	-1591	-1964	-3913	-3835	-2174	-2162
-2206	-2138	-1593	-1968	-3921	-3845	-2177	-2166
-2208	-2140	-1597	-1969	-3926	-3857	-2182	-2170
-2211	**-2142**	**-1598**	**-1972**	**-3931**	**-3869**	**-2184**	**-2174**
-2210	3	-4	3	-3879	-3743	-2104	-2080
3	0	0	1	-3855	-3761	-2123	-2097
1	-2	0	-1	-3834	-3779	-2137	-2110
0	-2	0	0	-3817	-3797	-2149	-2125
-1	-2	0	-2	-3802	-3786	-2162	-2136

Table 5 Continued

20-May-09	Failure	Loads	Of	Brazilian	Tests	
Solid_1				Solid_2		
		Load (#)				Load (#)
1:58:54 PM		-10217		2:59:15 PM		-10853
1:58:55 PM		-10271		2:59:16 PM		-10909
1:58:56 PM		-10329		2:59:17 PM		-10968
1:58:57 PM		-10386		2:59:18 PM		-11026
1:58:58 PM		-10440		2:59:19 PM		-11083
1:58:59 PM	**Failure**	**-10495**		**2:59:20 PM**	**Failure**	**-11138**
1:59:00 PM		-7403		2:59:21 PM		-1829
1:59:01 PM		-5065		2:59:22 PM		-1774
1:59:02 PM		-4446		2:59:23 PM		-1782
1:59:03 PM		-4278		2:59:24 PM		-1777
1:59:04 PM		-4179		2:59:25 PM		-1761
1LH 6.25_A1				1LH 6.25_A2		
		Load # (#)				Load # (#)
2:17:23 PM		-1688		3:24:05 PM		-1774
2:17:24 PM		-1707		3:24:06 PM		-1781
2:17:25 PM		-1728		3:24:07 PM		-1789
2:17:26 PM		-1739		3:24:08 PM		-1799
2:17:27 PM		-1787		3:24:09 PM		-1808
2:17:28 PM	**Failure**	**-1825**		**3:24:10 PM**	**Failure**	**-1816**
2:17:29 PM		-5		3:24:11 PM		-4
2:17:30 PM		1		3:24:12 PM		-1
2:17:31 PM		1		3:24:13 PM		1
2:17:32 PM		1		3:24:14 PM		0
2:17:33 PM		-1		3:24:15 PM		1

Figure 62 is an example of the data for load versus time that was recorded from the Tinus-Olsen test machine. Specimen 1LH6.25_A1 was loaded at a faster rate than specimen 1LH6.25_A2. At the near failure loads specimen 1LH6.25_A1 was loaded at about 27 lbs/sec and specimen 1LH6.25_A2 was loaded at about 8 lbs/sec. Specimen 1LH6.25_A1 failed at a load of 1825 lbs (8.12 kN) and specimen 1LH6.25_A2 failed at a load of 1816 lbs (8.08 kN).

The results showed that the failure load was not affected by the strain rate. A strain rate of 0.02 inches per minute was used for most of the tests.

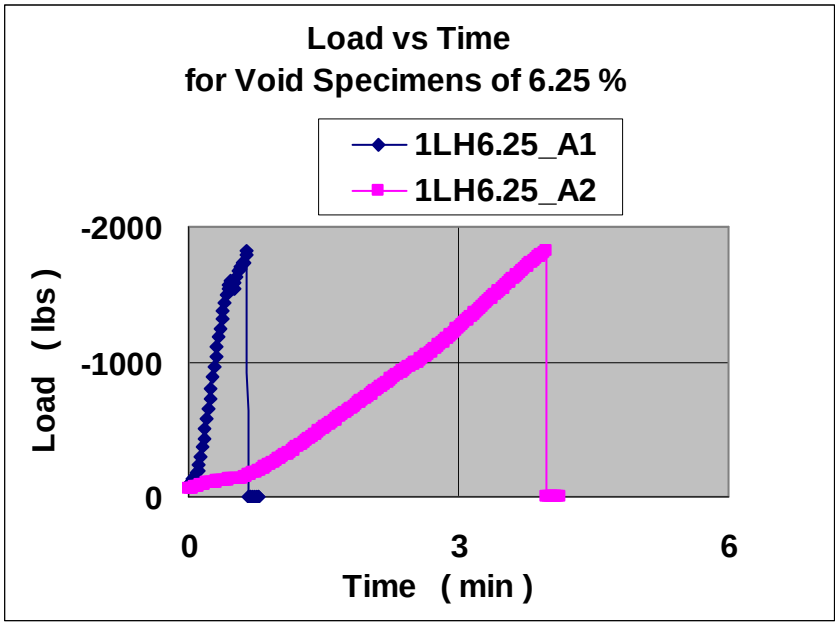

Figure 62 Load versus Time for Specimens 1LH6.25_A1 and 1LH6.25_A2

APPENDIX IV

INPUT DATA FOR UDEC PROGRAM

UDEC requires input data from the properties of the material being tested. Table 6 shows the properties that were used in the modeling of the Hydro-Stone TB specimens.

Table 6 UDEC Input Data for Hydro-Stone TB Specimens

UDEC Data			
Type	Description	Value	Units
den	Density	1.63 E -4	lbs/in^3 / in/sec^2
bu	Bulk Modulus	1.76 E 6	psi
sh	Shear Modulus	0.905 E 6	psi
jten	Tensile Strength	8 E 2	psi
Φ	Friction Angle	35	deg
jcoh	Cohesion	2.08 E 3	psi
jkn	Joint Normal Stiffness	2.4 E 6	psi / in
jks	Joint Shear Stiffness	1.2 E 6	psi / in

UDEC defines density as being the quotient of the weight per unit volume of the material and the acceleration of gravity.

The bulk modulus is a function of the Young's modulus and Poisson's ratio. It is defined by the equation $K = E / 3(1-2\upsilon)$. Values of $E = 2.32(10)^6$ psi and $\upsilon = .28$ were used (Rigby 2007).

The shear modulus is also a function of E and υ, which is defined by the equation $G = E / 2(1-\upsilon)$.

The tensile strength is the ultimate tensile strength of the Hydro-Stone TB. The average of four experimental tests on solid specimens, as shown in Chapter 3, resulted in an average ultimate tensile strength of 800 psi.

An exact value of the friction angle, φ, for Hydro-Stone TB was not known. Tests on actual rocks have shown that φ can vary from 7 to 51 degrees (Goodman, 1989). A value of 35 degrees was used successfully in the UDEC program for tuff rock (Rigby, 2007). 35 degrees was used for this project.

The cohesion is the ordinate on the vertical shear axis of the Mohr's circle diagram. The cohesion for Hydro-Stone TB was determined from the geometry of Mohr's circle using an unconfined compression strength of 7,976 psi (Rigby, 2007) and φ = 35 deg.

The joint normal stiffness is the quotient of the stress at a point and the displacement which is caused by the stress. The unconfined compressive stress of 7,976 psi was used, and the displacement was determined as the strain for a unit length of one inch. With these values the normal stiffness is the same as the elastic modulus.

The joint and normal stiffness were varied on several examples and there was no change in the resulting stress distributions. UDEC's manual for Verification Problems & Example Applications defines the normal and shear stiffness, as being for sub joints, and then gives estimated input values.

Normal and shear stiffness have been defined as the ratio of the change in stress to the change in strain, which is a function of the dilation angle and other values such as roughness coefficients for the joints (Brady and Brown, 1985).

The dilation angle was considered zero in the UNLV analysis, and joint roughness coefficients are not known for Hydro-Stone TB. Therefore, Young's modulus was used as an approximation for the normal joint stiffness and one half of Young's modulus was used as the shear joint stiffness. Table 7 shows the UDEC input program for the Dog Bone 1 model analysis.

Table 7 Input Data for UDEC Dog Bone 1 Analysis

```
new
ro .01
bl     -4 -10   -4 10   4 10    4 -10
     cr     -2   -10     -4   -7
     cr      2   -10      4   -7
     cr     -4    -5     -2   -2
     cr     -2    -2     -2    2
     cr     -2     2     -4    5
     cr      4    -5      2   -2
     cr      2    -2      2    2
     cr      2     2      4    5
     cr     -2    10     -4    7
     cr      2    10      4    7
     cr      0   -10      0   10
   tunnel      0    6      1.0      16
   tunnel      0   -6      1.0      16
de ra bl     2   118   308   598   1621
de ra bl  1069  2472  4961  3683  6159
gen edge  .2
se pl windows
prop mat 1  dens  1.63e-4   bu  1.76e6   sh  .905e6
prop jmat 1 jkn 2.46  jks 1.2e6  jfric 35 jcoh 2.08e3  ten 8e2
bo str  0  0      1.0e3     ra  -2  2      9.9     10.1
bo str  0  0      1.0e3     ra  -2  2     -10.1    -9.9
bo xvel  0  ra  -.2   .2     -.2   .2
bo yvel  0  ra  -.2   .2     -.2   .2
hi syy  0  10
hi  yd  0  10
hi syy  0 -10
hi  yd  0 -10
step  20000
pl hi 1 vs 2
```

Table 8 shows the UDEC input program for the 6-inch by 6-inch elastic model analysis.

Table 8 Input Data for UDEC 6-inch by 6-inch Model Analysis

```
new
ro  .01
bl   -3  -3    -3  3    3  3    3   -3
gen edge .2
se pl windows
prop mat 1   d 1.63e-4   k 1.76e6    g .906e6
bo yvel= 3e-1  xvel=0  ra -3.00 3.00   2.99  3.01
bo yvel=-3e-1  xvel=0  ra -3.00 3.00  -3.01 -2.99
bo yvel=  0    xvel=0  ra  -.01  .01   -.01   .01
step 5000
pl bl syy
pl bl sxx
```

APPENDIX V

UDEC DATA FOR BRAZILIAN SPECIMENS

The voids in the Brazilian test specimens were located as shown in Table 9. Each specimen was 4 inches in diameter and 2 inches in length. The hole locations were measured from the center of the specimen.

Table 9 Locations of Void Holes in Brazilian Specimens

		Distance from Center (0, 0)					
	Hole	Hole #1		Hole #2		Hole #3	
	Diameter	X	Y	X	Y	X	Y
Specimen	(in)	(in)	(in)	(in)	(in)	(in)	(in)
2SH6.18_A1	0.7031	0	0.75	0	-0.75		
2SH6.18_A2	0.7031	0	0.75	0	-0.75		
2SH6.18_B1	0.7031	0	0	0	1.176		
2SH6.18_B2	0.7031	0	0	0	1.176		
2SH6.18_C1	0.7031	-0.75	0	0.75	0		
2SH6.18_C2	0.7031	-0.75	0	0.75	0		
2SH6.18_D1	0.7031	-0.5	-0.5	0.5	0.5		
2SH6.18_D2	0.7031	-0.5	-0.5	0.5	0.5		
1LH6.25_A1	1	0	0.833				
1LH6.25_A2	1	0	0.833				
1LH6.25_B1	1	0	0				
1LH6.25_B2	1	0	0				
2LH12.50_A1	1	0	0.833	0.722	-0.42		
2LH12.50_A2	1	0	0.833	0.722	-0.42		
3LH18.75_A1	1	0	0.833	0.722	-0.42	-0.5	-1
3LH18.75_A2	1	0	0.833	0.722	-0.42	-0.5	-1

The UDEC data input for the solid and voided models are shown in the tables below.

Table 10 UDEC Data for Solid_1, Solid_2, Solid_3 and Solid_4 Models

```
new
ro .01
bl  -2.25 -2.25   -2.25  2.25   2.25 2.25   2.25 -2.25
cr  -2.25  0      2.25  0
tun  0    0      2   64
cr    .375  2.25    .375  1.95
cr   -.375  2.25   -.375  1.95
cr   -.375 -2.25   -.375 -1.95
cr    .375 -2.25    .375 -1.95
de ra bl   2   118    9379   9719
gen edge .2
zone model mohr
zone bulk 1.76e6   shear .905e6
zone coh 2.08e3  fric 35  ten 8e2
se pl windows
prop mat 1   den 1.63e-4   bulk 1.76e6   shear .905e6
prop jmat 1  jkn 2.4e6    jks 1.2e6   jfri 35   jcoh 2.08e3  jten 8e2
bo yvel =  -3e-1  xvel = 0.0    ra  -.375   .375   2.2   2.3
bo yvel =   3e-1  xvel = 0.0    ra  -.375   .375  -2.3  -2.2
bo yvel =  0.0    xvel = 0.0    ra -0.01   0.01   -0.01  0.01
hist sxx     0      0
hist xdisp   0      0
hist syy      .37    2
hist yd       .37    2
hist syy      .3     2
hist yd       .3     2
hist syy      .2     2
hist yd       .2     2
hist syy      .1     2
hist yd       .1     2
hist syy     0       2
hist yd      0       2
damp auto
step 68000
plot hist 1 vs 2
```

Table 11 UDEC Data for 1LH6.25_A1 and 1LH6.25_A2 Models

```
new
ro .01
bl  -2.25 -2.25   -2.25  2.25   2.25 2.25   2.25 -2.25
cr  -2      .8333    2      .8333
tun  0    0      2   64
tun  0  .8333   .5   32
cr    .375  2.25     .375  1.95
cr   -.375  2.25    -.375  1.95
cr   -.375 -2.25    -.375 -1.95
cr    .375 -2.25     .375 -1.95
de ra bl   2   2006    4367    14893
gen edge .2
zone model mohr
zone bulk 1.76e6   shear .905e6
zone coh 2.08e3  fric 35  ten 8e2
se pl windows
prop mat 1   den 1.63e-4   bulk 1.76e6   shear .905e6
prop jmat 1  jkn 2.46e6    jks 1.23e6   jfri 35   jcoh 2.08e3  jten 8e2
bo yvel =  -3e-1  xvel = 0.0    ra  -.375   .375   2.2   2.3
bo yvel =   3e-1  xvel = 0.0    ra  -.375   .375  -2.3  -2.2
hi sxx       -.53,    .8333
hi xd        -.53,    .8333
hi sxx        0      1.34
hi xd         .53    1.34
hi sxx        0       .32
hi xd         .53     .32
hi syy        .37    2
hi yd         .37    2
hi syy        .3     2
hi yd         .3     2
hi syy        .2     2
hi yd         .2     2
hi syy        .1     2
hist yd       .1     2
hi syy        0      2
hi yd         0      2
hi syy        0     -2
hi yd         0     -2
damp auto
step 17880
pl hi  3 vs  4
```

Table 12 UDEC Data for 1LH6.25_B1 and 1LH6.25_B2 Models

```
new
ro .01
bl  -2.25 -2.25   -2.25  2.25   2.25 2.25   2.25 -2.25
cr  -2      0    2      0
tun  0    0      2    64
tun  0    0      .5   32
cr    .375  2.25     .375  1.95
cr   -.375  2.25    -.375  1.95
cr   -.375 -2.25    -.375 -1.95
cr    .375 -2.25     .375 -1.95
de ra bl   2   1926    4287    14521
gen edge .2
zone model mohr
zone bulk 1.76e6   shear .905e6
zone coh 2.08e3  fric 35  ten 8e2
se pl windows
prop mat 1   den 1.63e-4   bulk 1.76e6   shear .905e6
prop jmat 1  jkn 2.46e6    jks 1.23e6   jfri 35   jcoh 2.08e3  jten 8e2
bo yvel =  -3e-1  xvel = 0.0    ra  -.375   .375   2.2   2.3
bo yvel =   3e-1  xvel = 0.0    ra  -.375   .375  -2.3  -2.2
hi sxx       -.53,   0
hi xd        -.53,   0
hi sxx        0      .53
hi xd         0      .53
hi sxx        .53    0
hi xd         .53    0
hi sxx        0     -.53
hi yd         0     -.53
hi syy        .3     2
hi yd         .3     2
hi syy        .2     2
hi yd         .2     2
hi syy        .1     2
hist yd       .1     2
hi syy        0      2
hi yd         0      2
hi syy        0     -2
hi yd         0     -2
damp auto
step 14370
pl hi   3 vs  4
pl hi  15 vs 16
```

Table 13 UDEC Data for 2LH12.50_A1 and 2LH12.50_A2 Models

```
new
ro .01
bl  -2.25 -2.25   -2.25  2.25   2.25 2.25   2.25 -2.25
cr   -.8   2     1.6    -1.6
tun  0    0      2       64
tun  0       .8333   .5     32
tun  .7217   -.4167   .5     32
cr    .375  2.25     .375  1.95
cr   -.375  2.25    -.375  1.95
cr   -.375 -2.25    -.375 -1.95
cr    .375 -2.25     .375 -1.95
de ra bl  2   20015   11185   16449   14163   18159
gen edge .2
zone model mohr
zone bulk 1.76e6    shear .905e6
zone  coh 2.08e3    fric 35     ten 8e2
se pl windows
prop mat 1   den 1.63e-4   bulk 1.76e6   shear .905e6
prop jmat 1  jkn 2.46e6    jks 1.23e6   jfri 35   jcoh 2.08e3  jten 8e2
bo yvel= -3e-1   xvel = 0.0    ra -.375  .375   2.2  2.3
bo yvel=  3e-1   xvel = 0.0    ra -.375  .375  -2.3  -2.2
damp auto
hi syy    0      2
hi  yd    0      2
hi syy    0     -2
hi  yd    0     -2
hi sxx    0      1.34
hi  xd     .5    1.34
hi sxx     .72    .10
hi  xd     .72    .10
hi sxx     .7    -.9
hi  xd     .7    -.9
step 12000
pl hi 1 vs 2
pl hi 3 vs 4
pl hi 5 vs 6
pl hi 7 vs 8
pl hi 9 vs 10
```

Table 14 UDEC Data for 3LH18.75_A1 and 3LH18.75_A2 Models

```
new
ro .01
bl  -2.25 -2.25   -2.25  2.25   2.25 2.25   2.25 -2.25
cr   -.8   2     1.6    -1.6
cr  -2     0     1      -2
tun  0    0      2       64
tun  0       .8333   .5     32
tun  .7217   -.4167   .5     32
tun -.500   -1.0000   .5     32
cr    .375  2.25     .375  1.95
cr   -.375  2.25    -.375  1.95
cr   -.375 -2.25    -.375 -1.95
cr    .375 -2.25     .375 -1.95
de ra bl  2   25028   19752   11310   14568   21462   17546   23172
gen edge .2
zone model mohr
zone bulk 1.76e6     shear .905e6
zone  coh 2.08e3     fric 35     ten 8e2
se pl windows
se pl clip bw
prop mat 1   den 1.63e-4   bulk 1.76e6   shear .905e6
prop jmat 1  jkn 2.46e6    jks 1.23e6   jfri 35   jcoh 2.08e3  jten 8e2
bo yvel= -3e-1   xvel = 0.0    ra -.375  .375   2.2  2.3
bo yvel=  3e-1   xvel = 0.0    ra -.375  .375  -2.3  -2.2
damp auto
hi syy    0      2
hi  yd    0      2
hi syy    0     -2
hi  yd    0     -2
hi sxx    0      1.34
hi  xd     .5    1.34
hi sxx     .72    .10
hi  xd     .72    .10
hi sxx     .7    -.9
hi  xd     .7    -.9
step 18000
pl hi 1 vs 2
pl hi 3 vs 4
pl hi 5 vs 6
pl hi 7 vs 8
pl hi 9 vs 10
```

Table 15 UDEC Data for 2SH6.18_A1 and 2SH6.18_A2 Models

```
new
ro .01
bl  -2.25 -2.25   -2.25  2.25   2.25 2.25   2.25 -2.25
cr   -2   .75    2    .75
cr   -2  -.75    2   -.75
tun  0    0      2       64
tun  0      .75    .3516     32
tun  0     -.75    .3516     32
cr    .375  2.25     .375  1.95
cr   -.375  2.25    -.375  1.95
cr   -.375 -2.25    -.375 -1.95
cr    .375 -2.25     .375 -1.95
pa
de ra bl  2   20015   11185   16449   14163   18159
gen edge .2
zone model mohr
zone bulk 1.76e6    shear .905e6
zone  coh 2.08e3    fric 35     ten 8e2
se pl windows
prop mat 1   den 1.63e-4   bulk 1.76e6   shear .905e6
prop jmat 1  jkn 2.46e6    jks 1.23e6   jfri 35   jcoh 2.08e3  jten 8e2
bo yvel= -3e-1   xvel = 0.0    ra -.375  .375   2.2  2.3
bo yvel=  3e-1   xvel = 0.0    ra -.375  .375  -2.3  -2.2
damp auto
hi syy    0      2
hi  yd    0      2
hi syy    0     -2
hi  yd    0     -2
hi sxx    0      1.12
hi  xd    .36    1.34
step 20000
pl hi 1 vs 2
pl hi 3 vs 4
pl hi 5 vs 6
```

Table 16 UDEC Data for 2SH6.18_B1 and 2SH6.18_B2 Models

```
new
ro .01
bl  -2.25 -2.25   -2.25  2.25   2.25 2.25   2.25 -2.25
cr   -2   1.176    2    1.176
cr   -2   0        2    0
tun  0    0      2       64
tun  0    1.176    .3516     32
tun  0    0        .3516     32
cr    .375  2.25     .375  1.95
cr   -.375  2.25    -.375  1.95
cr   -.375 -2.25    -.375 -1.95
cr    .375 -2.25     .375 -1.95
de ra bl  2    19836    2211    4572    6802    9130
gen edge .2
zone model mohr
zone bulk 1.76e6    shear .905e6
zone  coh 2.08e3    fric 35     ten 8e2
se pl windows
prop mat 1   den 1.63e-4   bulk 1.76e6   shear .905e6
prop jmat 1 jkn 2.46e6  jks 1.23e6   jfri 35   jcoh 2.08e3  jten 8e2
bo yvel= -3e-1   xvel = 0.0    ra -.375  .375   2.2  2.3
bo yvel=  3e-1   xvel = 0.0    ra -.375  .375  -2.3  -2.2
damp auto
hi syy    0      2
hi  yd    0      2
hi syy    0     -2
hi  yd    0     -2
hi sxx    0      1.12
hi  xd    .36    1.34
step 25000
pl hi 1 vs 2
pl hi 3 vs 4
pl hi 5 vs 6
```

Table 17 UDEC Data for 2SH6.18_C1 and 2SH6.18_C2 Models

```
new
ro .01
bl  -2.25 -2.25   -2.25  2.25   2.25 2.25   2.25 -2.25
cr   -2   0       2    0
tun  0    0      2       64
tun  -.75    0    .3516     32
tun   .75    0    .3516     32
cr    .375  2.25     .375  1.95
cr   -.375  2.25    -.375  1.95
cr   -.375 -2.25    -.375 -1.95
cr    .375 -2.25     .375 -1.95
de ra bl  2   19237   2086   4447   6677   9005
gen edge .2
zone model mohr
zone bulk 1.76e6    shear .905e6
zone  coh 2.08e3    fric 35     ten 8e2
se pl windows
se pl clip bw
prop mat 1   den 1.63e-4   bulk 1.76e6   shear .905e6
prop jmat 1  jkn 2.46e6    jks 1.23e6   jfri 35   jcoh 2.08e3  jten 8e2
bo yvel= -3e-1   xvel = 0.0    ra -.375  .375   2.2  2.3
bo yvel=  3e-1   xvel = 0.0    ra -.375  .375  -2.3  -2.2
damp auto
hi syy    0      2
hi  yd    0      2
hi syy    0     -2
hi  yd    0     -2
hi sxx    0      1.54
hi  xd    .36    1.54
step 60000
pl hi 1 vs 2
pl hi 3 vs 4
pl hi 5 vs 6
```

Table 18 UDEC Data for 2SH6.18_D1 and 2SH6.18_D2 Models

```
new
ro .01
bl  -2.25 -2.25   -2.25  2.25   2.25 2.25   2.25 -2.25
cr   -2   -2       2    2
tun  0    0      2      64
tun  -.5   -.5    .3516     32
tun   .5    .5    .3516     32
cr    .375  2.25     .375  1.95
cr   -.375  2.25    -.375  1.95
cr   -.375 -2.25    -.375 -1.95
cr    .375 -2.25     .375 -1.95
de ra bl  2   19413   2186   15471   4787    17557
gen edge .2
zone model mohr
zone bulk 1.76e6    shear .905e6
zone  coh 2.08e3    fric 35     ten 8e2
se pl windows
se pl clip bw
prop mat 1   den 1.63e-4   bulk 1.76e6   shear .905e6
prop jmat 1  jkn 2.46e6    jks 1.23e6   jfri 35   jcoh 2.08e3  jten 8e2
bo yvel= -3e-1   xvel = 0.0    ra -.375  .375   2.2  2.3
bo yvel=  3e-1   xvel = 0.0    ra -.375  .375  -2.3  -2.2
damp auto
hi syy    0      2
hi  yd    0      2
hi syy    0     -2
hi  yd    0     -2
hi sxx    0      .86
hi  xd    .36    .86
step 17500
pl hi 1 vs 2
pl hi 3 vs 4
pl hi 5 vs 6
```

Figure 63 shows the triangular block mesh that is made for the two small hole specimens, 2SH6.18_D, in the Itasca UDEC 2D program. UDEC 2D creates blocks that have a maximum dimension of 0.2 inches. Deformable finite-difference zones are created in each block. There were 3357 zones created for the Mohr-Coulomb failure criteria analysis in the 2SH6.18_D models.

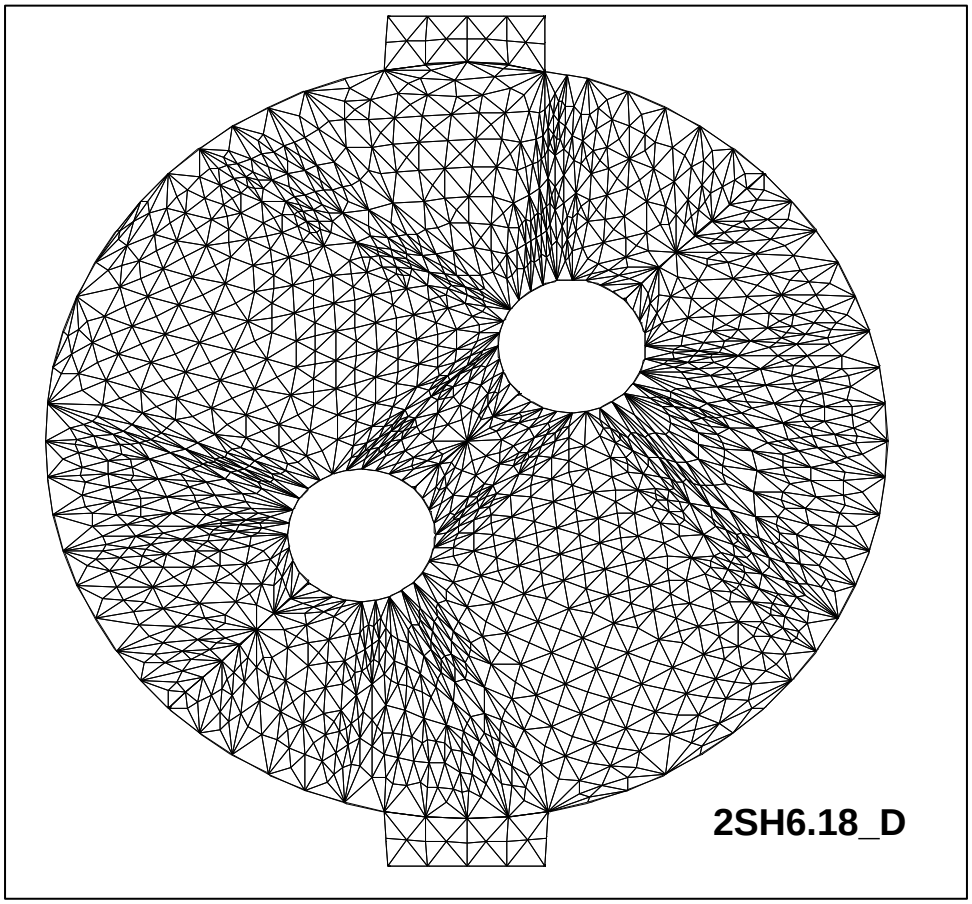

Figure 63 UDEC Mesh for 2SH6.18_D Models

Input data for the UDEC 2D programs are shown in Tables 6 through 18 of Appendixes IV and V.

The mesh edge length that was used for all of the UDEC models was 0.2 inches. An analysis was made for the 1LH6.25_B model with an applied load of 750 lbs at the top and bottom of the model to determine the effect of various mesh sizes on the horizontal stresses at the bottom of the hole, which is the location where the first stress failure occurs. The effect of mesh size on the stresses at the bottom of the hole is shown in Figure 64. The edge length was reduced from 0.20 inches to 0.04 inches in increments of 0.02 inches. At a length of .04 inches computer malfunction notices began to appear and no further length reductions were made.

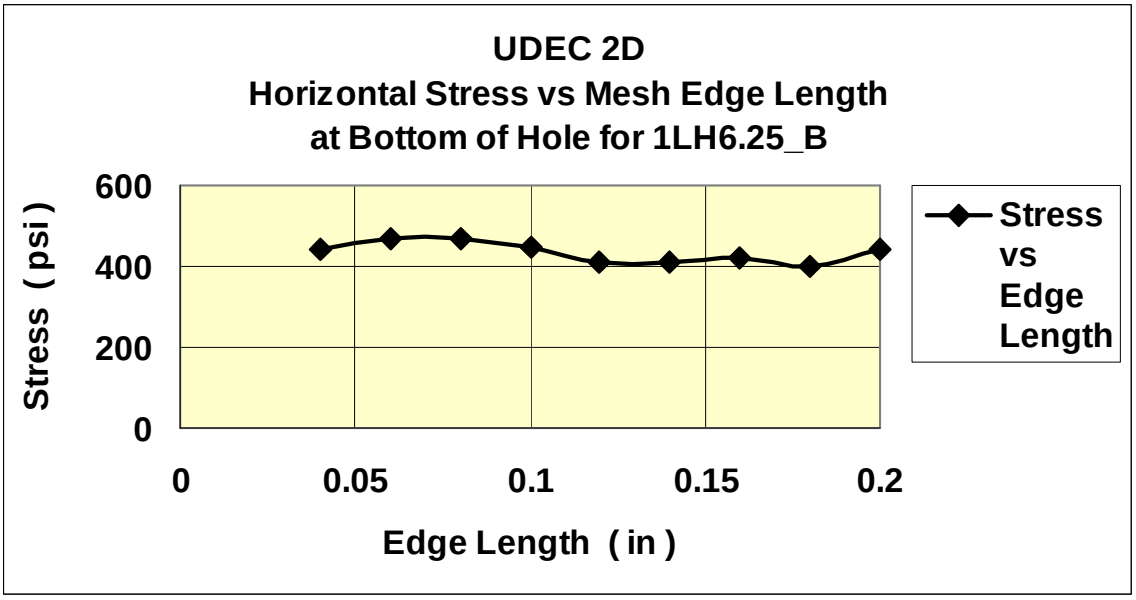

Figure 64 UDEC Horizontal Stress versus Edge Length

Figure 64 shows that the horizontal stresses were the same value of 440 psi for the maximum and minimum edge lengths shown.

Table 19 UDEC Ultimate Tensile Stresses (UTS)

1	2	3	4	5
Spec Name	UDEC Stress, Syy (psi)	Corrected D Equation	Corrected D (in)	UDEC UTS (psi)
Solid	5700	D - 0.0000	4	680
2SH6.18_A	905	D - 0.7031	3.2969	158
2SH6.18_B	800	D - 0.7031	3.2969	105
2SH6.18_C	X	D - 0.7031	3.2969	X
2SH6.18_D	980	D - 0.7031	3.2969	129
Avg				131
1LH6.25_A	560	D – 1.0000	3	89
1LH6.25_B	940	D - 1.0000	3	150
Avg				120
Avg 6.2 %				127
2LH12.50_A	480	D - 1.0000	3	76
3LH18.75_A	425	D - 1.0000	3	68

The columns in Table 19 show the following:

Column 1 is the name of the specimen.

Column 2 is the vertical stress at the top of the model, which is determined from the UDEC output.

Column 3 is the diameter correction equation for the reduced diameter of the specimen for the void space, as described in Appendix II.

Column 4 is the corrected diameter of the specimen.

Column 5 is the Ultimate Tensile Stress (UTS), as determined from the Brazilian equation, (Goodman, 1989), as shown in Appendix II.

APPENDIX VI

UDEC MOHR-COULOMB EQUATIONS

The Mohr-Coulomb failure criterion is applied to deformable zones in a UDEC model. The failure envelope is applied to both shear and tensile failure. The equations that follow are the same as shown in the text, “Theory and Background,” (Itasca, 2000).

Hooke’s law in terms of changes in principal stresses and strains in a plane strain analysis for elastic zones are:

$$\begin{aligned}\Delta\sigma_1 &= \alpha_1\Delta\varepsilon_{e1} + \alpha_2\left(\Delta\varepsilon_{e2} + \Delta\varepsilon_{e3}\right)\\ \Delta\sigma_2 &= \alpha_1\Delta\varepsilon_{e2} + \alpha_2\left(\Delta\varepsilon_{e1} + \Delta\varepsilon_{e3}\right)\\ \Delta\sigma_3 &= \alpha_1\Delta\varepsilon_{e3} + \alpha_2\left(\Delta\varepsilon_{e1} + \Delta\varepsilon_{e2}\right)\end{aligned} \qquad (1)$$

where

$\Delta\sigma_1, \Delta\sigma_2, \Delta\sigma_3$ are changes in elastic stresses, and

$\Delta\varepsilon_{e1}, \Delta\varepsilon_{e2}, \Delta\varepsilon_{e3}$ are changes in elastic strains.

$$\alpha_1 = K + \frac{4G}{3}$$

$$\alpha_2 = K - \frac{2G}{3}$$

$$K = \frac{E}{1-2\upsilon}$$

$$G = \frac{E}{2(1-\upsilon)}$$

The Mohr-Coulomb failure envelope for shear failure is:

$$f^s = \sigma_1 - \sigma_3 N_\phi + 2c\sqrt{N_\phi} \qquad (2)$$

where

$$N_\phi = \frac{1+\sin\phi}{1-\sin\phi},$$

f^s is the limiting shear stress,

σ_1 and σ_3 are normal principal stresses,

ϕ is the friction angle, and

c is the cohesion.

The shear stress has the flow rule:

$$g^s = \sigma_1 - \sigma_3 N_\varphi \qquad (3)$$

where

g^s is the limiting shear stress'

$N_\varphi = \frac{1+\sin\varphi}{1-\sin\varphi}$ and

φ is the dilation angle.

For stresses and strains in the plastic zone, the flow rule is:

$$\Delta\varepsilon_{pi} = \lambda^s \frac{\partial g^s}{\partial \sigma_i} \qquad \text{i = 1, 2 and 3} \qquad (4)$$

where

$\Delta\varepsilon_{pi}$ are changes in plastic strains,

$$\lambda^s = \frac{\sigma^s(\sigma_1', \sigma_3')}{(\alpha_1 - \alpha_2 N_\varphi) - (\alpha_2 - \alpha_1 N_\varphi) N_\phi}$$ and

σ_1', σ_3' are total normal principal stresses.

After partial differentiation, the plastic flow rule Is:

$$\Delta\varepsilon_{p1} = \lambda^s$$

$$\Delta\varepsilon_{p2} = 0 \qquad (5)$$

$$\Delta\varepsilon_{p3} = -\lambda^s N_\varphi$$

During plastic flow, the total sums of the elastic and plastic changes in strains are:

$$\Delta\varepsilon_i = \Delta\varepsilon_{ei} + \Delta\varepsilon_{pi} \qquad i = 1, 2 \text{ and } 3 \qquad (6)$$

These total strains are used to determine the total stresses that are compared with the stress of the Mohr-Coulomb envelope, f^s, in Equation (2).

The Mohr-Coulomb failure envelope for tensile failure is:

$$f^t = \sigma^t - \sigma_3 \qquad (7)$$

where

f^t is the limiting tensile stress and

σ^t is the ultimate tensile strength of the material.

In the case of tensile failure, the plastic flow rule is:

$$\Delta\varepsilon_{pi} = \lambda^t \frac{\partial g^t}{\partial \sigma_i} \qquad \text{i = 1, 2 and 3} \qquad (8)$$

where

$$\lambda^t = \frac{\sigma^t(\sigma_3{}^I)}{\alpha_1}$$

and tensile stress has the flow rule:

$$g^t = -\sigma_3 \qquad (9)$$

After partial differentiation:

$$\Delta\varepsilon_{p1} = 0$$

$$\Delta\varepsilon_{p2} = 0 \qquad (10)$$

$$\Delta\varepsilon_{p3} = -\lambda^t$$

The total sums of the elastic and plastic changes in strains are determined similar to Equation (6) and are used to determine the total stresses of the Mohr-Coulomb failure envelope, f^t, in Equation (7).

The method shown above is described in the UDEC text, “Theory and Practice,” Paragraph 2.4.2, titled, “Mohr-Coulomb Model,” pages 2-16 to 2-21 (Itasca, 2000).

REFERENCES

Abramson, L.W., Lee, T.S., Sharma, S. and Boyce, G.M. (2002). Slope Stability and Stabilization Methods, 2nd Edition, *John Wiley & Sons, Inc*.

Arioglu, N., Girgin Z.C. and Arioglu, E. (2006). Evaluation of Ratio between Splitting Tensile Strength and Compressive Strength for Concretes up to 120 MPa and its Application in Strength Criterion. *American Concrete Institute Materials Journal,* Jan-Feb 2006, pp 18-24.

ASTM C 496/C 496M (2004). Standard Test Method for Splitting Tensile Strength of Cylindrical Concrete Specimens. *American Society of Testing Materials, International.*

Avar, B.B. and Hudyma, N. W. (2006). Observations on the influence of lithophysae on elastic (Young's) modulus and uniaxial compressive strength of Topopah Tuff at Yucca Mountain, Nevada, USA. *International Journal of Rock Mechanics and Mining Sciences,* No. 44, Jun 2006, pp 266-270.

Avar, B.B., Hudyma, N. and Karakouzian, M. (2003). Porosity dependence of the elastic modulus of lithophysae-rich tuff: numerical and experimental investigations. *International Journal of Rock Mechanics and Mining Sciences,* Vol. 40, Issue 6, Sep 2003, pp 919-928.

Bardet, J. (1997). Experimental Soil Mechanics. *Prentice Hall, Inc.*

Brady, B.H.G. and Brown, E.T. (1993). Rock Mechanics for Underground Mining. 2nd Edition. *Chapman and Hall.*

Chawla, M. (2007). Influence of Lithophysal Geometry on Uniaxial Compression of Tuff-Like Rock. M.S. Thesis, *Department of Civil and Environmental Engineering, Howard R. Hughes College of Engineering, University of Nevada*, Aug 2007.

Christensen, D.W. and Bonaquist, R.F. (2004). Evaluation of Indirect Tensile Test (IDT) Procedures for Low-Temperature Performance of Hot Mix Asphalt, NCHRP Report 530. *Transportation Research Board of the National Academies.*

Goodman, R.E. (1993). Engineering Geology – Rock in Engineering Construction*. John Wiley & Sons, Inc.*

Goodman, R.E. (1989). Introduction to Rock Mechanics. 2nd Edition, John Wiley & Sons, Inc.

Hoek, E. and Brown, E.T. (1997). Practical Estimates of Rock Mass Strength. *International Journal of Rock Mechanics & Mining Sciences, Vol. 34, No. 8,* pp 1165-1186.

Hudyma, N., Avar, B.B. and Karakouzian, M. (2004). Compressive strength and failure modes of lithophysal-rich Topopah Spring Tuff specimens and analog models containing cavities. E*ngineering Geology,* Vol. 73, Issues 1-2, May 2004, pp 179-190.

Itasca (2000). Universal Distinct Element Code User's Guide. *Itasca Group Consulting Group, Inc.*

Itasca (2000). Universal Distinct Element Code Theory and Practice. *Itasca Group Consulting Group, Inc.*

Jumikis, A.R. (1983). Rock Mechanics, 2nd Edition, *Gulf Publishing Co.*

Karakouzian, M. and Rigby, D.B. (2007). Mechanical Behavior and Modeling of Lithophysal Rock Using Analog Material. *Paper Submitted to: U. S. Department of Energy, NSHE/YMP Nuclear Waste Cooperative Agreement,* Aug 2007.

Lin, Z. and Wood, L. (2003). Concrete Uniaxial Tensile Strength and Cylinder Splitting Test. *Journal of Structural Engineering,* ASCE, Vol. 129, No 5, May 2003, pp 692-698.

Marshak, S. (2006). Essentials of Geology. 2nd Edition, *Norton & Co.*

Obert, L. and Duvall, W.I. (1967). Rock Mechanics and the Design of Structures in Rock. *John Wiley & Sons, Inc.*

Peterson, R.E. (1974). Stress Concentration Factors. *John Wiley & Sons, Inc.*

Pilkey, W.D. (1994). Stress, Strain, and Structural Matrices. *John Wiley & Sons.*

Rahn, P.H. (1996). Engineering Geology. *Prentice-Hall PTR.*

Rigby, D.B. (2004). Lithophysal Rock Mass Mechanical Properties of the Repository Host Horizon. *DOE United States Government Identifier, 800-K0C-SS00-00200-000-00A,* Nov 2004.

Rigby, D.B. (2007). Influence of Lithophysal Geometry on the Uniaxial Compression of Tuff-Like Rock. *Department of Energy Technical Report TR-07-001*, Task ORD- FY04-013, http://hrcweb.nevada.edu/QA/Report/TR-07-001.pdf, Jun 2007.

Sheorey, P.R. (1997). Empirical Rock Failure Criteria. *A.A. Balkema Publishers, USA.*

Sullivan, M. (2002). College Algebra, 6th Edition. *Prentice Hall.*

Teufel, L.W. and McNamee, M.J. (1990). Tensile Strength Testing of Topopah Spring Tuff. *Sandia National Laboratories, DOE contract number DE-AC04-76DP00789,* printed 1990.

Timoshenko, S. and Goodier, J.N. (1970). Theory of Elasticity. 3rd Edition, *McGraw-Hill Book Company.*

VITA

Graduate College
University of Nevada, Las Vegas

James Allen Nott

Degrees:

Bachelor of Science, Civil Engineering, 1956
University of Maryland, College Park, Maryland, USA

Master of Science in Engineering, Structural Engineering, 1962
George Washington University, Washington, D.C., USA

Awards and Honors:

American Legion School Award, 1947
Eagle Scout, 1948
Award for Superior Achievement, DOD, US Navy, DTMB, 1962
Performance Awards, DOD, US Army, COE, 1986 and 1990
American Society of Civil Engineers
- Editor, Student Newsletter, University of Maryland, 1955
- Fellow, 1997
- Life Member, 1998

Tau Beta Pi, UNLV, 2007
Phi Kappa Phi, UNLV, 2008
Golden Key, UNLV, 2009
Order of the Engineer, UNLV, 2009
National Scholars Honor Society, Magnacumlaude, 2009

Publications:

Nott, J.A. (1962). Investigation on the Influence of Stiffener Size on the Buckling Pressure of Circular Cylindrical Shells Under Hydrostatic Pressure.

George Washington University Masters Thesis, Feb 1962
Society of Naval Architects and Marine Engineers, Journal of Ship Research, Vol. 6, No. 2, Oct 1962, pp 24-32.
Department of the Navy, David Taylor Model Basin Report 1688, Jan 1963.

Nott, J.A. (1963). Structural Design of Viewing Ports for Oceanographic Vehicles, *Department of the Navy, David Taylor Model Basin Report 1737,* Mar 1963.

Nott, J.A. and Ward, G.D. (1965) Evaluation of Stresses in Web-Stiffened Cylindrical Sandwich Shells subjected to Uniform External Pressure, *Department of the Navy, David Taylor Model Basin Report 2092,* Sep 1965.

Nott, J.A. (1966). Axisymmetric Stresses in Orthotropic, Web-Stiffened Sandwich Cylinders Loaded with Uniform External Pressure, *Department of the Navy, David Taylor Model Basin Report 1859,* Apr 1966.

Dissertation Title:

Tensile Strength and Failure Criterion of Analog Lithophysal Rock

Dissertation Examination Committee:

Chairperson and Committee Member, Dr. Moses Karakouzian
Committee Member, Dr. Nadar Ghafoori
Committee Member, Dr. Samaan Ladkany
Committee Member, Dr. Douglas Rigby
Graduate Faculty Representative, Dr. Samir Moujaes